THESIS

Investigating Synoptic Variations in Atmospheric CO_2 Using Continuous Observations and a Global Transport Model.

Submitted by

Nicholas C. Parazoo

Department of Atmospheric Science

In partial fulfillment of the requirements

for the Degree of Master of Science

Colorado State University

Fort Collins, Colorado

Spring 2007

COLORADO STATE UNIVERSITY

March 1, 2007

WE HEREBY RECOMMEND THAT THE THESIS PREPARED UNDER OUR SUPER-
VISION BY NICHOLAS C. PARAZOO ENTITLED Investigating Synoptic Variations in
Atmospheric CO_2 Using Continuous Observations and a Global Transport Model. BE
ACCEPTED AS FULFILLING IN PART REQUIREMENTS FOR THE DEGREE OF
MASTER OF SCIENCE.

Committee on Graduate Work

_____

_____

_____

_____
Advisor

_____
Department Head

ABSTRACT OF THESIS

Investigating Synoptic Variations in Atmospheric CO_2 Using Continuous Observations
and a Global Transport Model.

Global chemical transport models are commonly used in tracer transport inversion studies to estimate global distributions of CO_2 sources and sinks in the land and ocean from atmospheric CO_2 observations. There is much uncertainty in this technique due to under-representation of terrestrial processes by weekly flask observations over mountains and oceans compared to continuous observations over continental interiors, which in contrast contain much information about potential roles of the terrestrial biosphere in the global atmospheric carbon cycle. This information is typically stored in synoptic variations, which are still poorly understood. It is therefore important to understand the biological and atmospheric processes that cause those variations, in particular those under the influence of mid-latitude cyclones, in order to accurately represent them within transport models, theoretically improving the inversions and aiding in their interpretation.

For this study, an atmospheric transport model (PCTM) capable of resolving synoptic motions, coupled to a land surface model (SiB) through GEOS4 meteorology reanalysis, is run in forward mode in an effort to reproduce observed synoptic variations over the continent. PCTM is then used diagnostically to analyze processes that produce those variations. To assist this analysis, we formulate a budget equation that governs changes to CO_2 within the planetary boundary layer. This equation is a simplified version of PCTM that includes forcing terms such as transport by vertical and horizontal mixing and biogenic fluxes be-

tween plants and the atmosphere. Maps of each term are made to quantify and visualize interactions.

Evaluation of PCTM and GEOS4 suggests that assimilated meteorology is important for simulating timing of frontal passage events. Although fossil fuel buildup and over-estimation of winter respiration skew the amplitude of frontal CO_2 variations, timing and shape of variations are consistent with observations. The budget equation demonstrates skill in reconstructing CO_2 tendencies simulated by PCTM. Averaged over monthly scales during the growing season the equation suggests that horizontal mixing is negligible and vertical mixing is weak compared to vegetative uptake. At synoptic scales, under the influence of mid-latitude cyclones, horizontal and vertical mixing work together to cause strong and sudden variations along surface cold fronts. Results from this study should aid in future interpretation of continental observations, forward transport simulations, and CO_2 inversions. Furthermore, techniques developed in this study are general enough to be used for analysis of other weather related CO_2 variations outside of mid-latitudes.

Nicholas C. Parazoo
Department of Atmospheric Science
Colorado State University
Fort Collins, Colorado 80523-1371
Spring 2007

ACKNOWLEDGEMENTS

DEDICATION

CONTENTS

FIGURES

TABLES

Chapter   1

INTRODUCTION

1.1   Background

Fossil fuel burning and deforestation are major sources for global increases in atmospheric CO_2 (or CO_2 mixing ratio, referred to from here on out as just CO_2) during the last century, which can be seen from globally integrated ice core and high precision CO_2 measurements (Intergovernmental Panel on Climate Change (IPCC), 2001, Figure 1.1). Currently, only about half of anthropogenic CO_2 emissions remain in the atmosphere; the
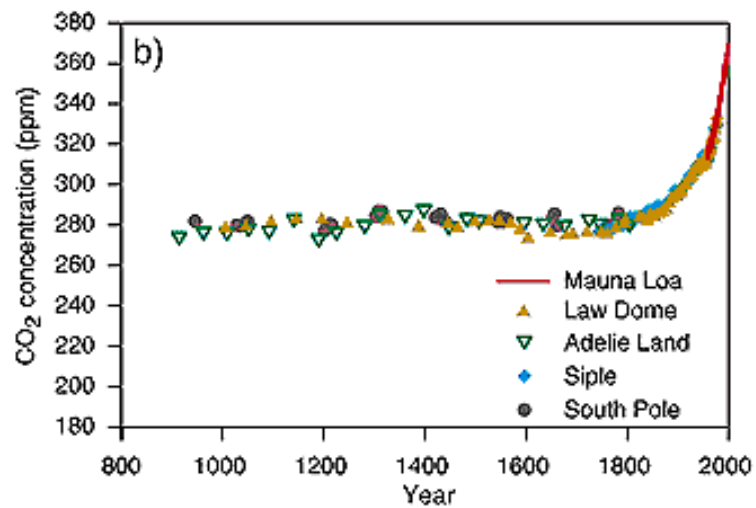
Figure 1.1: Growth rate of atmospheric CO_2 according to several estimates. IPCC, 2001.

rest is removed by some combination of terrestrial biosphere and oceanic uptake (IPCC, 2001). A basic goal of carbon cycle science has been to determine the relative roles of the ocean the terrestrial biosphere in removing CO_2 from the atmosphere. Much effort has gone

into estimating the spatial structure and magnitude of terrestrial and oceanic sources and sinks (Schimel et al., 2001).

A popular method for making estimates of net sources and sinks over large areas in the time mean has been tracer-transport inversions, where information about observed atmospheric CO_2 and three dimensional modeled atmospheric transport fields such as wind velocity, diffusion, and convective transport are used to infer surface source and sink distributions (see Figure 1.2). This is also referred to as the "top-down" approach since source

Inverse Modeling

wind   Air Parcel   wind

Air Parcel

Sources   Sinks

Air Parcel

Sample   Sample

Changes in CO_2 in the air tell us about sources and sinks
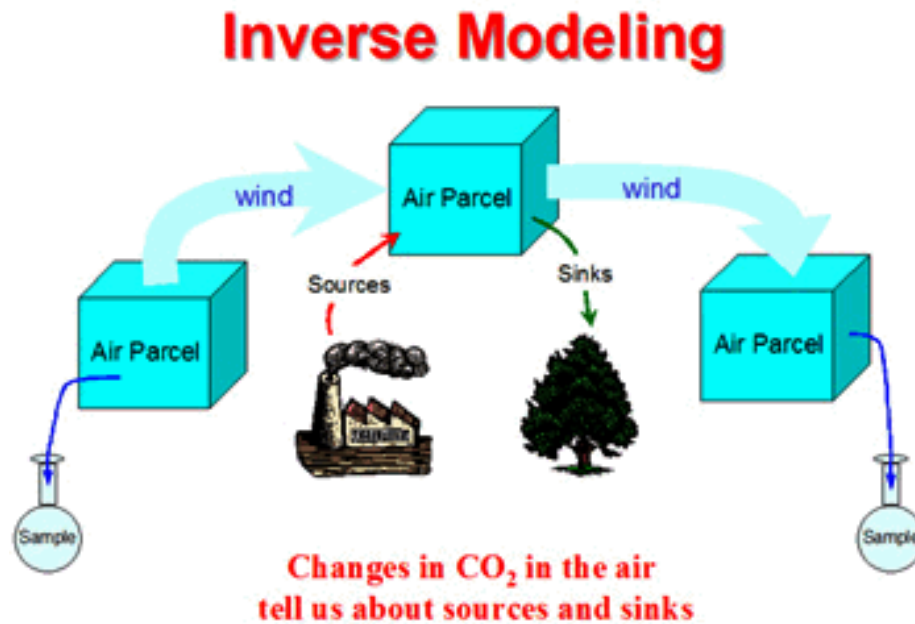
Figure 1.2: Diagram of Inverse Modeling.

and sink distributions are estimated without knowledge of details regarding finer-scale variability or underlying processes that cause the fluxes.

Global inversions of atmospheric CO_2 flask data using atmospheric transport models such as General Circulation Models (GCMs) and Chemical Transport Models (CTMs) typically find a Northern Hemisphere (NH) midlatitude terrestrial sink (Gurney et al., 2003; Fan et al., 1998), which is in agreement with direct observations (Baldocci et al., 2001) and inventory estimates (Houghton, 1999; Pacala et al., 2001), but estimates of its magnitude vary widely from -0.6 to -2.3 Gt C yr (Heimann, 2001). Estimates of its spatial distribution

are also uncertain. Reasons for uncertainty include the sparsity of available observations (Bakwin et al., 1998); numerical inaccuracy and limited spatial resolution of transport models (Gurney et al., 2002); uncertain representation of linkages between photosynthesis, surface fluxes, and weather (Baker et al., 2003); inaccurate or unrepresentative meteorology used to drive transport (Kawa et al., 2004); and the under-representation inherent in the use of monthly mean remote marine boundary layer observations in the inversions compared to high frequency observations within continental interiors (Geels et al., 2004).

Until recently, many CO_2 measurement sites have been deliberately placed in regions remote from terrestrial sources and sinks such as mountain tops and remote marine locations (Fan et al., 1998). It has become apparent, however, that continental sites would do a better job addressing the role of the terrestrial biosphere in the global atmospheric carbon cycle (Gloor et al., 2001). Continental CO_2 records are available at hourly resolution and contain high-frequency information regarding the interaction between the terrestrial biosphere and the atmosphere at diurnal and synoptic ($\sim$ days) time scales (Geels et al., 2004).

One of the biggest problems with increasing the density and frequency of continental boundary layer CO_2 observations is how data users interpret the high frequency variations. Diurnal variability was discussed in detail in Chen et al. (2004). It is controlled by alternating signals of net ecosystem exchange of CO_2 (NEE) between night and day and modified by the rectifier effect (Denning et al., 1996a,b), or the covariance between planetary boundary layer (PBL) growth/decay and biotic activity. This effect typically leads to CO_2 buildup within the nocturnal PBL, where plant and soil respiration (net efflux) and shallow PBLs can enhance CO_2 concentrations, and depletion in the daytime PBL, where convective PBLs (which act to spread concentrations over a larger volume) and photosynthetic drawdown (net uptake) can reduce atmospheric concentrations. The rectifier can vary largely from day to day depending on synoptic conditions and is most influential during the growing season.

Synoptic variations, which are frequently associated with large spikes or dips in the observations over scales of a few hours due to passing weather disturbances and surface cold

fronts, are often regarded as observation "noise" because they are difficult to explain and reproduce with models. Midlatitude cyclones are often the culprit of such variations and can be described briefly as meteorological phenomena controlled by frontal systems that form in response to baroclinic disturbances in the upper atmosphere, which are a result of meridional temperature gradients created by differential solar heating from equator to pole. These cyclones can span 1000's of kilometers in width and typically pass along the surface propelled by itself and the mean flow until energy driving the cyclone is cut off.

Synoptic systems can have important impacts on the distribution of CO_2 in the atmosphere along the frontal zone through several well known physical and biological mechanisms mentioned in the literature (Geels et al., 2004; Hurwitz et al., 2004). First, they can introduce nonlocal influence through lateral advection of horizontal CO_2 gradients. Next, vertical motion through frontal lifting over air mass boundaries along the frontal zone, mass flux convergence near the surface, and cumulus convection can enhance mixing of vertical CO_2 gradients between the PBL and free troposphere. Finally, ecosystem respiration and photosynthesis can react in various ways to changing weather associated with frontal events.

This last mechanism is more closely associated with the coupling of meteorology and biology than the others, which are governed more by the dynamics of atmospheric transport. The three mechanisms combined lead to a coupling of atmospheric transport, synoptic weather, and biology, making synoptic variability one of the more challenging scales of variability to study and understand. It also makes it one of the most interesting because of the information contained within air masses traveling across the continent (Law et al., 2002), which can be exploited through regional inversions. To utilize high frequency continental measurements for use in inverse studies given an observational network as envisioned by the North American Carbon Program (NACP, see Figure 1.3), better representation of the above mechanisms, as well as a better understanding of how the above mechanisms work together to drive high frequency variations, is needed. This can be evaluated in forward model comparison with observations.
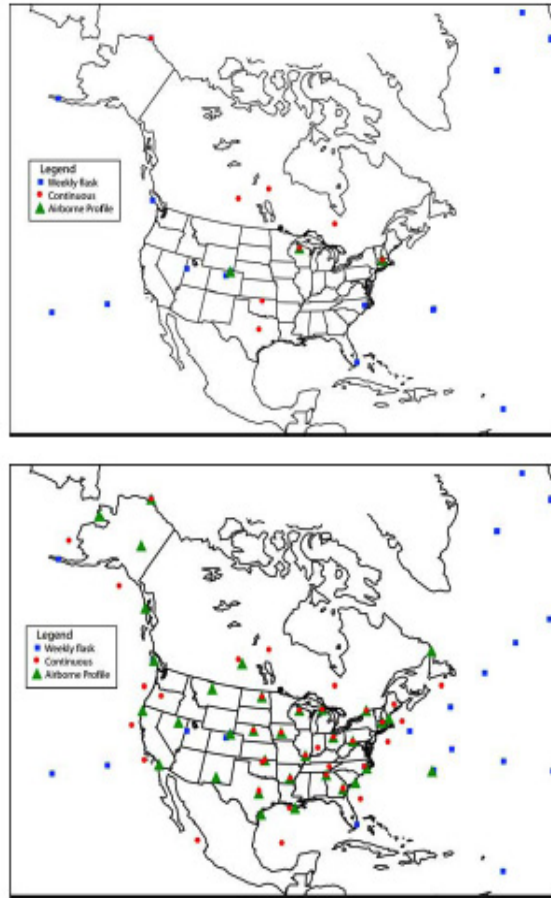
Figure 1.3: The NACP Concentration Network. The upper panel is the current network and the lower is that envisioned under Phase 2 of NACP implementation.

Several studies have looked at individual frontal cases with forward models. Chan et al. (2004), Wang et al (2005), and Corbin et al (2005), for example, used coupled land surface atmosphere mesoscale models to evaluate mesoscale and synoptic CO_2 variability during cold and warm frontal events in the summertime North America (NA). Chan and Wang found evidence that biospheric fluxes are strongly coupled to radiative forcing changes under cloud cover. They also found that mesoscale circulations and horizontal advection contribute to much of the signal during these events. Furthermore, the study by Corbin et al (2006) indicates that a clear sky CO_2 bias occurs in observations at a northern Wisconsin site with CO_2 near the surface enriched during cloudy days. The study concluded that although radiative forcing was important, horizontal advection was probably the main mechanism

for the high CO_2 during several events in August 2004.

These studies, however, were not able to incorporate larger scale perturbations into the experiments because of uniform lateral boundary conditions. In addition, coupled models generate their own weather which is not always consistent with observed weather. Mesoscale models are also impractical for simulations exceeding several weeks, a time scale necessary for global atmospheric circulations to affect local variations in weather, which makes it hard to analyze multiple events over a seasonal or annual time scales. Although high-resolution prognostic coupled models have the advantage of feedback between surface fluxes and PBL properties and are necessary for future detailed predictive studies, global chemical transport model studies of tracer transport driven by analyzed weather are good diagnostic supplements in process-based experiments. Transport models offer the advantage of analysis of the climatology of synoptic CO2 variations rather than individual events and may lead to a better understanding of the processes causing variations in atmospheric CO_2 at regional scales (Nicholls et al., 2003).

1.2 Objectives of this Study

A major obstacle in interpreting synoptic variations, in this case those associated with midlatitude cyclones, is understanding how the two major processes important for CO_2 variations, i.e., surface fluxes and atmospheric transport, interact. An appropriate modeling study would therefore involve two major components: 1) analysis of each process, and the meteorology which links them, to determine if the transport and land surface models are realistic compared to a set of observations, and 2) use of models for analysis of the processes that produce the variations.

This study therefore has two parts. The first part (Chapter 3), which addresses the first component listed above, evaluates the ability of the Parameterized Chemical Transport Model (PCTM), coupled offline to the Simple Biosphere model (SiB) and weather reanalysis provided by NASAs Goddard Earth Observation System version 4 Data Assimilation

System (GEOS4-DAS), to reproduce CO_2 observations at several well-calibrated continuous (hourly) stations in NA. Biogenic surface fluxes in SiB are evaluated at seasonal and synoptic scales to test sensitivity to both climate and weather. Transport is only evaluated at the synoptic scale; this is done by first analyzing GEOS4 directly and then its ability to transport CO_2 through PCTM during cold front passage. Frontal identification is needed for evaluation of transport; we therefore test an algorithm for identifying cold fronts in time at a point in space (part of GEOS4 analysis). Other surface fluxes separate from SiB, which include fossil fuels and oceanic fluxes, are only analyzed in terms of known inadequacies (Chapter 2).

The second part (Chapter 4), which addresses the second component and depends on the degree to which observations can be reproduced at seasonal and synoptic time scales, then uses PCTM and SiB to evaluate physical and biological processes causing the synoptic variations. Model evaluation in Chapter 3 focused on frontal variations to evaluate transport and sensitivity of NEE to frontal weather; analysis is extended, however, in Chapter 4 to the entire region under the influence of cyclonic activity. The 'budget equation', also described in Chapter 4, is the designated tool for this analysis.

Chapter 2 discusses: 1) models used in this experiment, 2) input and driver data used by the models, 3) the experiment, 4) algorithm for frontal identification 5) and observations used to evaluate model performance. The focus of Chapter 3 can be summarized as evaluation of model performance. Chapter 3 is therefore a testbed for use of the models as a set of diagnostic tools for analyzing mechanisms (Chapter 4).

Previous studies have successfully used SiB in an atmospheric GCM (Denning et al., 1995, 1996; Randall et al., 1996) and in a mesoscale atmospheric model (Denning et al., 2003). A study using PCTM driven by GEOS4 reanalysis found seasonal cycles and synoptic variability to be reasonably well reproduced compared to flask data and continuous records using only monthly mean terrestrial CO_2 Carnegie-Ames-Stanford-Approach (CASA) fluxes (Kawa et al., 2004). Ability to capture synoptic variations, which are driven largely by

transport variations, was attributed to the use of assimilated meteorological fields, which are better suited for short term events than GCM fields (Douglass et al., 2003). The current study uses a similar model experiment except that hourly CO_2 fluxes more tightly coupled to actual meteorological fields are used such that a large amount of the variation of observed data due to biology is expected to be captured. Other major differences include a more detailed analysis of physical mechanisms leading to synoptic variability and the use of continuous continental observations for evaluating potential spatial and temporal variations in synoptic signals that occur across the continent.

One major motivating reason to study synoptic weather systems with respect to regional CO_2 distributions is the information about the surface contained within the moving air masses as they travel across the continent. Unlike diurnal variations, which are influenced primarily by local forcing, and seasonal variations, which reflect hemispheric forcing, synoptic variations contain a wealth of information about regional source and sink distributions (Law et al., 2002). Since cyclones are a major mechanism for translating upstream fluxes into downstream CO_2 variations, it is important to understand the underlying processes associated with cyclones so that regional inversion studies can improve. Combined with bottom-up approaches, which consist of investigations of local processes, construction of simulation models from "input" data sets such vegetation and soil maps, and extrapolation with spatial data to larger scales (see Figure 1.4), a "model-data fusion" approach can be used to provide multiple constraints (see Figure 1.5) to the carbon cycle to estimate where net annual sources and sinks may exist across the continent (Denning et al., 2005).

To illustrate, the bottom up approach can be accomplished with SiB, which is the land surface model of choice in this study to estimate spatial and temporal NEE distributions across the continent. SiB, however, by design contains no net annual sources or sinks because it does not model longer scale processes such as ecosystem disturbance (agriculture, fire, succession, etc.) and interannual climate variability, which are potentially major factors in whether a region may balance NEE annually or not. If PCTM, given surface fluxes from

Bottom-Up Scaling Approach
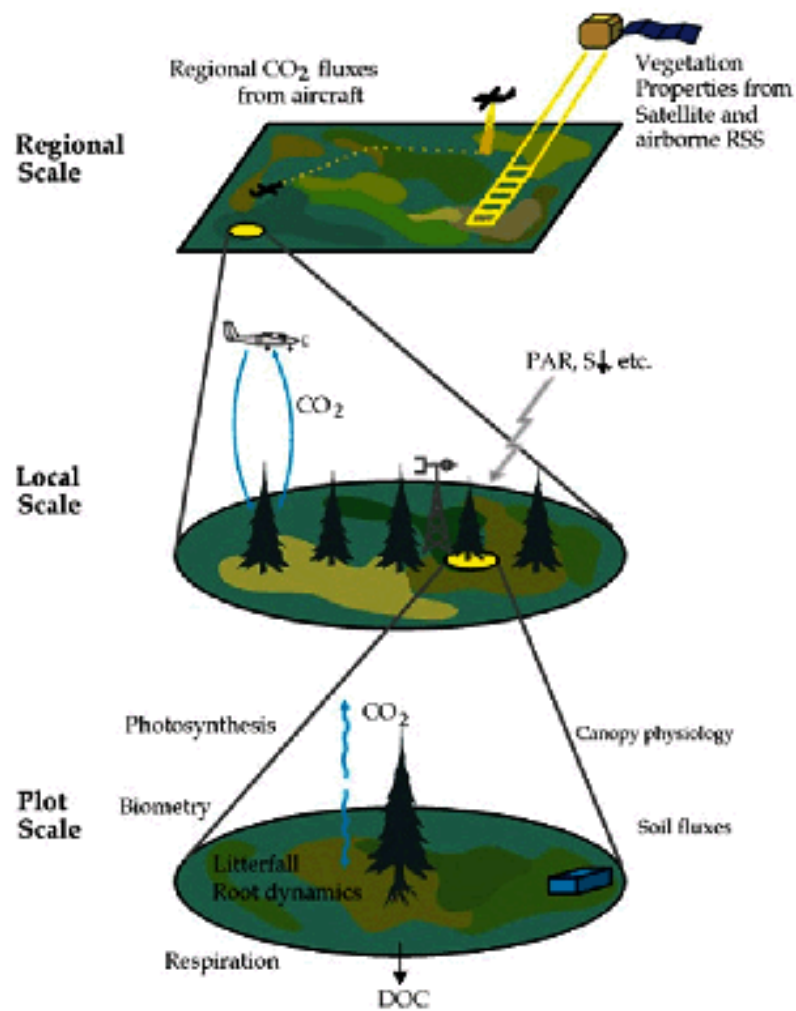
Figure 1.4: Summary of Bottom-Up Scaling.

SiB, correctly simulates the climatological (long term average, annual to decadal) frontal influence of biology on fluxes of CO_2 to the atmosphere upstream from an observing station, then this is evidence that the region of influence is correctly modeled by SiB and is likely not a strong source or sink. This scenario could be diagnosed by long term agreement between observed and modeled CO_2 downstream of moving weather systems; i.e., the average frontal signal over many years matches observations. If, however, there is strong long term disagreement between observed and modeled frontal CO_2, this is evidence that there may
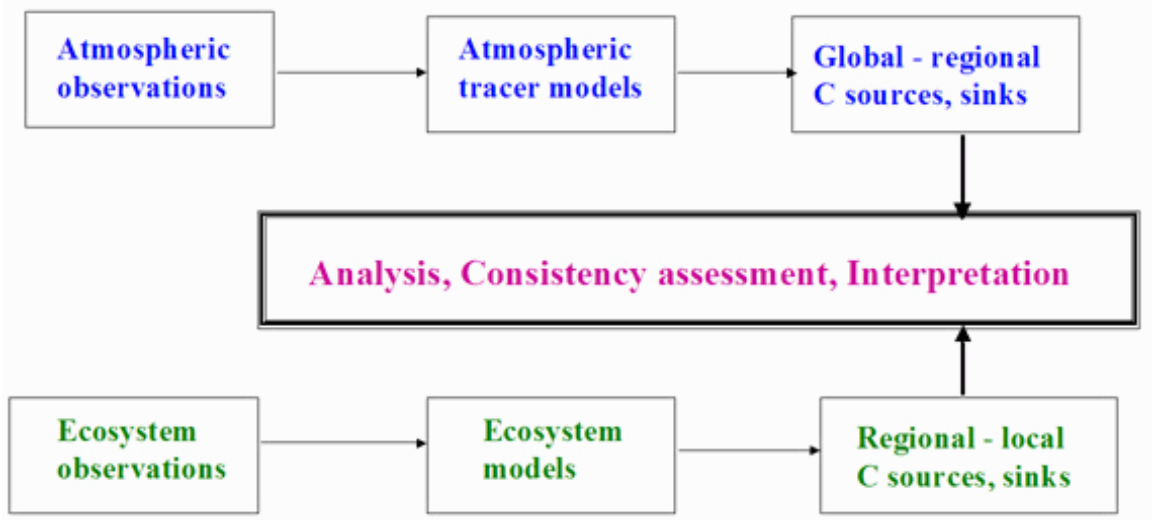
Figure 1.5: Summary of "Multiple Constraint" Approach.

be some region of influence upstream that behaves like a net annual source or sink. An optimization procedure that combines information from SiB fluxes, assuming no weather related vegetation stress exists, with inverted fluxes of atmospheric CO_2 to estimate biases in SiB can be utilized such that corrections can be made to SiB so that net sources and sinks are included.

Another major overall objective of this study is, depending on the degree to which observations can be reproduced in our modeling experiments, to then use model output to evaluate physical and biological processes that cause synoptic variations using simplified budgets of CO_2 in the PBL. Insight gained from a study of mechanisms can aid in interpretation of observed atmospheric CO_2 data which undergoes variations more closely related to atmospheric transport by midlatitude cyclones. Although the focus of this study is to obtain a better grasp on synoptic variations in NA, we try to be as general as possible in analysis of mechanisms in Chapter 4. The hope is to use the same type of analysis on much broader scales so that CO_2 variations in the Tropics or in Europe can be interpreted using a similar approach (also discussed in Conclusions chapter).

Until mesoscale models can run on a global domain in a computationally inexpensive way, they will always have the issue of prescribing inflow at the lateral boundaries.

The previous mesoscale studies mentioned above used constant inflow such that large scale perturbations that theoretically should be interacting with the domain are damped out. One other major goal of this study is to evaluate the prospect of using output from global transport models, in particular PCTM coupled offline to SiB, as lateral boundary forcing for regional simulations.

Chapter   2

EXPERIMENTAL METHODS

2.1   Model Description

2.1.1   SiB Description

SiB was developed by Sellers et al. (1986) to calculate surface energy budgets in climate models and after substantial modification (Sellers et al., 1996a,b) became SiB2. Vegetation parameters are derived directly from processed satellite data. The parameterization of stomatal and canopy conductance used in the calculation of the surface terrestrial energy budget involves the direct calculation of carbon assimilation by photosynthesis (Farquhar et al., 1980), making possible the calculation of CO_2 exchange between the land and atmosphere (Denning et al., 1996, 2003). Photosynthetic carbon assimilation is linked to stomatal conductance and thence to the surface energy budget and atmospheric climate by the Ball-Berry equation (Collatz et al., 1991, 1992). SiB includes a prognostic canopy airspace of temperature, moisture, and CO_2. Soil respiration is modeled as a function of temperature and moisture of each layer of soil, and is scaled to achieve carbon balance over an annual cycle (Denning et al., 1996a). This scaling means that modeled NEE becomes less realistic since net annual sources and sinks within a grid cell cannot be modeled and so SiB is not expected to corrected capture the magnitude of annual NEE at locations for this reason and other reasons discussed in Chapter 3.

Additional modifications have occurred since SiB2. For example, the ability to accumulate up to five layers of snow, each with unique thermodynamic properties, has been

added, improving the treatment of soil insulation and thermal properties in the winter. A more realistic root profile is used, along with better treatment of soil water stress and frozen soil. We use an improved normalized difference vegetation index (NDVI) interpolation scheme for better estimate of the time mean of NDVI. Finally, respiration now includes an autotrophic component, accounting for maintenance and growth. The revised model is referred to as SiB3.

Land surface parameters for SiB3 were specified from satellite imagery and soil texture data following the methods of Sellers et al. (1996b) and Los et al. (2000). Boundary conditions at a grid point include land cover type (Hansen et al., 2000), 8km 30-day maximum value NDVI derived from advanced very high-resolution radiometer (AVHRR) data processed by the Global Inventory Modeling and Mapping Studies lab, version "g" (GIMMSg, Pinzon et al., 2006; Teillet et al., 2000), and soil properties (Soil Survey Staff, 1994). The use of observed NDVI creates spatial heterogeneity in canopy properties.

Time invariant biophysical parameters include canopy height, leaf angle distribution, leaf transmittance, photosynthetic parameters, and soil properties. Time-varying biophysical parameters are calculated from NDVI and include leaf area index, fraction of absorbed photosynthetic active radiation (fPAR).

2.1.2   PCTM Description

The chemical transport model used for CO_2 forward simulations has been adapted from a full-chemistry and transport model (e.g., Douglass and Kawa, 1999), technical aspects of which are discussed in Nielson (2000). Three-dimensional tracer advection in PCTM is based on the transport code of Lin and Rood (1996), which uses a flux form semi-Lagrangian formulation (FFSL). Several modifications were made to PCTM for mass conservation (Kawa et al., 2004). Transport in PCTM can be driven by model simulated fields or weather reanalysis. This study uses $1.25°$ x $1°$ GEOS4-DAS weather reanalysis, which includes 6-hourly horizontal wind, cloud mass flux, and turbulence parameters.

Surface CO_2 boundary conditions include terrestrial, oceanic, and anthropogenic fluxes.

The PCTM solves the constituent continuity equation

$$\frac{\partial \chi}{\partial t} = -\vec{\mathbf{V}} \cdot \nabla \chi + \mathrm{L}\left(\chi\right) + \mathrm{P}\left(\chi\right) \tag{2.1}$$

where χ is the constituent mixing ratio concentration, t is time, $\vec{\mathbf{V}}$ is the total velocity vector, and P and L are the production and loss rates, respectively using a technique known as process splitting (Nielson, 2000).

The Lin and Rood scheme offers several major advantages of FFSL necessary to maintain the statistics of advected tracers. One includes independence of stability on time step (Lin and Rood, 1996). In addition, the scheme meets the physical constraints of tracer advection and accounts for the problem of consistency between the tracer continuity equation and the underlying equation of continuity of air due to process splitting techniques (Lin and Rood, 1996). The accuracy of the code for large-scale transport is well documented (Kawa et al., 2004).

PCTM simulations that use analyzed meteorology face the problem of local nonconservation of mass that arises during the assimilation process, which leads to inconsistencies between surface pressure tendencies and mass flux convergence. This, in turn, introduces errors in the advected tracer field. Kawa et al. (2004) add a pressure fixer (Rotman et al., 2001) to the model, which acts to remove zonally distributed pressure errors without inducing a vertical wind change, and find that inconsistencies were removed.

Since subgrid-scale vertical processes are important for atmospheric trace gases, vertical motion is included in PCTM by means of vertical advection (vertical wind derived from vertical mass flux (hPa)), cumulus convection, and boundary layer subgrid scale vertical diffusiviity (turbulent mixing). Vertical cloud transport is implemented in PCTM using a mass conserving, semi-implicit convective transport module [Kawa et al., 2004], formulated to be consistent with convective mass fluxes provided by the deep convection scheme used in the finite volume GCM (FVGCM) (Zhang and McFarlane, 1995).

2.2   Data Preparation

This section briefly discusses surface flux data, which act as sources and sinks of CO_2 to the atmosphere and include terrestrial fluxes, anthropogenic sources (industrial fossil fuels), and oceanic fluxes, as well as meteorological driver data used as input to PCTM.

2.2.1   Terrestrial Fluxes

Terrestrial land surface fluxes are provided by SiB3 at an hourly time step and represent both CO_2 sources and sinks. In this experiment, initial conditions for soil moisture and temperature are specified using an 18-year global spinup of SiB3 (January 1, 1982 to December 31, 1999) driven by the National Center for Environmental Prediction Department of Energy reanalysis (NCEP2) 1° x 1° global dataset (Kanamitsu et al., 2002). NCEP2 is also used to drive SiB for the PCTM simulation period (discussed in Section 2.3).

Land Surface Parameters and NDVI

The soil map for SiB is provided by the International Geosphere-Biosphere Programme (IGBP) at a resolution of 10 km and then modified to correspond to SiB classes. The biome map is a satellite data product of the University of Maryland with a resolution of 1 km, converted to 1° by 1° resolution (see Figure 2.1). Biome types are also converted to SiB classes.

SiB combines information about NDVI, biome, and soil type to determine surface characteristics, which are used in CO_2 flux calculations.

2.2.2   Fossil Fuel Fluxes

Anthropogenic CO_2 emission (kg $C/m^2/s$) is based on calculations done by Andres et al. (1996) at 1° by 1° resolution for the entire globe using fossil fuel consumption, cement manufacture, and population density data from 1998 and represents a source from the land to the atmosphere. Anthropogenic CO_2 is emitted constantly in PCTM simulations
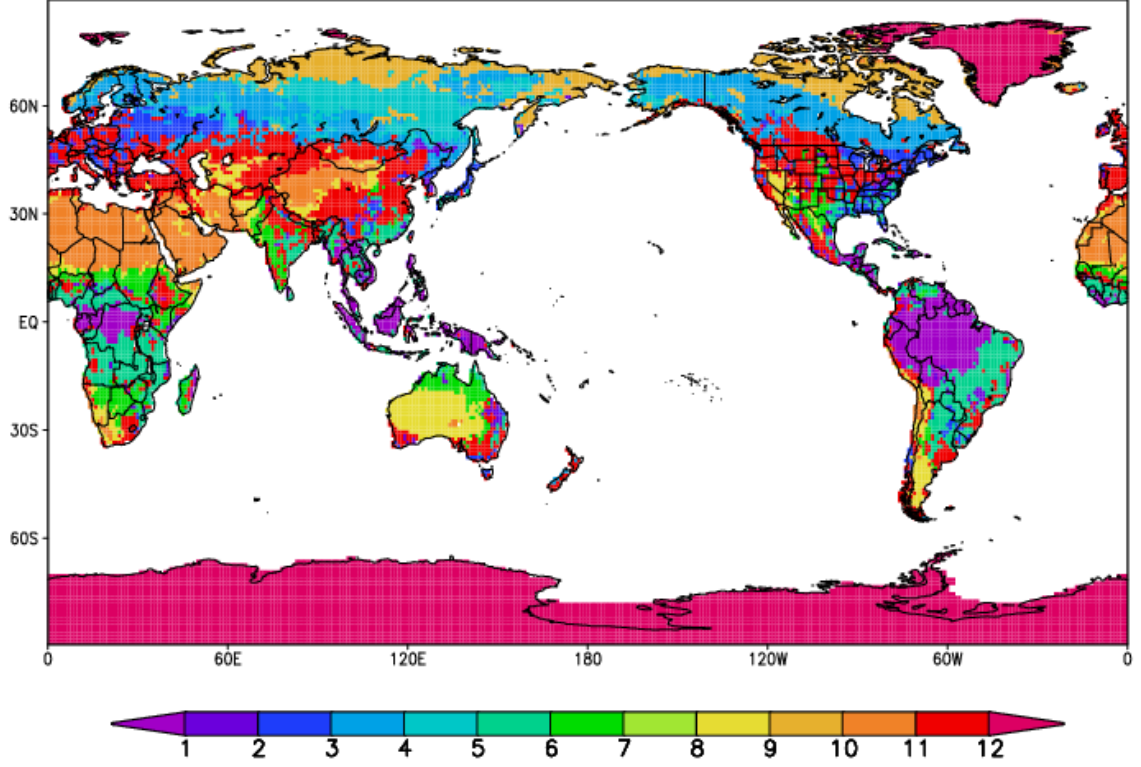
Figure 2.1: SiB Biome Map for GiMMSg NDVI. Vegetation Type by Number on Color Bar: 1) C3 Tall Broadleaf-Evergreen Trees, 2) C3 Tall Broadleaf-Deciduous Trees, 3) C3 Tall Broadleaf and Needleleaf Trees, 4) C3 Tall Needleleaf Trees, 5) C3 Tall Needleleaf-Deciduous Trees, 6) C4 Short Vegetation, Same as Types 6, 7, 8, 11 7) C4 Short Vegetation (Maize Optical Properties), 8) Same as 7, 9) Short Broadleaf Shrubs with Bare Soil, 10) C3 Short Ground Cover (Tundra), 11) C4 No Vegetation (Low Lat Desert), 12) Agriculture (Wheat) and C3 Grasslands, 13) Ice

at each grid point at each time step (7.5 minutes), where in reality emission strength is diurnally, weekly, and seasonally variable (Gurney et al., 2005). Its influence in the CO_2 concentration fields in the experiment are expected to have a noticeable impact, especially during the winter when the atmosphere is stable and biospheric flux is limited (Worthy et al., 1998). This is investigated in Chapter 4.

2.2.3   Oceanic Fluxes

Based on about 940,000 measurements of surface-water pCO_2, Takahashi et al. (2002) calculated monthly and annual mean net sea-air CO_2 flux with spatial resolution of 4° by 5°

for reference year 1995. This calculation assumes the magnitude of the flux is a function of the air-sea pCO_2 difference and gas transfer velocity, which is parameterized as a function of 10 m climatological wind speed. Atmospheric pCO_2 is computed as a function of zonal mean CO_2, water vapor pressure, surface water temperature and salinity. This study uses monthly mean fluxes and a regridded version of the original dataset into 1° by 1°. These fluxes represent sources and sinks from the ocean depending on geographic location and time of year (Takahashi et al., 2002). Fluxes at major lakes that are resolved in this experiment are set to zero.

2.2.4   GEOS4-DAS

This study uses analyzed meteorological fields from NASA's GEOS4-DAS. Kawa et al. 2004, Douglass et al. 2003, and Bloom et al., 2005, discuss this data in detail. To summarize their discussion, GEOS4-DAS is based on a FVGCM and the physical space statistical scheme (Kawa et al., 2004). Observations used in the finite volume data assimilation system (FVDAS) include both meteorological products and satellite data. FVGCM is based on the Lin-Rood dynamical core (Lin and Rood, 1996) Physical parameterizations are determined using the National Center for Atmospheric Research Community Climate Model, Version 3 (CCM3) package (Kiehl et al., 1998), which include deep convection (Zhang and McFarlane, 1995), shallow convection (Hack, 1994), and PBL turbulence (Holtslag and Boville, 1993). Transport fields used by PCTM include horizontal winds, which are used for advective processes, and cloud mass fluxes and turbulence, which are used for vertical diffusive processes. These are available at 1.25° by 1° (longitude by latitude) with 55 hybrid vertical levels up to 1mb.

2.3   Methods

The experiment was run from 2000-2004 at 1.25° by 1° with 25 of the 55 available hybrid vertical levels from the surface up to 1mb with a time step of 7.5 minutes. Surface

flux input follows guidelines from the Transcom continuous data experiment (Law et al., 2005). The first three years of simulation (2000-02) are used to spin up the atmosphere from constant background conditions using 2002 hourly SiB fluxes (as well as ocean and fossil fuel fluxes). 2003-04 hourly SiB fluxes are used for the analysis portion of the simulation, which occurs from 2003-04. Surface flux maps are regridded to the experiment grid using the conservative remapping scheme of the SCRIP software package (Jones, 1999). CO_2, which is given as a mole fraction in units of parts per million (ppm), is treated as a passive tracer such that no chemical reactions occur and the CO_2 field does not affect weather. SiB, fossil fuel, and ocean tracers are run separately in the experiment. The total CO_2 distribution is the sum of tracers. Background CO_2 is arbitrary and set to zero.

In order to perform a model-observation analysis of synoptic variations associated with cold fronts we needed some general way to define frontal zones in which these signals occur. This study focuses on surface-based cold fronts in part because their surface signatures tend to be more sharply defined than other surface fronts, making them easier to identify and study (Schultz, 2005). We characterize surface fronts according to the Clarke and Renard (1965) definition, who define a front as "the warm-air boundary of a synoptic-scale baroclinic zone of distinct thermal gradient... Further, the frontal-zone boundaries are considered as quasi first-order thermal and moisture discontinuities." Clarke and Renard also define a frontal locator function that this study adapts to identify the time of cold front passage at the grid cell containing an observation site. Temporal gradients of temperature and water vapor are used together with wind shifts and pressure minima to locate the warm-air boundary. Since gaps are often present in the observed meteorology, we use GEOS4 reanalysis to identify fronts. In Chapter 3 we show that GEOS4 meteorology is consistent with that observed during frontal events.

A preliminary comparison of observed and modeled atmospheric CO_2 made it very clear that PCTM was not correctly capturing the amplitude of diurnal variability. In particular, nocturnal buildup was consistently too weak at all sites, especially during summer

and at higher latitudes, yet daytime drawdown appeared correct. We noticed that this was most likely a result of the low temporal resolution of subgrid scale vertical diffusion (1 value every 6 hours) in the reanalysis files. Turbulent diffusion (i.e., vertical mixing by turbulence) serves an important role in PCTM in mixing terrestrial fluxes from the surface throughout the PBL, where lower values cause weaker mixing and therefore higher CO_2 near the surface in the presence of respiration. In the summer at higher latitudes where nights are short, insufficient temporal coverage of vertical diffusion led to a misrepresentation of nightime mixing just after sunset with daytime values of diffusivity and therefore weak nocturnal buildup. To rectify this we added a weight to vertical diffusivity proportional to the cosine of solar zenith angle such that only nighttime values are used for mixing from sunset to sunrise. The result improved nocturnal buildup but was still not enough to capture its amplitude as seen in the observations (see Figure 2.2). The diurnal cycle, however, is not the focus of this study.

2.4   Study Sites

Several well calibrated continuous CO_2 continental sites have recently been established in NA in an effort to gain a better understanding of the terrestrial biosphere and interactions with the atmosphere. This study utilizes data from eight stations from 2003-04, including three tall towers (see Figure 2.3), for analysis and model evaluation. Meteorological and CO_2 flux measurements were recorded at several of the sites; these are used to evaluate GEOS4 reanalysis and SiB fluxes. Table 2.1 has information about some of the site specifications.

The Meteorological Service of Canada (MSC) manages Fraserdale and Prince Albert (see FRS and SOBS in Figure 2.2, respectively). Continuous measurements at Fraserdale, located in Kapuskasing, Ontario, started in June 1989 by the Canadian Greenhouse Gases Measurement Laboratory (GGML). Fraserdale is described in detail in Higuchi et al., 2003; briefly, it located in north central Ontario and is strongly influenced by the eastern boreal
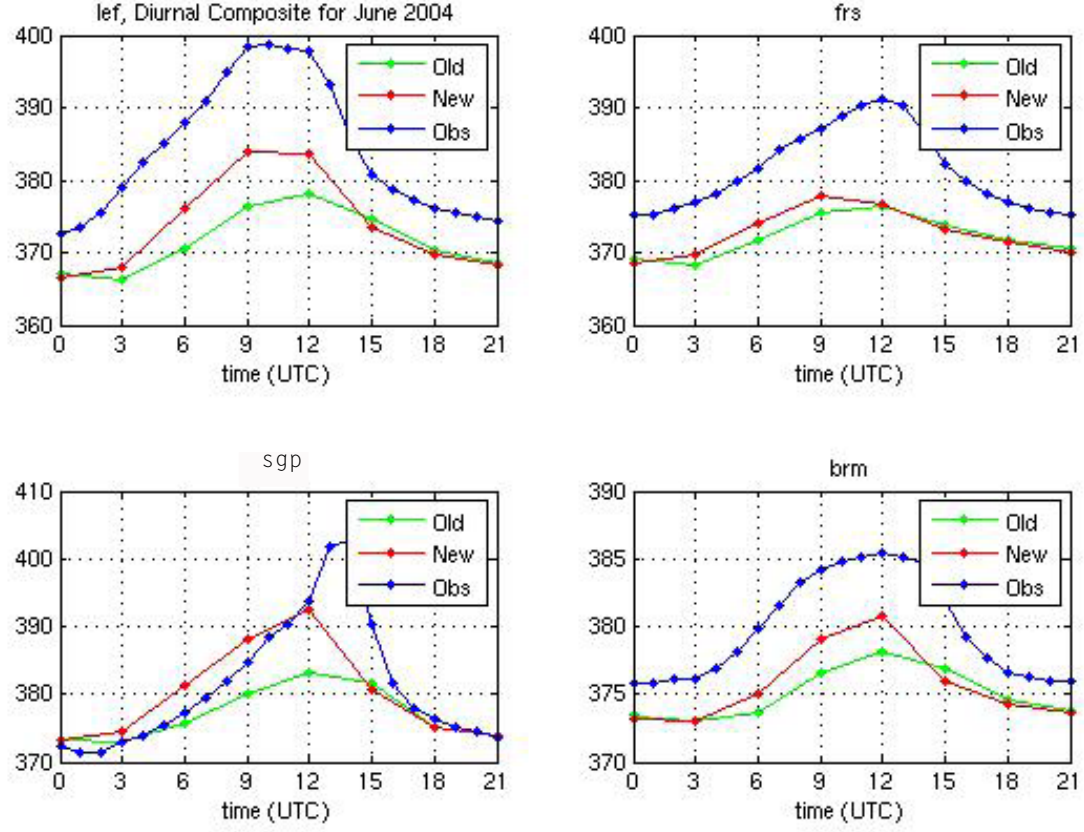
Figure 2.2: Observed and simulated diurnal CO_2 composites. Blue lines are observed, green lines are simulated without the solar zenith angle weight added to vertical diffusivity, and red are simulations with the weight. Each composite is the average of all diurnal cycles in June 2004 at the grid cell containing the observations.

forest and northern wetland regions around Hudsons Bay. Several air masses influence the site depending on the location of the Arctic front; these include maritime tropical, Arctic, and modified Pacific air masses. Anthropogenic influence is dominated by cities farther south during sustained southerly winds.

Continuous CO_2 measurements began at the eddy covariance tower at the Boreal Ecosystem Research and Monitoring Sites (BERMs) southern old black spruce (SOBS) location in Prince Albert, Saskatchewan, Canada in 2002 (Chan et al., 2004). This station is influenced predominately by the western boreal forest. Anthropogenic influence is limited.

We have also acquired continuous CO_2 measurements from Western Peatland (WPL),
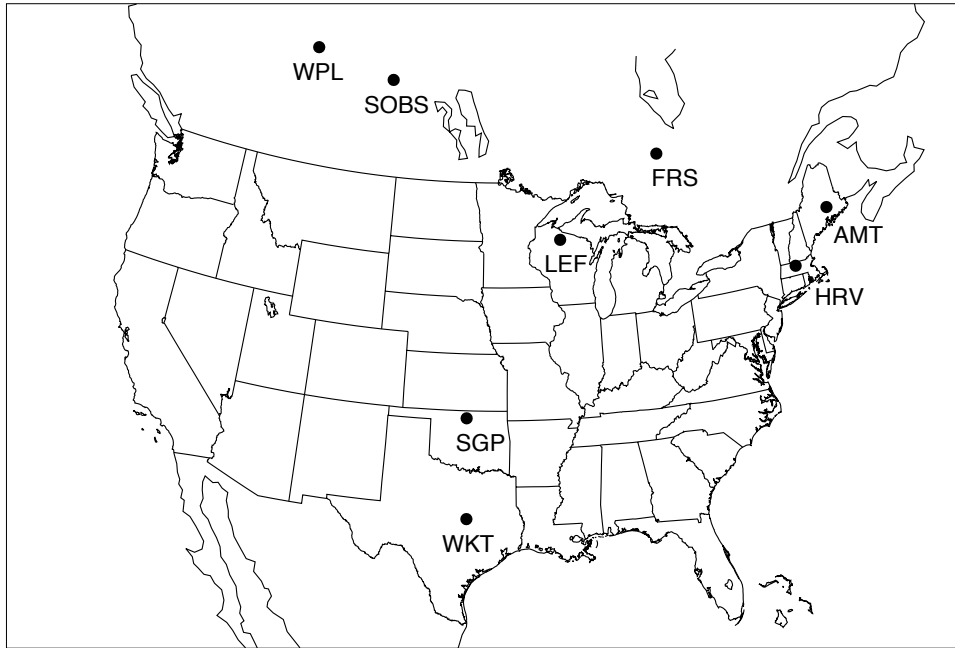
Figure 2.3: Locations of well calibrated CO_2 measurement stations in North America that report at least semi-continuously from 2003-04.

a Fluxnet-Canada Research Network (FCRN) eddy covariance site near Fort McMurray, Alberta. See Syed et al., 2004 for site details.

In the United States, the National Oceanic and Atmospheric Administration Global Monitoring Division (NOAA GMD) has established a network of tall towers in the continental United States intended to extend the long-term trace gas monitoring program to continental areas as part of the Carbon Cycle Greenhouse Gases (CCGG) cooperative air sampling network (Bakwin et al., 1998). Several other smaller towers across the United States have also joined the network. The tall towers, including WLEF (LEF), KWKT (WKT), and AMT record CO_2 measurements every hour at several levels from the surface to the top of the tower. The smaller towers include Southern Great Plains (SGP) and Harvard Forest (HRV).

The tall tower sites managed by NOAA GMD undergo a robust calibration process. The Infra-Red Gas Analyzer (IRGA) LiCor instruments are calibrated for short-term drifts

STATION	LAT (°N)	LON (°W)	HGT (M)	MET	NEE
LEF	45.95	90.27	30	Y	Y
SGP	36.61	97.49	60	Y	Y
FRS	49.88	81.57	40	N	N
WPL	54.95	112.47	9	Y	Y
AMT	45.03	68.68	107	N	N
HRV	42.54	72.17	30	Y	Y
WKT	31.6	97.22	61	N	N
SOBS	53.98	105.12	25	Y	Y

Table 2.1: Information about study sites. Latitude (LAT) and longitude (LON) are given in degrees. Instrument height (HGT) refers to the measurement height (in meters above ground level) of CO_2, MET, and NEE observations used in this study. Columns of meteorology (MET) and NEE indicate whether the site reports those measurements (Y) or not (N).

with a calibration gas every 36 minutes and with a sequence of four certified standards of NOAA GMD every three hours. Measurements are taken at multiple levels with calibration uncertainty of 0.07 ppm, analyzer drift uncertainty of 0.1 ppm, and analytical uncertainty of 0.2 ppm at LEF, 0.3 ppm at AMT, and 0.6 ppm at WKT (Andrews et al., 2007; Bakwin et al., 1998).

The LEF tower near Park Falls in northern Wisconsin is described in Bakwin et al. (1998). LEF has continuous measurements at six levels from 11 m up to 396 m above the ground. The region surrounding the tower is characterized by mixed forest, wetlands and some agriculture with heavy population to the SE and agriculture to the SW. The second tall tower used is WKT in Moody, Texas, which makes measurements at six levels from 9 m to 457 m. The region is within a strong east-west moisture gradient, and local land use is dominated by cattle grazing. Data from WKT is hourly averaged and assumed valid at

30 minutes past the hour.

The AMT tower near Argyle, Maine makes continuous measurements at 11 m and 107m. The site is characterized by coniferous and deciduous forest with ocean to the east and heavy population to the SW. Data from AMT is hourly averaged and assumed valid at 30 minutes past the hour. The SGP tower, in north central Oklahoma, is managed by the Lawrence Berkeley National Laboratory and makes measurements at 2, 4, 25, and 60m. It is located within the Atmospheric Radiation Measurement Cloud and Radiation Testbed (ARM-CART) region, where local topography is flat, land use is mostly agriculture, and land cover is winter wheat, summer crops, and some pasture (Ameriflux). The Harvard Forest site in Massachusetts is surrounded by hilly terrain and a regrowing temperate deciduous forest which accumulated 2.0 ± 0.4 tC/ha/yr during 1993-2000 (Barford et al., 2001).

In addition to CO_2 measurements, several of the stations use the eddy covariance technique (Baldocchi et al., 2003) to measure net exchange of CO_2 between the landscape and the atmosphere (see Table 2.1), which are used for evaluating the response of SiB fluxes to synoptic and seasonal weather. The same five sites also make continuous meteorological measurements. These are useful diagnostics for trying to explain changes in CO_2 mixing ratio and NEE due to short term and long term changes in weather. These data will be important for evaluating synoptic variations in GEOS4 reanalysis.

Fossil fuel fluxes also contribute significantly to synoptic variations in some areas, so it is important to consider potential anthropogenic influences. There are several major population centers in the fossil fuel map used in this study. Table 2.2 lists some of the more potentially important cities in terms of approximate model distances to towers (based on grid cell centers) and annual fossil fuel emission estimates. Cities with relatively minor emissions according to the fossil fuel map are not included in the table.

Comparisons to model results are made as closely to lowest model level ($\sim$ 50m) as possible, with observations ranging from 9m to 107m. In most cases the observations are

	City / Annual Emission (kg C/m2/yr) / Distance (km) / Direction From Site
LEF	Chicago(Milwaukee)/2.4/550/SE, Minneapolis/.68/250/SW
SGP	Houston(Austin)/.70/750/S, Dallas/.56/400/S, Kansas City/.48/400/E
SOBS	Edmonton/.25/700/W
FRS	Chicago(Milwaukee)/2.4/900/SW, Detroit(Cleveland)/1.65/850/S
AMT	New York/4.43/650/SW
HRV	New York/4.43/200/SW
WPL	Edmonton/.25/125/E
WKT	Houston(Austin)/.70/350/SE, Dallas/.56/275/NE

Table 2.2: Annual emission estimates of closest major cities to observation sites used in this study.

recorded below the lowest model level such that the simulated diurnal cycle is expected to be weaker than observed. This is especially true for WPL, where measurements are made at 9m. In an effort to avoid extensive local influence in both model and observations, analysis is performed using mid-day CO_2 where possible, chosen such that turbulent mixing in the PBL is near its maximum and vertical tracer gradients in the PBL, including CO_2, are minimized.

2.5   Additional Data

NOAA GMD monthly mean flask observations from the Carbon Cycle and Greenhouse Gases (CCGG) Cooperative Air Sampling Network are used in Chapter 3 for analysis of background seasonal cycles, atmospheric growth rates, North-South CO_2 gradients, and model transport evaluation (see Figure 2.4). They are used again in Chapter 4 to study large scale latitude gradients surrounding NA. GLOBALVIEW aircraft data is used in Chapter 3 to evaluate vertical gradients in PCTM. Aircraft data from the CO_2 Budget and Regional Airborne Study-North America 2003 (COBRA-NA 2003) measurement program are used in Chapter 3 to evaluate vertical mixing in the summer in NA.
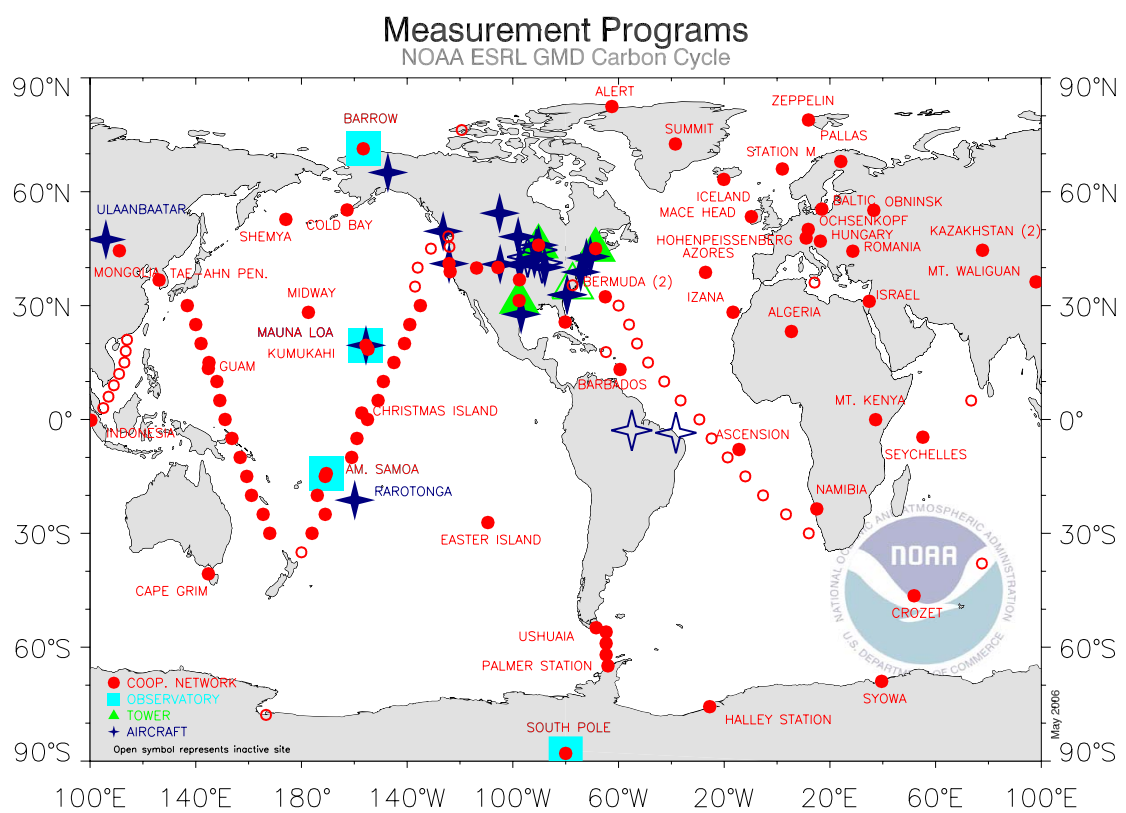
Figure 2.4: Locations of NOAA ESRL GMD Carbon Cycle flask stations. Courtesy NOAA GMD.

Chapter 3

MODEL EVALUATION

3.1   Synoptic Meteorology

Use of GEOS4 to drive transport is evaluated by: 1) comparison of PCTM to weekly CO_2 flask measurements and 2) comparison of GEOS4 to meteorology measurements recorded at LEF, SGP, and WPL. The first comparison tests the ability of GEOS4 to advect CO_2 gradients around. This is an important first step test to conduct before making comparisons to continuous measurements to ensure realistic large scale transport exists in the experiment. The goal of the second comparison is to make sure shape, timing, and magnitude of GEOS4 synoptic meteorology, including density gradients between air masses and wind shifts, is similar to that observed at several NA locations. Since cold fronts typically have a common set of characteristics not unique to location, and the goal of this research is to perform a systematic analysis of representative synoptic patterns across a broad range of sites, here we try to stress the ability of GEOS4 to capture representative synoptic meteorological patterns during cold front passage.

3.1.1   Flask Comparison

To test whether weekly model variations are realistic we regress flask observations onto model output at four Northern Hemisphere locations, three of which are remote (MLO, BMW, and MHD). A scatterplot of deseasonalized and detrended values, along with regression and correlation values, are shown in Figure 3.1. These sites have reasonable goodness of fit and correlations, with regressions between 0.510 and 0.759 and correlations between

0.486 and 0.597 (32.9% variance explained by the model on average). The statistics are
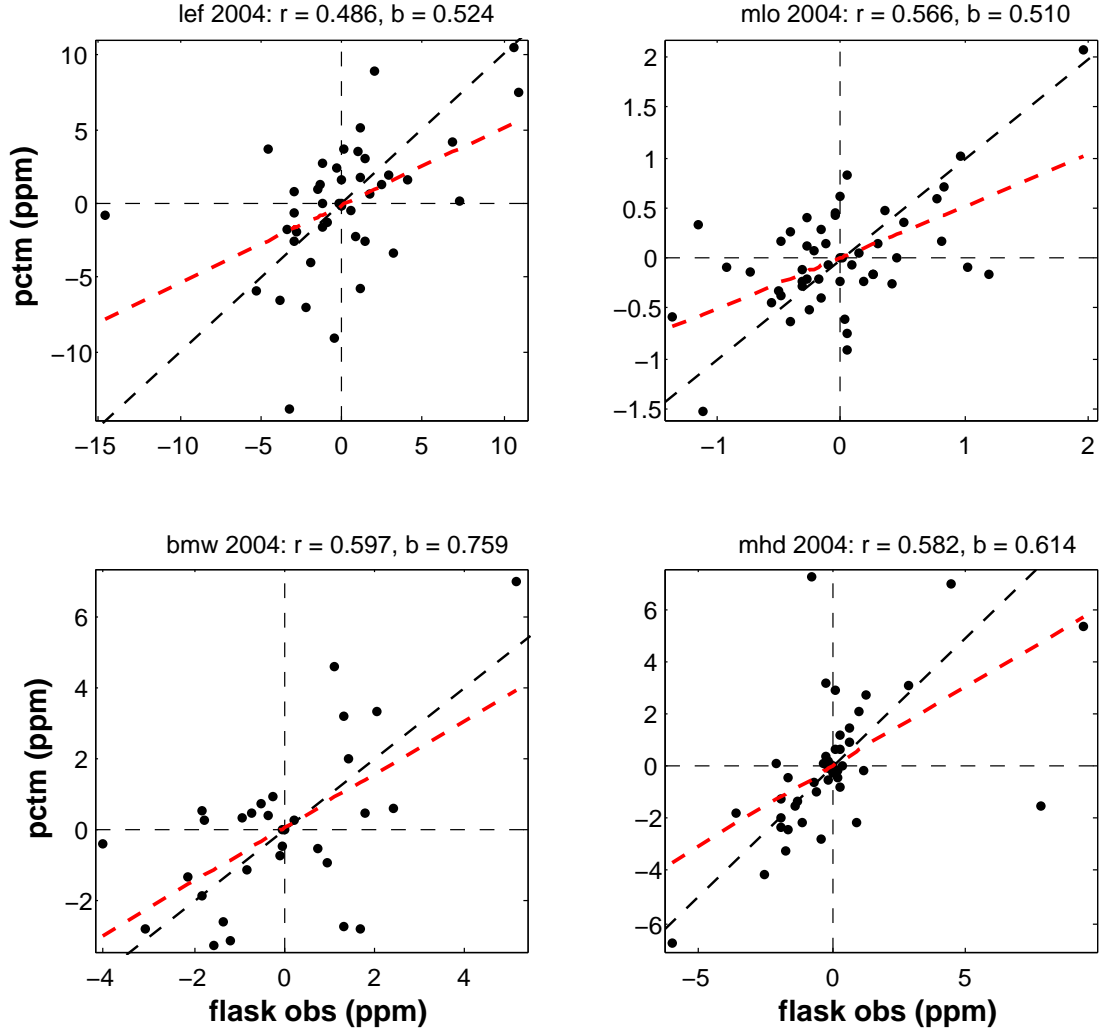
Figure 3.1: Scatterplots of 2004 NOAA GMD weekly flask data onto PCTM output (in ppm) sampled at the time of and approximate location of the flask data. Flask locations include Park Falls, Wisconsin, USA (LEF, 45.93N, 90.7W, 396masl), Mauna Loa, Hawaii (MLO, 19.54N, 155.58W, 3397masl), Tudor Hill, Bermuda (BMW, 32.27N, 64.88W), and Mace Head, Ireland (MHD, 53.33N, 9.9W). The correlation value (r) and regression coefficient (b) are shown above each plot, with the one-to-one line (black dashed) and regression line (red dashed) plotted for convenience.

broken down by year and season in Table 3.1. These values suggest that correlations and regressions are much stronger in the winter (52.8% of variance explained) than in the summer (18.6% variance explained) at these sites.

	Year			Winter			Summer		
Station	r	R^2	b	r	R^2	b	r	R^2	b
LEF	0.486	0.237	0.524	0.421	0.178	1.031	0.539	0.291	0.537
MLO	0.566	0.321	0.510	0.890	0.793	0.903	0.152	0.023	0.086
BMW	0.597	0.357	0.759	0.584	0.342	0.786	0.438	0.192	0.292
MHD	0.582	0.400	0.614	0.894	0.800	1.321	0.486	0.237	0.409

Table 3.1: Statistics comparing weekly flask observations to PCTM during 2004. r represents the correlation value, R^2 the amount of observed variance explained by PCTM, and b the regression.

These correlations indicate that PCTM simulates 23-40% of the variations correctly at weekly scales for the entire year and gets a large part of the magnitude of the variations correct. This is good but not great, and indicates problems with either SiB, GEOS4, or both. To delve into these problems further is beyond the scope of this research.

3.1.2   GEOS4 Comparison

Implicit in this section is assessment of the 'frontal locator' function. The goal of the technique is to identify the timing of frontal passage within a grid cell based on wind shift and density gradients. The locator function is applied to GEOS4 to identify timing. Assessment of the function is carried out by: 1) testing whether the appropriate density gradients exist surrounding frontal passage and 2) comparing the phase of several observed and analyzed meteorological variables.

Figure 3.2 shows winter composites of several meteorological variables used in this study for identifying cold fronts using the frontal locator function: temperature (t_a) and water vapor mixing ratio (q) are used to represent density gradients, both of which are strongest at the time of frontal passage as warm moist air masses are replaced by drier, colder ones; barometric surface pressure (p_s) is used to diagnose alternating ridge and trough movement; wind direction ($wdir$) helps to identify clockwise wind shifts characteristic of surface cyclones; and finally wind speed ($wspd$) is used to diagnose whether enhanced winds occur along the front. The composites are created by averaging at least five winter synoptic
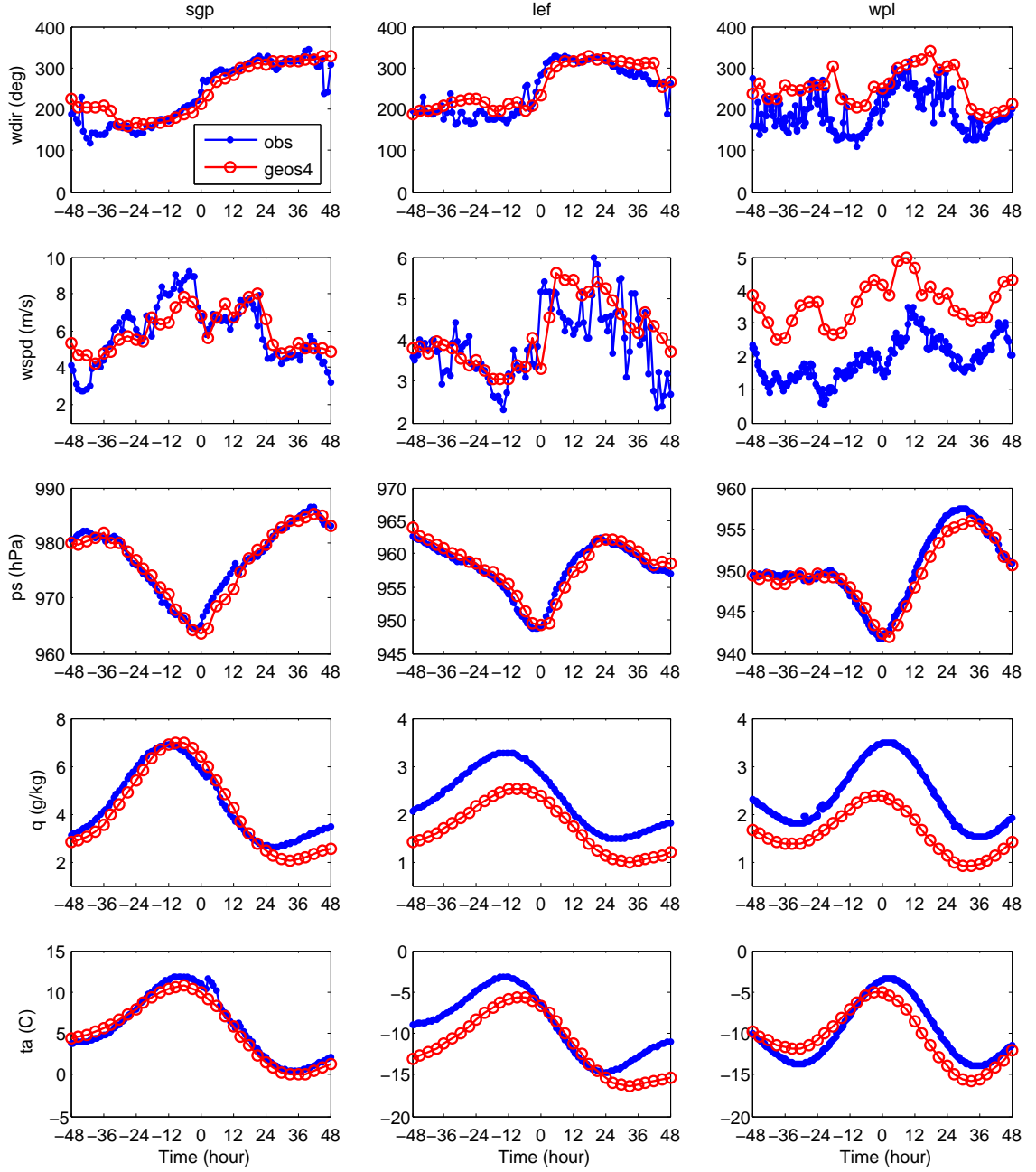
Figure 3.2: Composites of observed and GEOS4 meteorology fields during synoptic events at SGP (left column), LEF (middle column), and WPL (right column). The met fields from top to bottom are as follows: wind direction (degrees), wind speed (m/s), surface pressure (hPa), water vapor mixing ratio (g/kg), and air temperature (C). Blue lines are composites of hourly observations; red lines with open circles are composites of 3-hourly GEOS4 reanalysis for the grid cell containing the station. All GEOS4 fields are interpolated to 10 m from the lowest model level. Observations are taken at 10m. The diurnal cycle has been removed from air temperature and water vapor.

events (identified as described in section 2.1) together for 48 hours before and after the surface front passes through the grid cell. Diurnal and seasonal cycles are removed from q and t_a using a recursive filter so that only synoptic variability is conveyed. Only composites at LEF, SGP, and WPL are shown. The patterns seen in GEOS4 suggest that the frontal locator algorithm finds the appropriate cold front wind shifts, pressure minima, and density gradients. Observed and analyzed fields are generally in good agreement, both in shape and phase.

GEOS4 does not match observations perfectly. One disturbing mismatch is the average wind direction before and after frontal passage at WPL. The observations show southerly winds while the reanalysis is more westerly or southwesterly. This could have implications on air mass source regions identified by GEOS4 at WPL. Also, summer composites show similar but weaker synoptic patterns compared to winter because of reduced baroclinicity in the NH summer (see Figure 3.3). The weaker signals make timing of frontal passage more difficult to determine.

Figure 3.2 also shows that, even though the frontal gradient in q matches observations, its magnitude is underestimated at the northern stations in the winter, and even more so in the summer (not shown). The same comparison of frontal composites, this time using NCEP2 (which, as mentioned in Section 2.2.1, is used in this study to drive SiB), shows that q matches observations more closely (also not shown), instilling confidence that meteorology driving SiB is more realistic and less likely to stress plants. Furthermore, NCEP2 composites, like GEOS4, have the same synoptic patterns as observed, indicating that transport during frontal passage events in NCEP2, GEOS4, and observations are approximately synchronized.

3.2   Seasonal CO$_2$ Flux

This section aims to interpret modeled seasonal variations in NEE. It is difficult to reach conclusions regarding modeled NEE compared to eddy covariance based turbulent flux
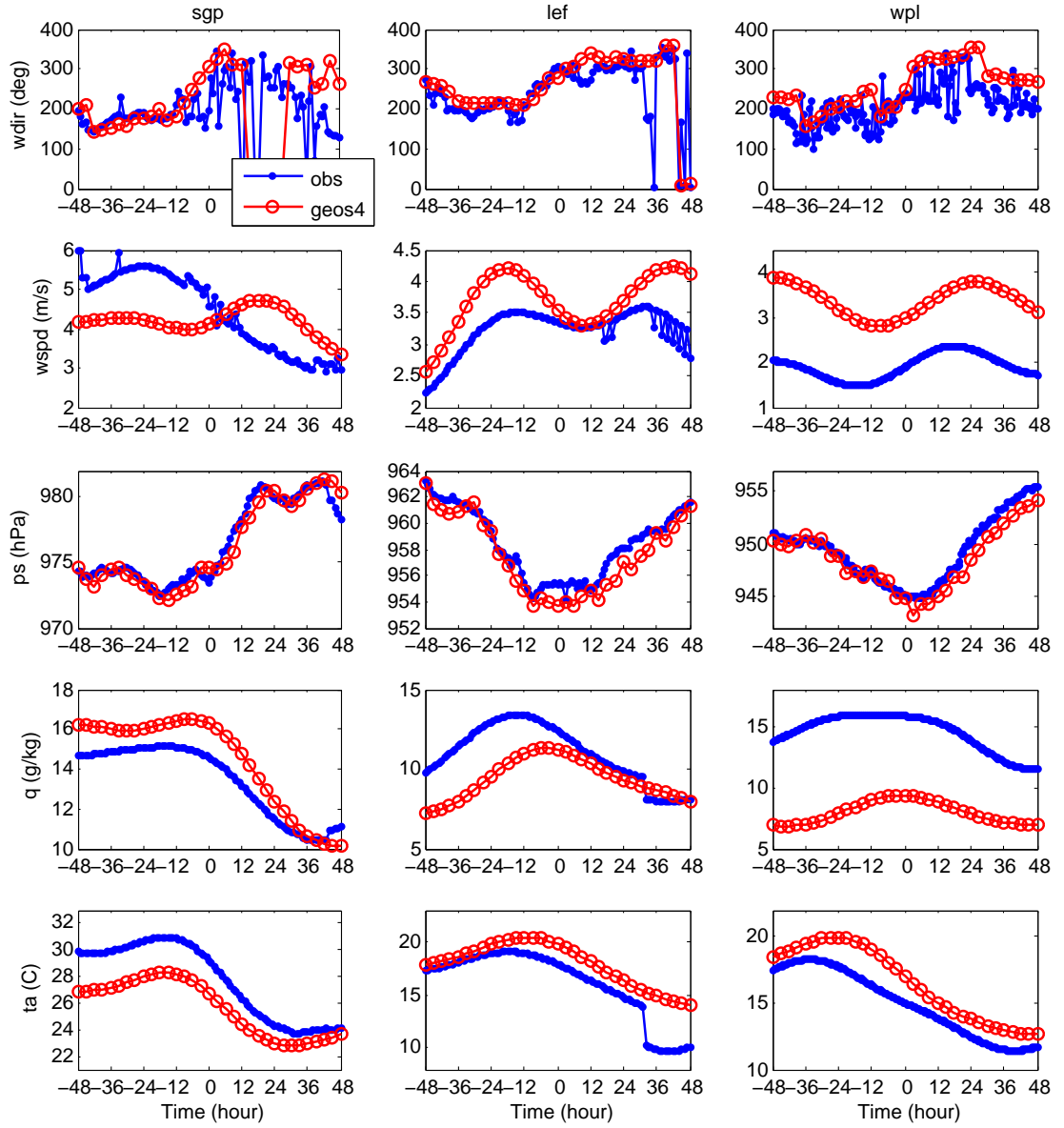
Figure 3.3: Same as Figure 3.2 except for summer cold fronts.

observations because of the uncertainties inherent in both. The goal here is to understand the limitations of both and then interpret the model with these uncertainties in mind.

Observations, for example, face the energy balance closure issue. Many FLUXNET sites, which have a wide range of vegetation type and stand age, have been shown to have a general lack of energy closure, where surface energy fluxes tend to be underestimated on average between 10 and 30%. Evidence suggests a link between the energy imbalance and CO_2 fluxes, with trends indicating that the magnitude of observed CO_2 uptake and respiration decreases as the energy imbalance increases (Wilson et al., 2002). We also need to be aware of what is known in the literature about the kinds of attributes that tend to make forests net annual sources or sinks. Regrowing forests, for example, tend to be stronger net sinks, while mature forests tend to me more neutral. This type of information will help in our interpretation of NEE.

SiB3, on the other hand, has the option to balance NEE annually at each grid point by scaling annual respiration (R_g) to equal annual photosynthetic uptake (or Gross Primary Production (GPP)), as described in Denning et al., 1996a. This parameterization allows for realistic seasonal, synoptic, and diurnal variations. The magnitude of seasonal variations depends on the amount of GPP in the summer (and winter depending on location) and the way SiB scales respiration throughout the year to balance uptake, which depends on soil moisture and temperature.

Figure 3.4 shows monthly averaged NEE at 19 sites in NA. For this experiment, which is designed so that NEE is in steady state such that GPP is balanced by R_g over one year (Jan 1 - Dec 31), we find three main patterns in SiB relative to observations: 1) summer NEE is too weak, 2) seasonal amplitude is too large, and/or 3) winter NEE is too large.

With regard to weak model summer uptake at many of these sites, including ARM, Bondville, Harvard, Howland, MMSF, Vaira, and Willow Creek, it is likely that these sites are actually strong summer sinks, which we do not allow SiB to deal with for this experiment since long-term sink/source strength is difficult to simulate because of many
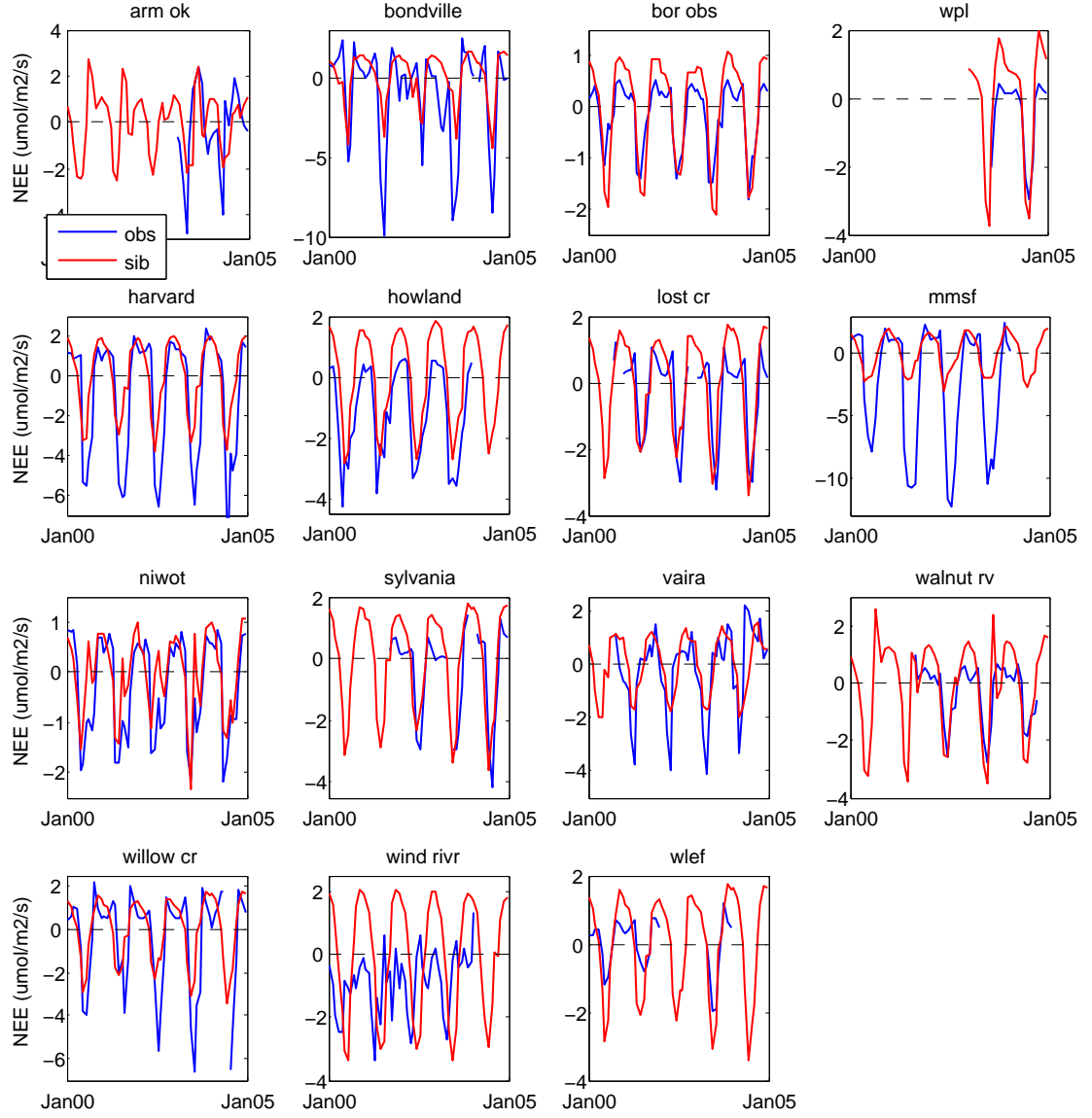
Figure 3.4: Monthly mean NEE from 2000-04. Blue is observed and red is from SiB3. All observations, except WPL, are taken from Ameriflux. Sites include (left to right, top to bottom): 1) ARM SGP, Lamont, OK, 2) Bondville, Il, 3) BOREAS Northern Old Black Spruce, Saskatchewan, Canada, 4) Western Peatland, Alberta, Canada, 5) Harvard Forest EMS Tower, MA, 6) Howland Forest, ME, 7) Lost Creek, WI, 8) Morgan Monroe State Forest, IN, 9) Niwot Ridge Forest, CO, 10) Sylvania, WI, 11) Vaira Ranch, CA, 12) Walnut River Watershed, KS, 13) Willow Creek, WI, 14) Wind River Crane Site, CA, and 15) WLEF, WI.

scientific unknowns or uncertainties. Although eddy covariance methods should not be

used to deduce long term sources and sinks because of all the inherent uncertainties in the

technique, the sites listed above are in areas prone to strong summer uptake. Harvard, for example, located in a regrowing forest in the Northeast, is one known sink (Barford et al., 2001) where net uptake is not simulated well in the summer. Other examples include agricultural sites like Vaira and Bondville, which are also much more productive in the summer than SiB. A comparison of model and observations at agricultural sites during a typical week in the summer shows observed net uptake as large as 30 μmol/m^2/s (not shown).

SiB can be treated as a sink if the strength of the sink is known. A simple test suggests that, if R_g in SiB is scaled so that it does not balance GPP over one year such that an annual sink is allowed and steady state is violated, part of the summer deficit at several sink sites can be compensated for. If, for example, a 1 μmol/m^2/s (378 g/m^2/yr) sink is imposed in the model at HRV (which is the average observed value at HRV from 2000-04), NEE becomes more negative in the summer and less positive in the winter (see Figure 3.5). The scaling of R_g does not affect GPP; instead, changes in NEE result from decreases in the amount of R_g allowed over one year, which essentially causes the NEE curve to shift down (the amount of shift for any given month or site depends on GPP, soil temperature, moisture, and other factors). The result approaches the observations but does not make up the entire deficit. The shift in the NEE curve appears to be independent of the driver data (although the magnitude of the shift varies).

A portion of the discrepancy in summer uptake at these sink sites may also be related to plant stress. Diurnal NEE composites of the global run sampled at HRV compared to observations at HRV show slight mid-afternoon stress in the model not present in the observations (see Figure 3.6). Point runs at HRV also show mid- afternoon stress, regardless of whether driven by observed meteorology or NCEP meteorology. Furthermore, global runs sampled at other sites experience similar stress, especially at SGP and HRV, although daytime minima is in better agreement with observations (see Figure 3.7).

It is clear that winter R_g is overestimated at most of these sites, but the magnitude of
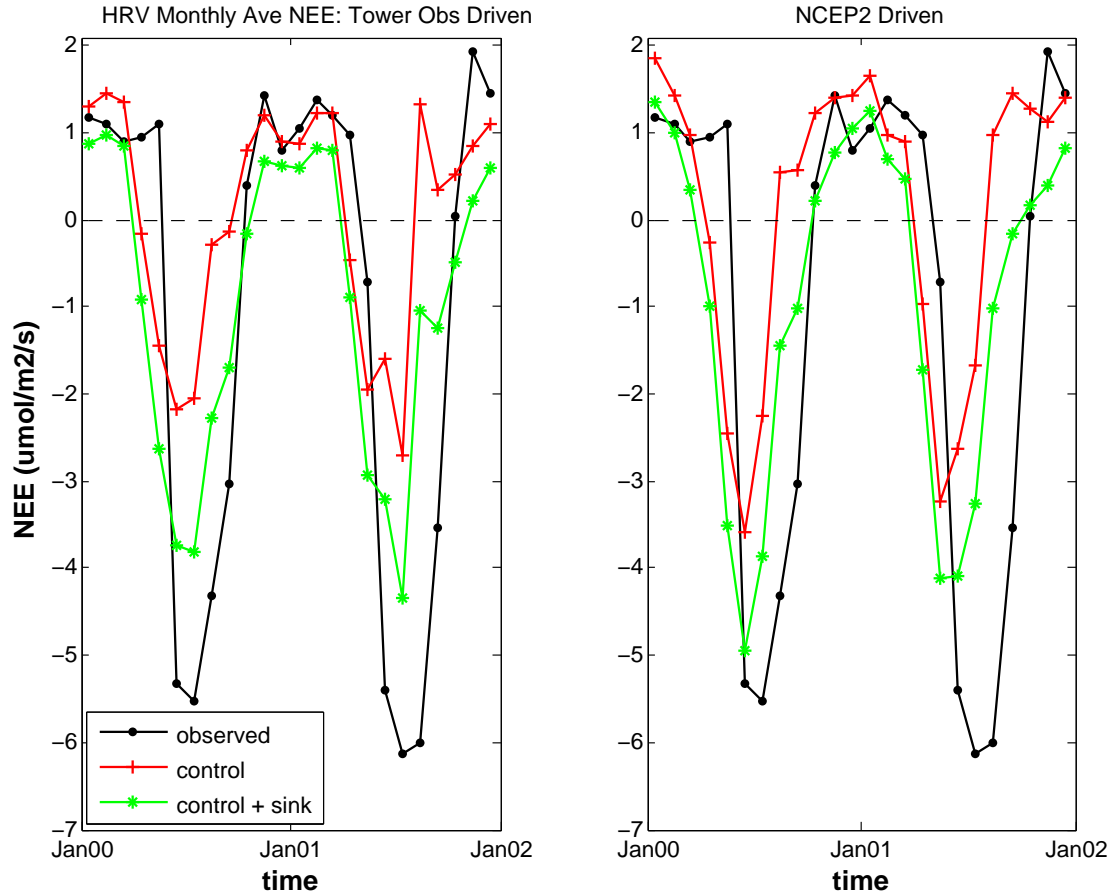
Figure 3.5: Monthly average observed and model NEE from 2000-01 at HRV. Model results are from point runs. SiB results on the left are driven by observed meteorology, on the right by NCEP2 meteorology. The black curve is observed, red is the control simulation, and green is the control plus a model sink.

the model/observed discrepancy is not clear because of potential errors in the observations. For example, it is possible that observed NEE was underestimated in some cases during stable atmospheric boundary layers (night, winter) due to advective carbon losses (Eugster and Siegrist, 2000), which might act to slightly decrease observed NEE in the winter but increase NEE in the summer. The energy closure issue may help to explain another portion of the difference.

There are several promising results in the simulations. One is the correct timing of leaf greenup in the Spring and leaf senescence in the Fall at all sites in Figure 3.4. Another is the ability of the model to capture the basic seasonal structure at each site, in particular the
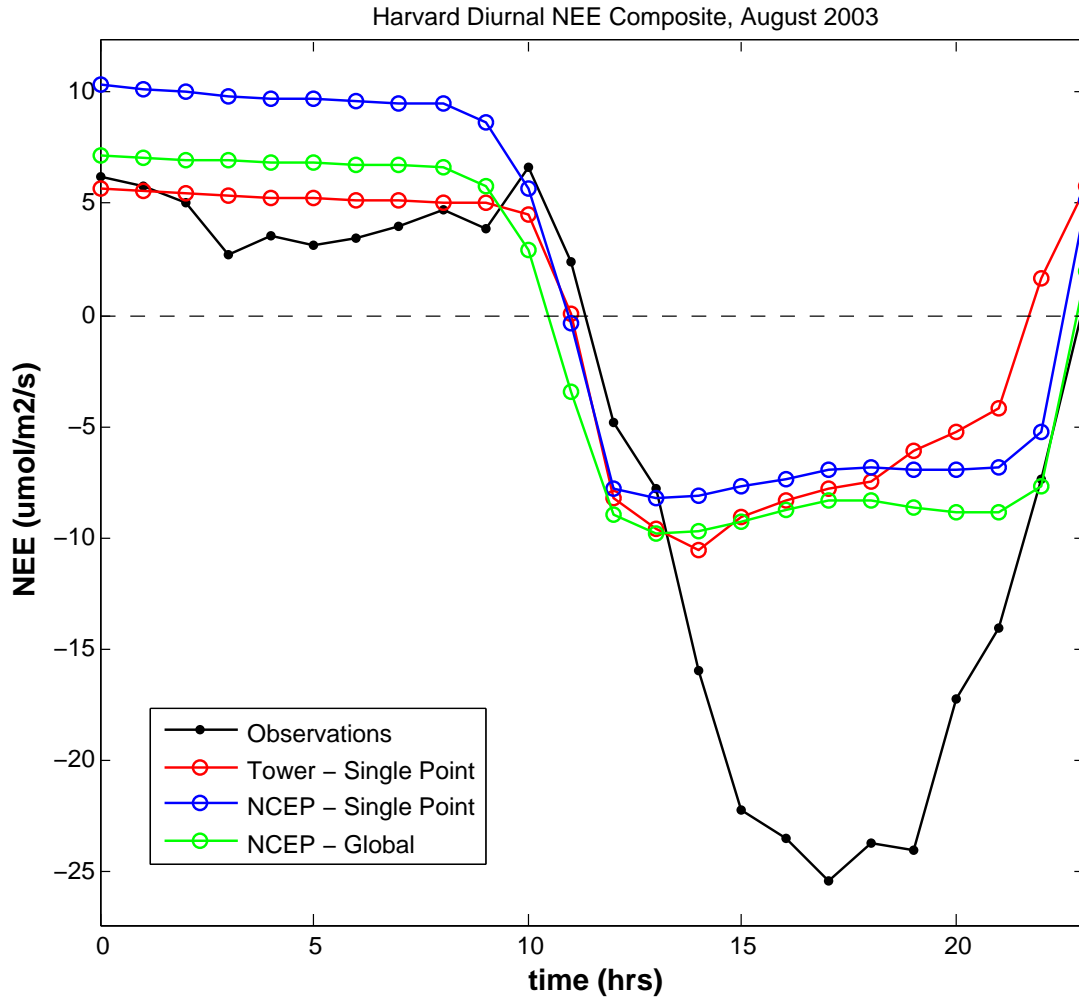
Figure 3.6: Diurnal NEE composite at HRV during August 2003, including observations (black dots), observed meteorology driven point run (red circles), NCEP2 driven point run (blue circles), and NCEP2 driven global run sampled at HRV (green circles).

complicated seasonal structure at SGP, where two annual minima exist in both the model and observations (more so in 2003) due to local agriculture. This surprising result also emphasizes the inherent value of NDVI in capturing seasonal changes in canopy phenology regardless of vegetation type. Another is the correctly simulated spike in respiration in the fall at several sites like WPL, Northern Old Black Spruce, and Walnut River, a tribute to the ability of SiB to represent decay of plant litter just prior to the onset of cold temperatures and snowfall.
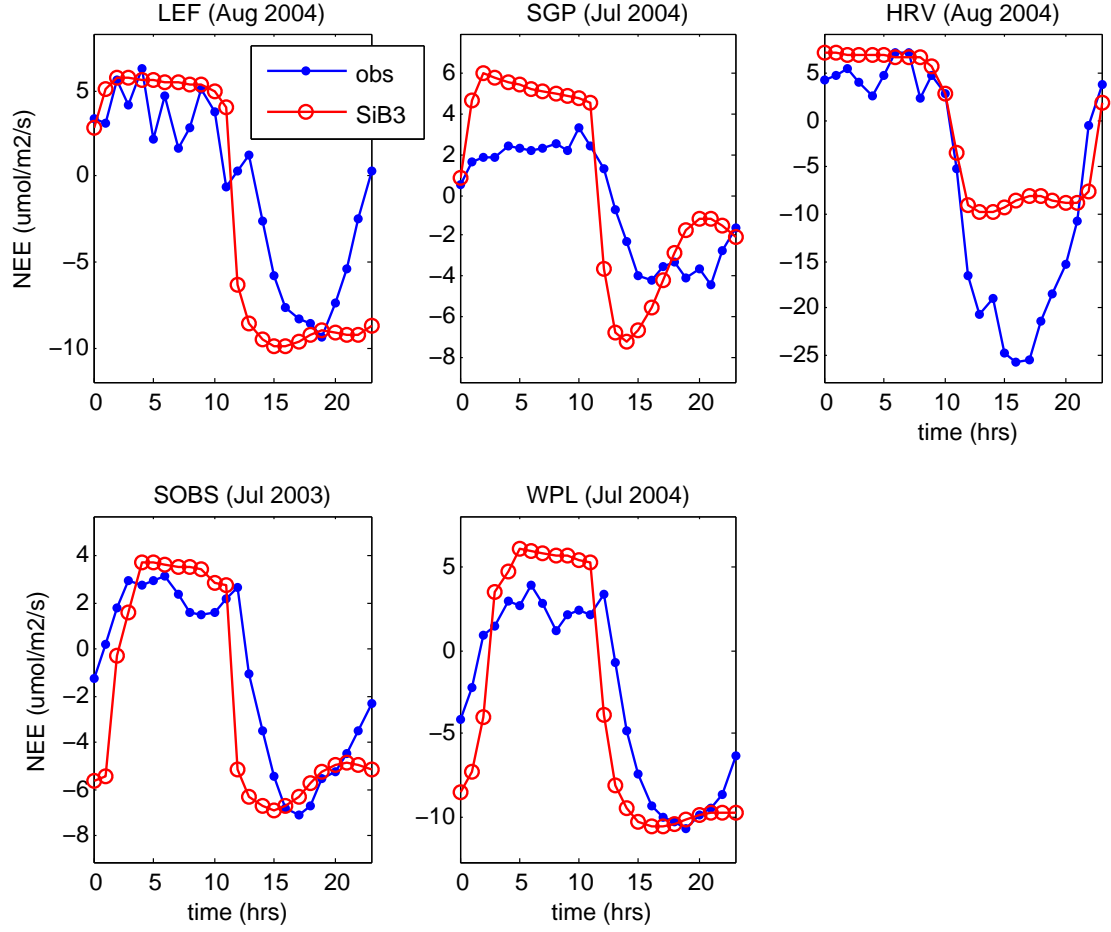
Figure 3.7: Diurnal NEE composites at various stations (station and month indicated above plot), including observations (blue dots) and NCEP2 driven global run sampled at station (red circles).

The most important conclusions to take from this section are that, regardless of whether errors in the observations exist or what the causes for overestimation of winter R_g are, SiB is probably overestimating NEE in the winter at most locations, even those that are in steady state in reality, and underestimating summer drawdown at sites that are net annual sinks because of the steady state assumption. This needs to be accounted for in our interpretation of seasonal and synoptic variations in atmospheric CO_2.

3.3   Atmospheric CO_2

One major result of the steady state assumption in SiB is that fossil fuels accumulate in the atmosphere at faster rates in the model than is observed. Consequently model background CO_2 should exceed that observed, especially in the Northern Hemisphere where the majority of fossil emissions occur and most of the world's long term surface sinks are thought to exist. Indeed, a comparison of global flask observations to PCTM gives this result. Assuming that CO_2 at flask sites approximately represent zonal distributions, a plot of annual mean flask observations compared to PCTM output at sites around the globe would approximately represent the North-South gradient (see Figure 3.8). The result of steady state in SiB, which is seen in the figure, is manifested in one way as a difference in zonal mean CO_2.

If continental sites are included in the above analysis, the North-South gradient is more difficult to discern because of spikes that occur over the continent. Furthermore, continental sites are less representative of zonal distributions because of strong local and regional influence. If we consider remote sites only, i.e., measurements collected over mountains and marine boundary layers exposed to less anthropogenic and terrestrial influence than continental sites, the difference in gradient is more apparent and representative of background conditions. The model/observed difference decreases with latitude moving south because of the long mixing time scale between hemispheres (~ 1 year).

3.3.1   Vertical Gradients

The effect of excessive winter R_g can be seen in winter vertical CO_2 profiles. Comparisons between aircraft data and PCTM are made in Figure 3.9 to show the large difference in vertical gradient in the model, especially in the winter near the surface. A portion of the stronger than observed gradient could also be a result of weak vertical mixing in the winter, a result that appears to be common in other transport models (Stephens et al, 2007). This result will be important in the following interpretation of seasonal cycles.
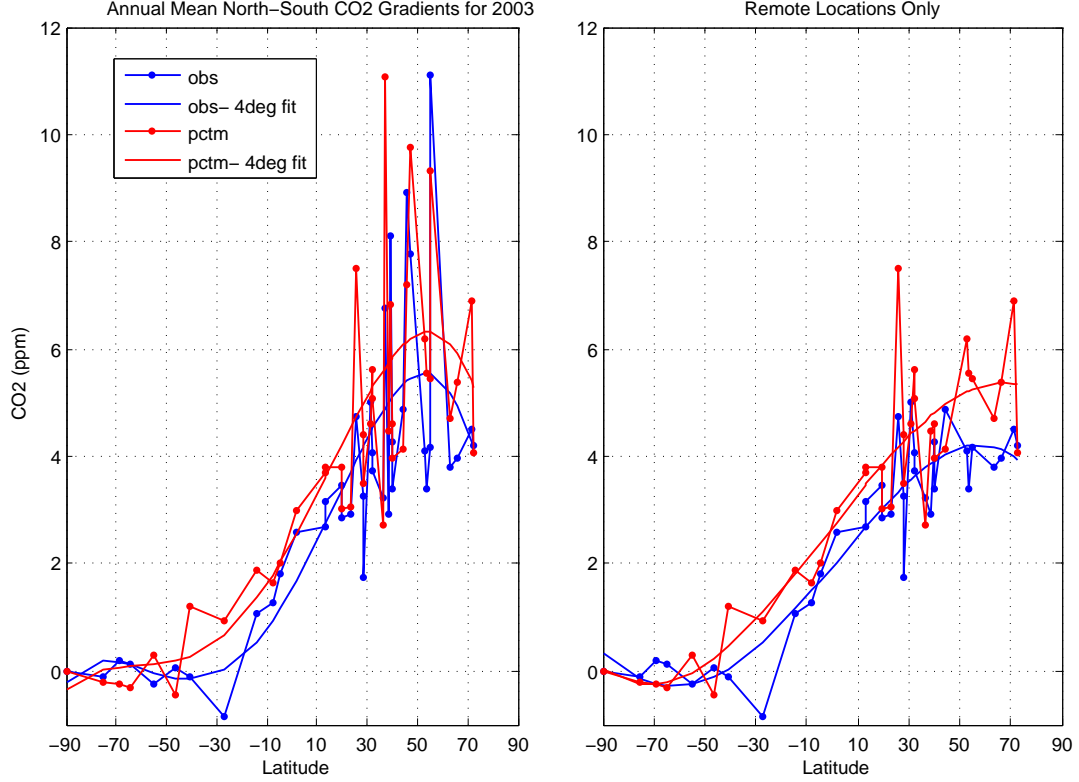
Figure 3.8: North-South CO_2 gradients (2003). Annual averaged monthly mean flask observations are shown in blue; annual averaged hourly PCTM sampled at the flask location is shown in red. Fourth-degree polynomial fits to each curve are included to get a better idea of the model/observed discrepancy. The left panel includes continental and remote sites; the right includes only remote sites.

3.3.2   Seasonal Cycles

Regarding analysis of seasonal CO_2, since hourly CO_2 is subject to huge and variable diurnal cycles which make seasonal variability difficult to interpret, we have focused here only on day-to-day variations of mid-afternoon concentrations. This means we can analyze values near the surface since daytime surface values are approximately representative of the entire PBL (e.g. Bakwin et al., 1998). Figure 3.10 shows seasonal cycles of monthly mean mid-afternoon observed and modeled CO_2 at each station from 2003-04.

An important result to notice is that the timing of leaf greenup in the spring and leaf senescence in the fall is simulated really well at all sites. Ability to model the timing
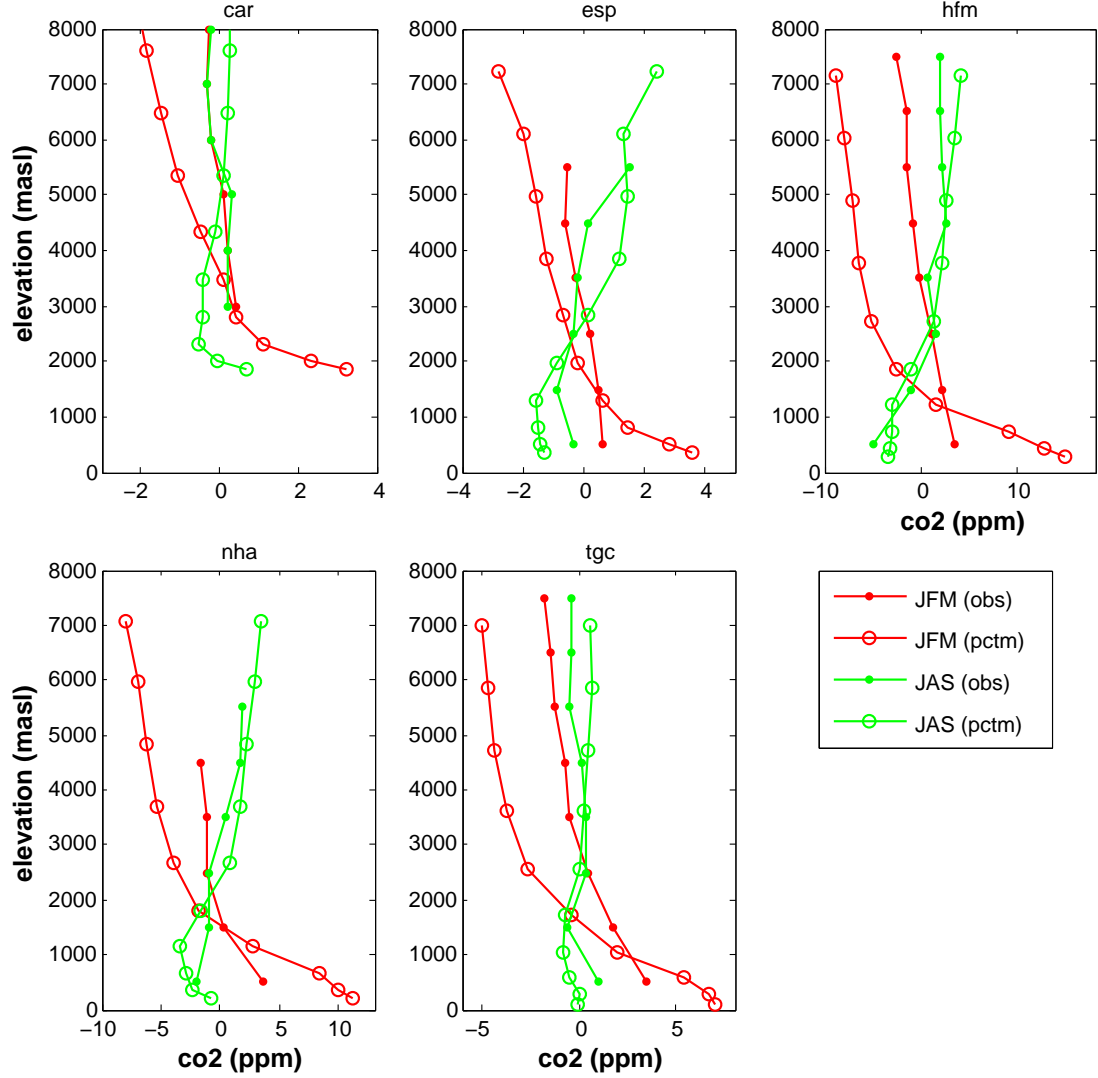
Figure 3.9: Vertical CO_2 gradient by season and site. Observed vales are smoothed aircraft measurements from GLOBALVIEW. GLOBALVIEW values are extracted from a curve fitted to measurement data that have been selected for conditions where the sampled air is thought to be representative of large well-mixed air parcels.Red dots represent observed January, February, March (JFM) averages from 2003-04, red circles are modeled JFM averages, green dots are observed July, August, September (JAS) averages, and green circles are modeled JAS averages. Mean vertical CO_2 has been removed from each curve. Vertical profiles are shown for Carr, CO, USA (CAR, [40.9N, 104.8W]), Estevan Point, British Columbia, Canada (ESP, [49.9N, 126.5W]), Harvard Forest, MA, USA (HFM, [42.5N, 72.2W]), Worcester, MA, USA (NHA, [42.9N, 70.6W]), and Sinton, TX, USA (TGC, [27.7N, 96.9W]).

and phase of seasonality reflects (among other things) proper: 1) interpolation of monthly composite NDVI, and 2) large scale transport of hemispheric CO_2. Correct timing of season
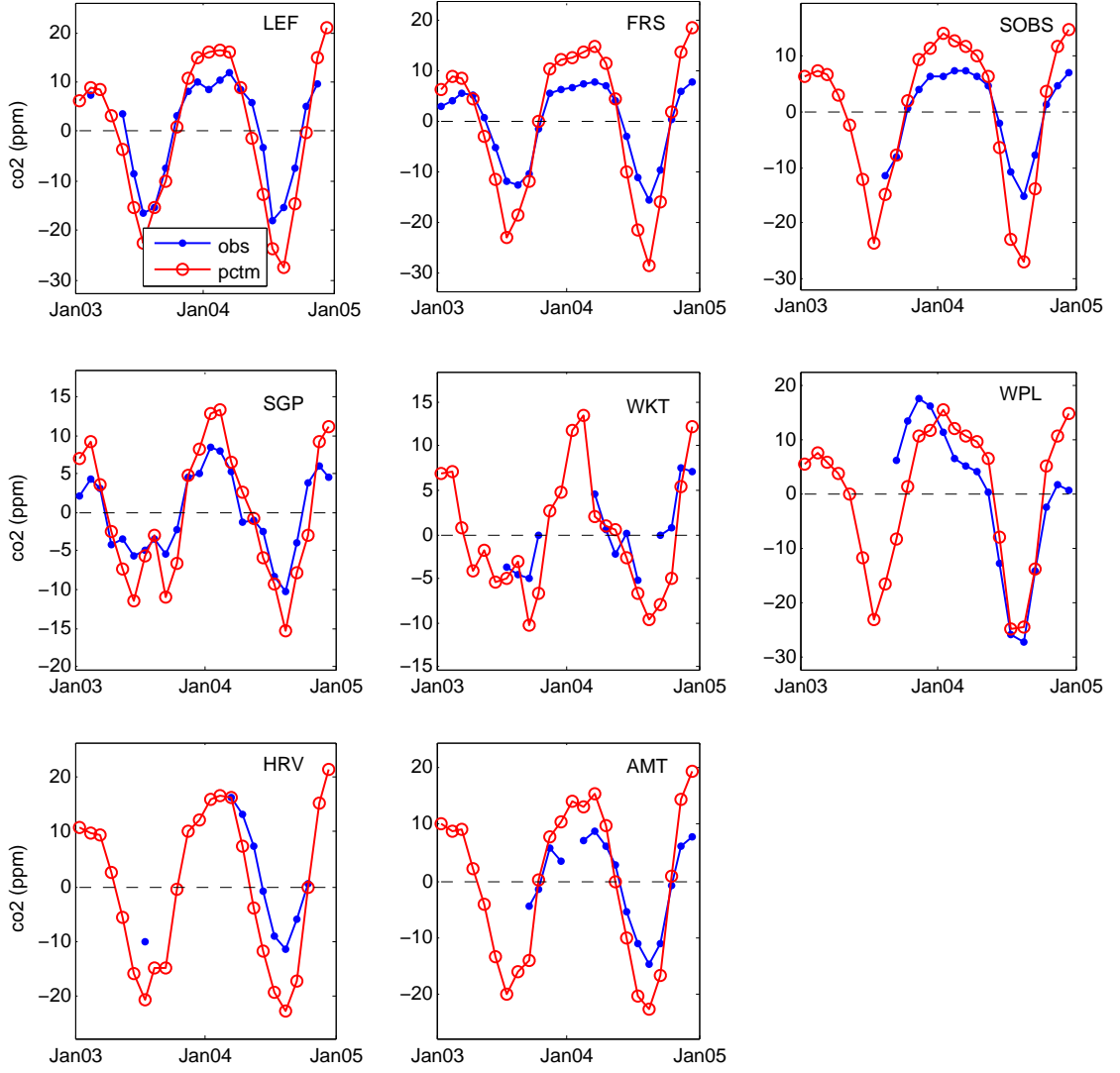
Figure 3.10: Comparison of seasonal cycles of observed (solid line with dots) and model (dashed line with open circles, fossil fuel + ocean + SiB3) monthly mean mid-afternoon CO_2 at 8 sites for years 2003-04. Both plots are detrended to account for differences in model/observed atmospheric growth rates and therefore adjusted to a mean of zero. Use of mid-afternoon values only removes diurnal variations.

is also important for realistic simulation of the magnitude of synoptic and diurnal cycles during transitional seasons, which is dictated in part by strength of vegetative uptake.

A comparison of figures 3.4 and 3.10 indicate that observed and simulated CO_2 in the PBL have similar seasonal cycles to NEE; CO_2 is generally taken out of the atmosphere in the summer when photosynthesis exceeds respiration (negative NEE) and released to the

atmosphere during the rest of the year when decomposition and respiration of vegetation dominate (positive NEE). Davis et al. (2003) observe that variations in PBL CO_2 are governed primarily by local NEE predominantly during fair weather.

It is interesting that at all sites except HRV the seasonal amplitude of both NEE and CO_2 are overestimated. At HRV, the amplitude of NEE is instead underestimated. This is explained by the relative areas of influence of CO_2 compared to NEE, where NEE is much more local than CO_2, which influences an area several orders of magnitude larger (Denning et al., 2003). The result is that seasonal cycles of daytime minima CO_2 are controlled more by regional and global CO_2 forcing than local forcing. The same principle holds for the other sites such the seasonal amplitude is more a reflection of large scale CO_2.

There are at least 3 likely causes for persistent overestimation of the amplitude of daytime minima seasonal CO_2 over NA. One of course is accumulation of fossil fuels in the atmosphere due to no model sink. This can be quantified to some degree by making a quick comparison of model growth to observed growth. This is done by comparing observed and modeled NH CO_2 on Jan 1, 2000 (beginning of simulation) and Jan 1, 2004 (4 yrs into simulation). Although any station in the world experiences the same atmospheric growth rate (see Figure 3.11), we use Mauna Loa as the proxy for growth rate. We compare two-year means surrounding Jan 1, 2000 and Jan 1, 2004 of Mauna Loa monthly mean flask observations and PCTM sampled at the Mauna Loa grid cell. We then solve for the 4-yr total model and observed growth, which turn out to be 12.45 and 7.87 ppm, respectively. This means the model growth rate exceeds that observed by approximately 1.14 ppm/yr in the NH, which should leave an excess of ~4.5 ppm on average in the model atmosphere at the start of 2004. This, however, is not enough to explain the discrepancies in Figure 3.10.

The second likely cause is the excessive model winter R_g at many of the flux sites in Figure 3.4. This appears to be a common problem in the model at higher latitudes and may aggregate over much of the Northern Hemisphere in the winter. Finally, Figure 3.9 suggested stronger than observed vertical CO_2 gradients in the winter, explained by some
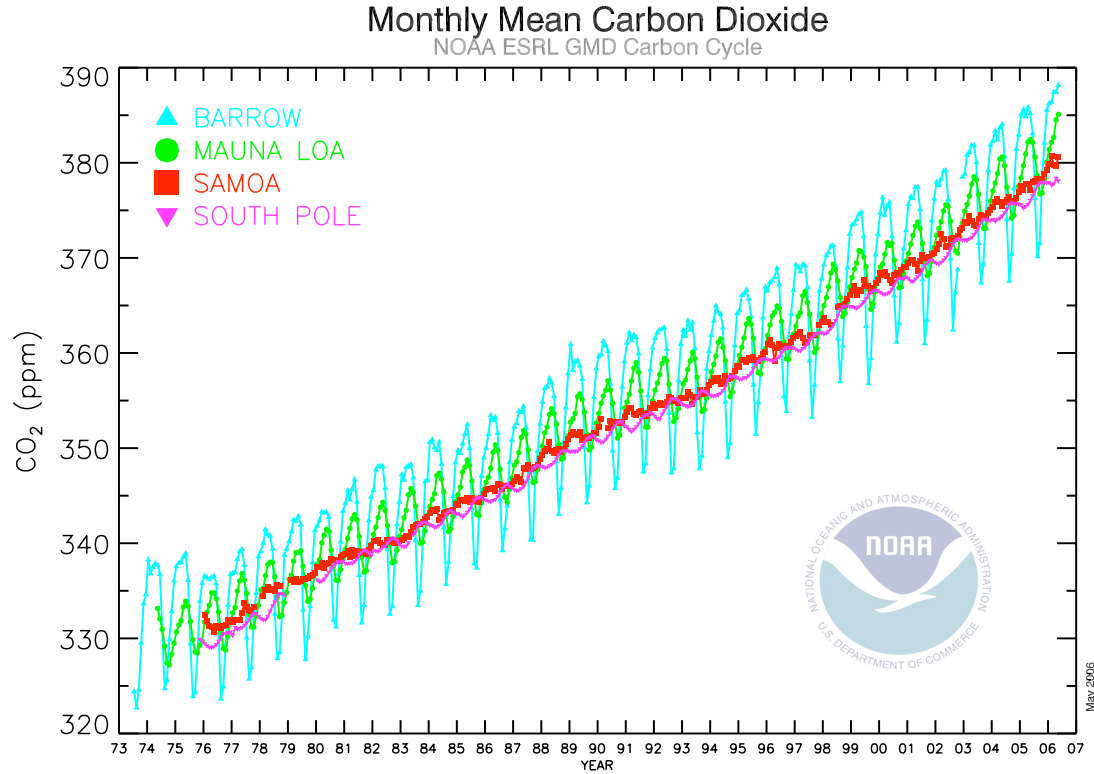
Figure 3.11: Growth of atmospheric CO_2 at NOAA GMD observatories. Courtesy NOAA GMD.

combination of excessive winter R_g and weak vertical mixing, the latter of which would act to enhance positive gradients already established by the former.

3.4   Comparison of Observed and Simulated Synoptic CO_2

Figure 3.12 shows mid-afternoon observed CO_2 at each station in 2004. It is clear that there are large day-to-day variations throughout the year, as much as 10-30 ppm at several sites, that cannot possibly be explained by day-to-day variations in NEE alone. Periods with large jumps are more likely to correspond to synoptic weather systems where CO_2 transport is more important. Davis et al. (2003) and Chen et al. (2004) also find that these transport events are important for local signals all year.

How does PCTM compare to these observed synoptic variations? Correlations of PCTM and flask observations made in Section 3.1.1 were found to be fairly good. Here
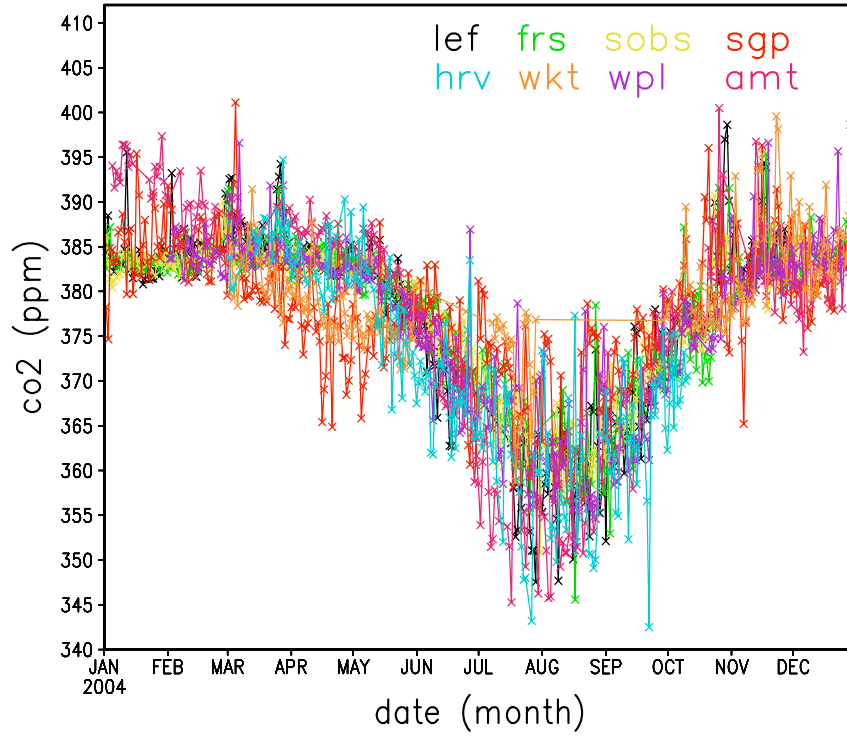
Figure 3.12: Seasonal cycles of observed mid-afternoon (21UTC) CO$_2$ for 2004.

we make similar correlations except with mid-afternoon continuous data over NA. These scatterplots are shown in Figure 3.13 and, as before, are broken down by season in Table 3.2. The regression and correlation values are slightly weaker for the entire year, with PCTM

	Year			Winter			Summer		
Station	r	R^2	b	r	R^2	b	r	R^2	b
LEF	0.525	0.277	0.658	0.503	0.253	0.799	0.534	0.286	0.596
SGP	0.624	0.390	0.782	0.614	0.378	0.931	0.712	0.508	0.974
SOBS	0.553	0.306	1.035	0.678	0.460	1.714	0.465	0.216	0.609
FRS	0.430	0.185	0.639	0.562	0.316	1.708	0.467	0.219	0.556
AMT	0.498	0.248	0.689	0.683	0.467	1.510	0.448	0.201	0.435
WPL	0.421	0.178	0.537	0.426	0.181	0.616	0.497	0.247	0.523
WKT	0.533	0.284	0.743	0.437	0.192	0.734	0.893	0.799	1.317
HRV	0.443	0.197	0.358	0.172	0.030	0.230	0.495	0.245	0.372

Table 3.2: Statistics comparing mid-day (21 UTC) continuous observations to PCTM during 2004. r represents the correlation value, R^2 the amount of observed variance explained by PCTM, and b the regression.
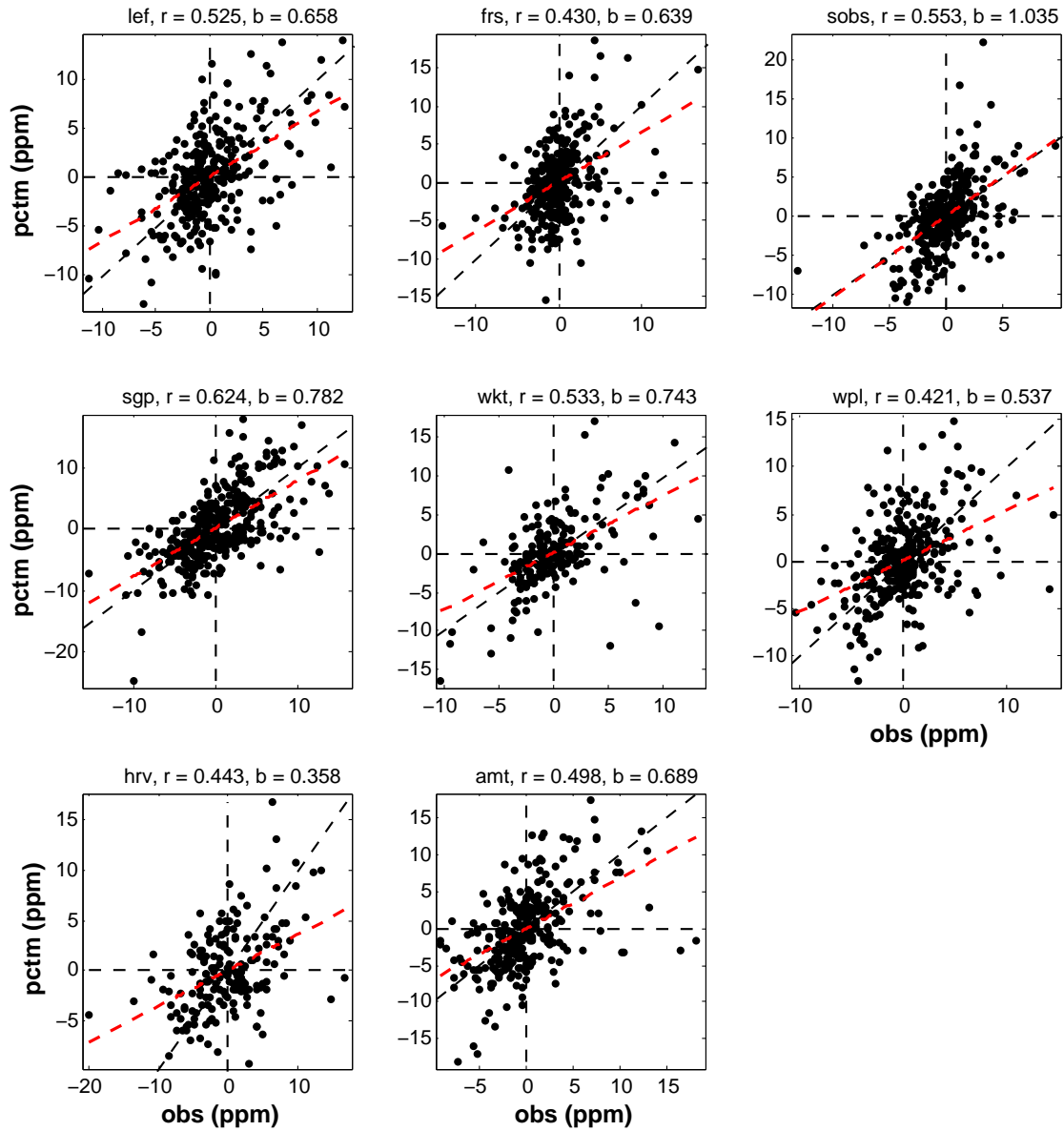
Figure 3.13: Scatterplots of 2004 mid-day (21 UTC) continuous data and PCTM output (in ppm) sampled at the time of and approximate location of the continuous data. The correlation value (r) and regression coefficient (b) are shown above each plot, with the one-to-one line (black dashed) and regression line (red dashed) plotted for convenience.

explaining between 17 and 40% of variations at the stations (25.8% on average). The average is slightly larger in the winter (28.5%) and, unlike the flask comparisons, the best in the summer (32%). These values suggest some success in simulating day-to-day variations over the continent in the summer and winter but that more than 70% of the synoptic variations

over the continent are still unexplained by the model.

At this point we find it appropriate to narrow the analysis to cold front events in NA, i.e., those that match the stringent frontal criteria outlined in Section 2.3. No effort has been made to create synoptic statistics for cold fronts only, but at first glance many of the summer and winter variations are in agreement. Here we look at frontal events at the continuous sites by applying the frontal locator function to the observed and modeled CO_2 field before and after frontal passage. In this analysis we are interested in whether: 1) unique patterns emerge at each station in the observations and model and, if so, if general shape is in agreement, 2) pattern phase is in agreement, and 3) pattern amplitude is in agreement. Figures 3.14 and 3.15 show the behavior of CO_2 during several selected events averaged together in the summer and winter, respectively.

Before analyzing Figures 3.14 and 3.15 it is important to note that there are certain signals we do not expect to resolve. For example, subgrid scale horizontal gradients in CO_2 flux (e.g. km) created by local spatial heterogeneity in vegetation are not resolved in this experiment (Gerbig et al., 2003). Local CO_2 gradients created by variable vegetative response to subgrid scale fluctuations in meteorology are also not resolved (Gerbig et al., 2003).

These limitations aside, PCTM does a reasonable job reproducing observed frontal variations. For reasons stated above the model is not expected to always capture the magnitude of day-to-day variations. We do, however, expect signal shape to be replicated if the model can establish the correct sign of horizontal and vertical gradients throughout the atmosphere. If gradients evolve correctly in the simulations, the assimilated meteorology has a better chance of transporting/mixing gradients around at the correct time and location. As can be seen in both Figures 3.14 and 3.15, these are the results we generally get.

With few exceptions, amplitude mismatches appear to be within the averaging error. Assuming the amplitudes are correct, however, there are possible explanations for the errors that may be worth pursuing in the future. Summer mismatches, for example, may result
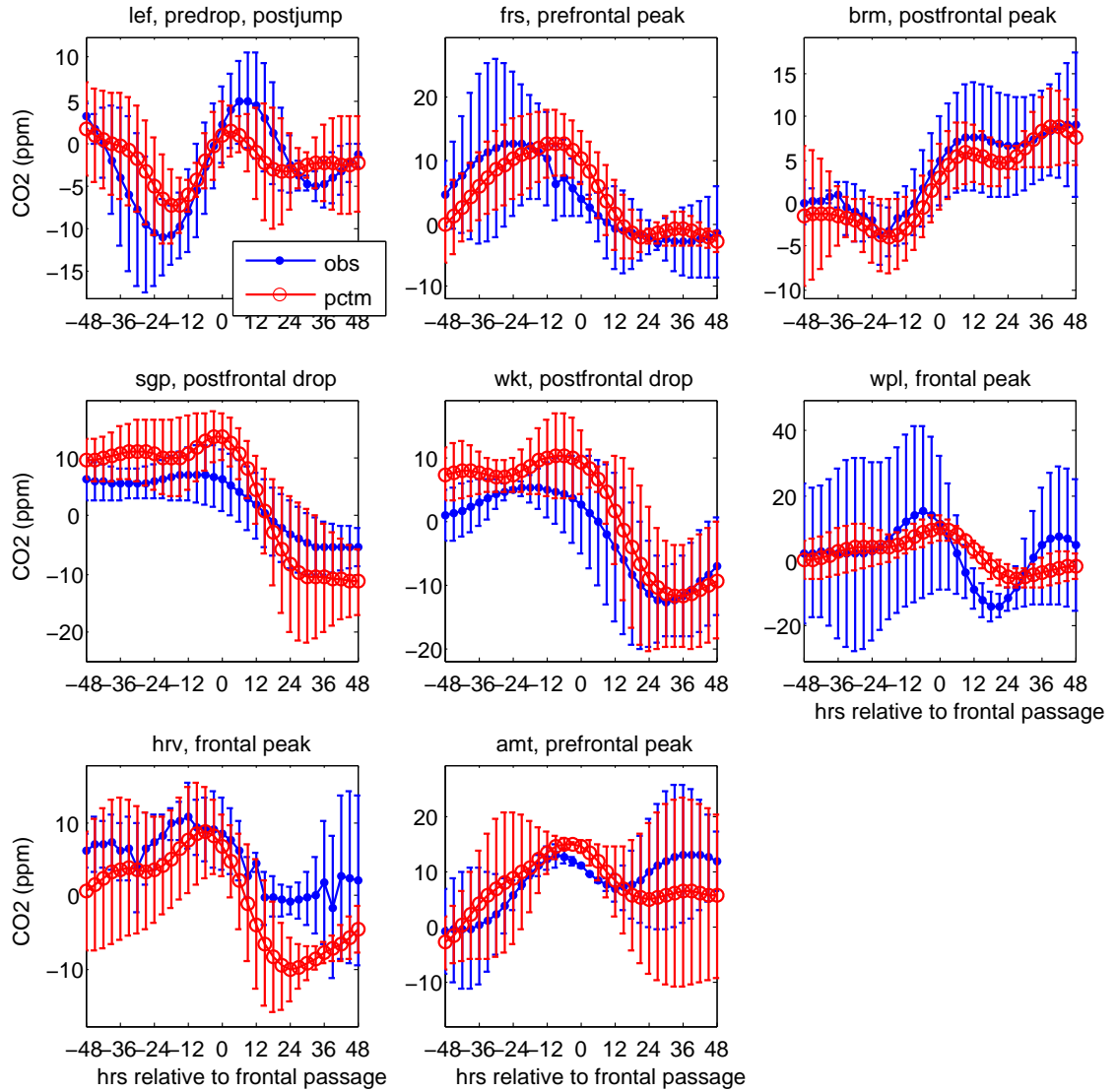
Figure 3.14: CO_2 composites by station during summer months (June, July, August, and September). These composites are created in the same way as GEOS4 composites; i.e., several frontal events between Jan 1, 2003 and Dec 31, 2004 are averaged together for 48 hours before and after frontal passage. The 'frontal locator' function, along with other meteorology criteria outlined in Section 2.3, is used to identify events. Diurnal and seasonal cycle are removed with a recursive filter. Error bars represent the standard deviation of the average of events.

from exclusion of model sinks, which, if included, would alter the magnitude of CO_2 anomalies advected along cold fronts upstream of the site. Amplitudes are typically overestimated in the winter for reasons such as fossil fuel buildup and over-estimation of respiration.
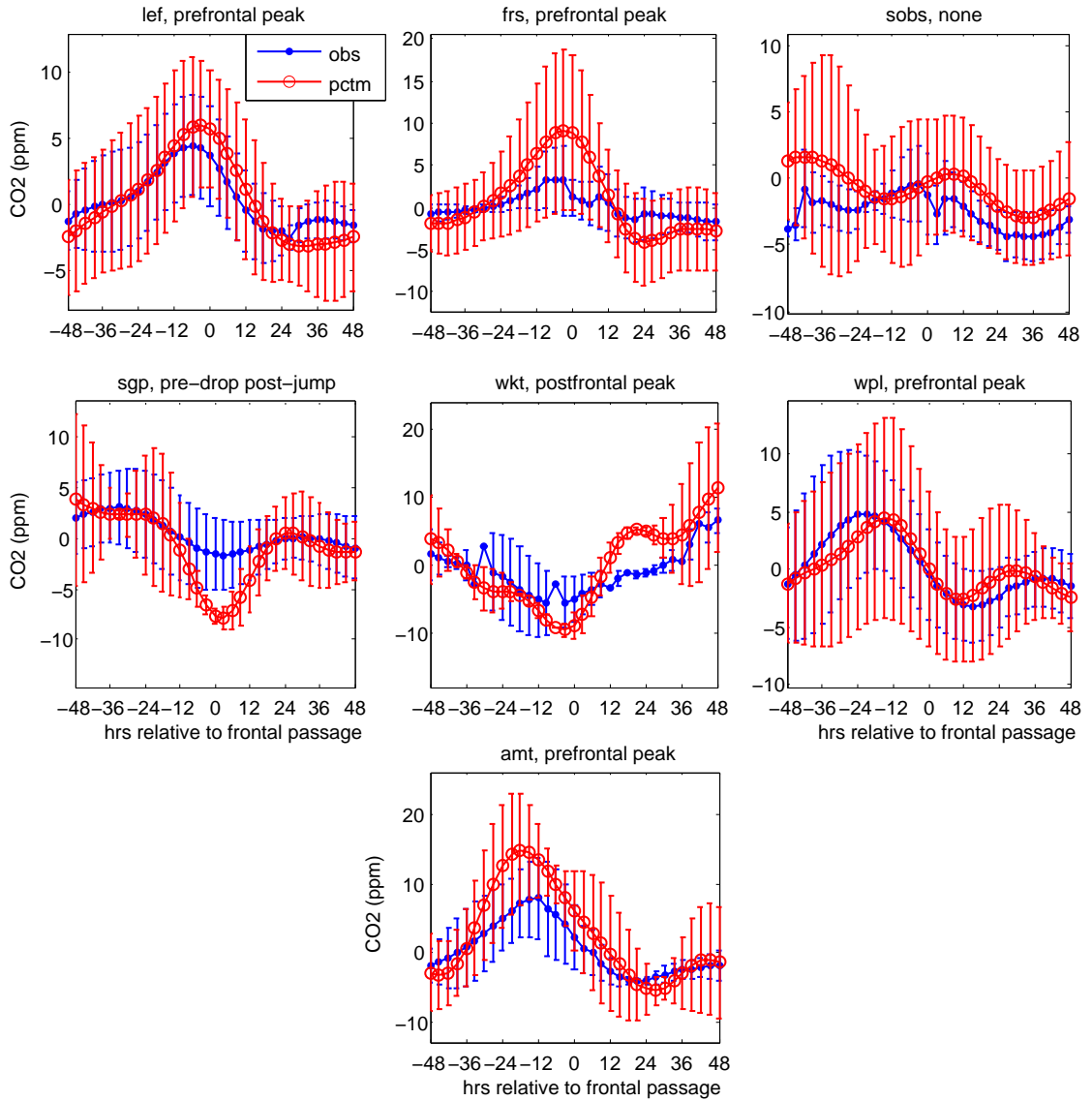
Figure 3.15: Same as Figure 3.14 but for winter. HRV is excluded because of missing data.

The more important result of Figures 3.14 and 3.15 for this study is that observed frontal CO_2 patterns are generally reproduced by PCTM in both summer and winter. Detectable day-to-day variability in the winter (non-growing season) observations suggests the presence of horizontal and/or vertical transport (since NEE is much weaker). Overall, these results suggest that PCTM is translating the correct CO_2 gradients to the correct locations at the correct time in the winter and summer, suggesting that the transport mechanisms for doing so are being modeled correctly much of the time.

3.5   Spatially Coherent Events

Since NEE is much weaker in NA in the winter, strong model and observed day-to-day winter variations at all sites indicate the significance of transport for synoptic signals. In addition, there are several important results in Figure 3.16 that suggest the importance of horizontal advection of CO_2 anomalies for synoptic variations. A few examples of spatial
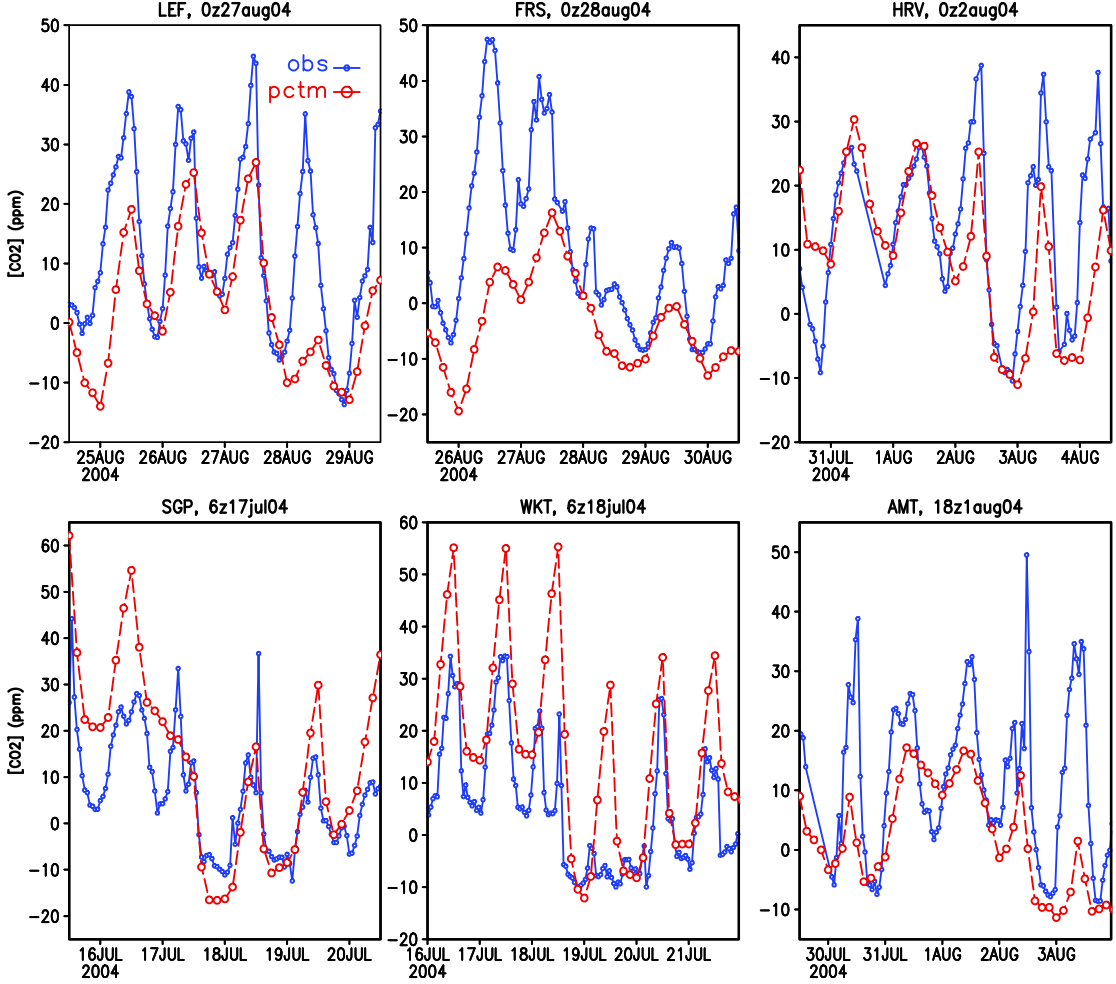
Figure 3.16: CO_2 signal during summertime frontal passage events in NA. The solid dotted line is observed and the dashed line with open circles is PCTM. The x-axis is in UTC. The time of frontal passage is indicated in the title of each plot in UTC.

coherence should demonstrate this. SGP and WKT, for example, show substantial depletion following frontal passage events from July 17-18. Since these stations are separated by

only a few hundred kilometers in the central Midwest and experience the same synoptic pattern when under the influence of a common meteorological system, some degree of spatial coherence between towers in this region is suggested. In this case a cold front moved far enough south to affect both stations. It is unlikely that a similar jump in CO_2 of this magnitude occurred at both stations a day apart because of similar local variations in NEE related to synoptic weather.

Another example of spatial coherence, this time in the Northeast, uses the same line of reasoning as with SGP and WKT for AMT and HRV. An event occurs at both stations from August 1-2, this time with frontal passage separated by only about 6 hours, that leads to a peak in CO_2 right around the time of frontal passage, first at HRV and then at AMT. The timing suggests spatially coherent southwesterly frontal movement in this region. Yet another example is seen in the upper Midwest with LEF and FRS. These stations experience frontal peaks about a day apart, first at LEF and then at FRS, from Aug 27 to Aug 28, suggesting southwesterly frontal movement and advection of a positive CO_2 anomaly.

These events support the idea that horizontal advection is an important component in creating the large CO_2 spikes/dips during frontal passage events. Additional support to this argument is given by the fact that the events are not limited to certain regions of NA. They occur in the lower Midwest, the Northeast, and around the Great Lakes region, suggesting that large deviations in CO_2 are more dependent on atmospheric transport than local vegetation. In Chapter 4 discussion is devoted to explaining how spatial gradients in CO_2 might be created, how horizontal and vertical advection may act on those gradients, and the importance of transport relative to local surface fluxes..

3.6   Comparison of Observed and Simulated Synoptic NEE

Apart from seasonal amplitude and overestimation of winter fluxes, SiB was shown in Section 3.2 to capture seasonal variability at several NA stations reasonably well, including seasonal structure and timing of leaf senescence and spring greenup. The ability of SiB

and PCTM to capture the shape of the synoptic CO_2 signal for several summer events was shown in Sections 3.4 and 3.5, with emphasis on the importance of transport. In this section the focus is directed towards modeled and observed synoptic variability of NEE to determine whether observed synoptic variations occur and if SiB captures them.

Figure 3.17 shows NEE during several summer frontal events. SiB appears to capture
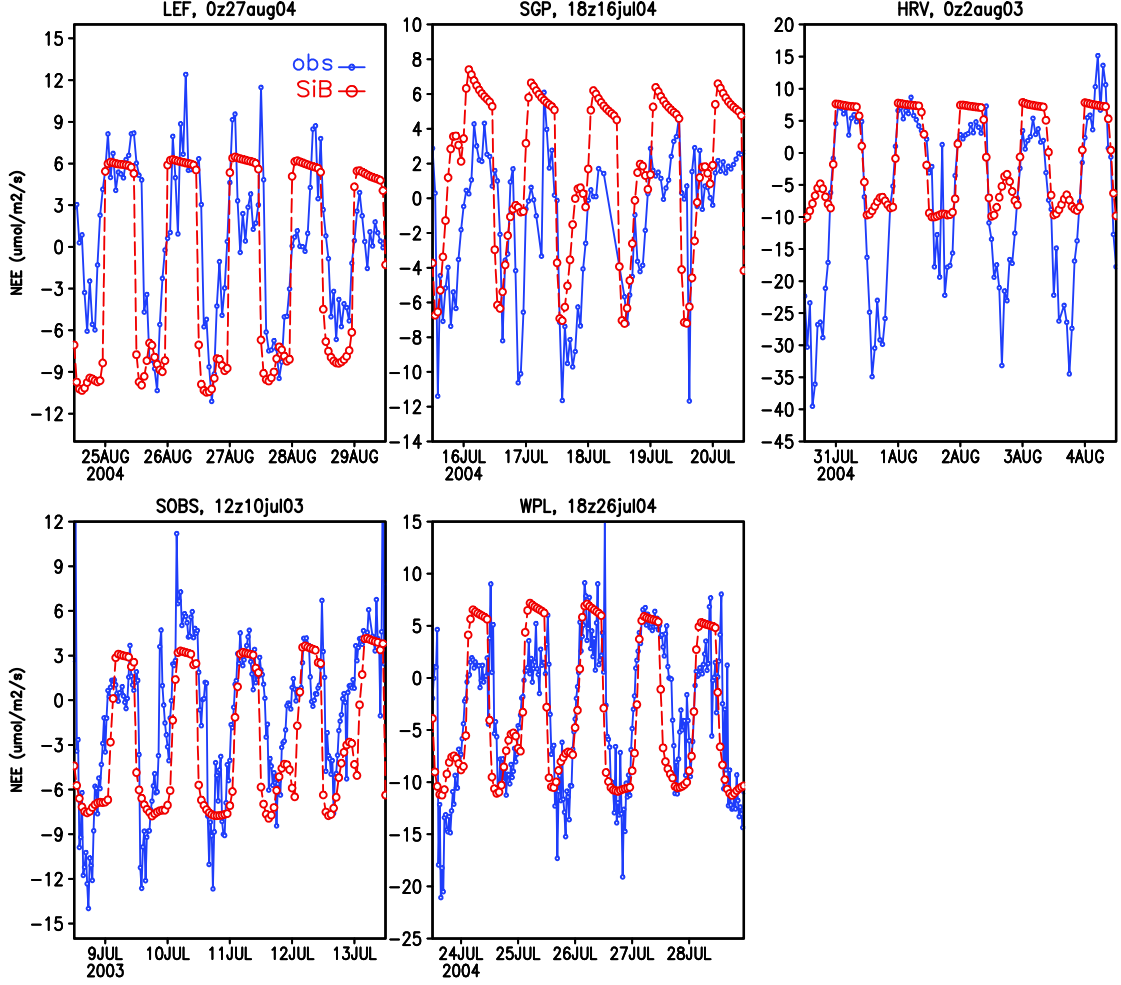
Figure 3.17: Modeled and observed NEE during several summer synoptic events. Open circles correspond to SiB and dots to observations.

the correct day-to-day variations at LEF and SOBS for these cases, where average model and observed daytime NEE decreases for two days after frontal passage. A similar result occurs in the late afternoon at SGP. The observed response at HRV and WPL, however,

differs from the modeled response.

The time series in Figure 3.17 suggest varying observed and modeled responses by site and day relative to frontal passage. The question now is how well SiB corresponds to observed frontal variations in general, and how this compares to observed/modeled NEE relationships for the entire summer. To start, frontal NEE regressions (see right column of Figure 3.18) show a persistent weak relationship between observed and modeled NEE independent of site (b = 0.08-0.283). HRV has the strongest correlation, with 27% of observed variations explained by SiB, but a weak regression (0.19), indicating the correlation is fairly strong but that model variations are significantly weaker than observed. The frontal relationships aren't much different than what is generally seen in the summer at this site.

LEF and SGP have weaker correlations ($\sim$ 10% of observed variations explained) and the regressions are still only weakly positive. LEF has the weakest regression of all. WPL also has a weak correlation and regression. These weak positive regressions indicate that, although the models respond in some systematic way to frontal variations, the response is weak compared to observations. It appears that observed frontal variations are almost always significantly stronger than modeled variations, especially at HRV and LEF.

Except for WPL, frontal relationships are not much different than summer relationships. At WPL, the regression and correlation are much weaker during frontal events, which means that, although frontal model variations do occur, they are much weaker and less consistent with observations than typically seen. One interesting point, however, is that sometimes average model frontal NEE is different than its average summer value without a similar difference in observed NEE, and vice versa; for example, average uptake at WPL and LEF is 22% and 30% more, respectively, during fronts than the rest of the summer, but observed uptake is about the same. Does this mean that frontal weather is causing enhanced uptake in the model compared to the rest of the summer at WPL and LEF?

Radiation could be one meteorological forcing that alters NEE during fronts, either by enhancing uptake (diffuse radiation during cloud cover) or suppressing it (radiation source
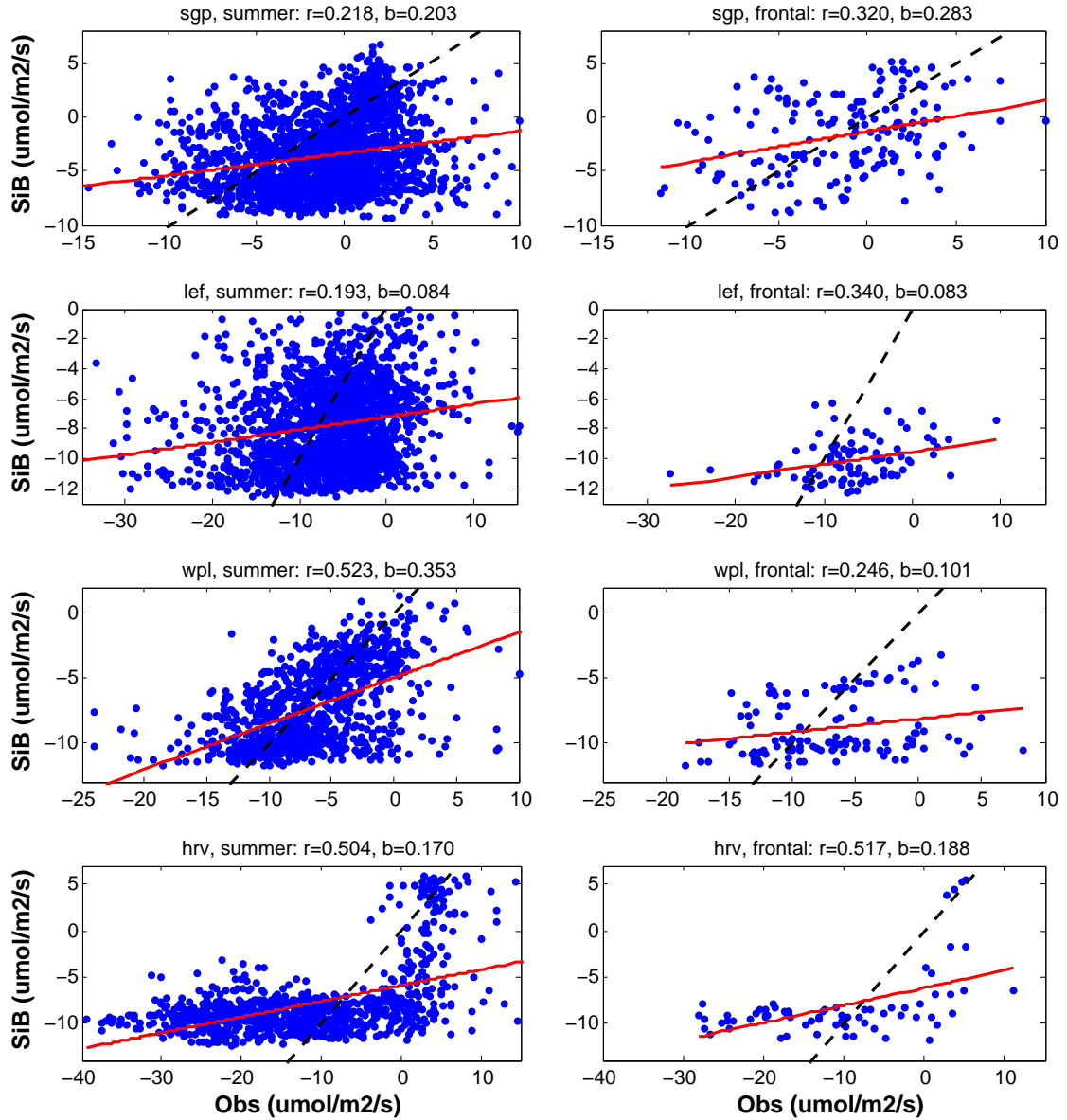
Figure 3.18: Scatterplots of SiB vs observed hourly daytime NEE at several sites for the entire summer (left column) and for multiple summer frontal events (right column) from 2003-04. Only NEE 36 hrs before and after frontal passage are included in the right column. The correlation (r) and regression (b) are included above each plot. The red line is the regression.

blocked off by clouds). There are of course a lot of other factors that may work with or against radiation and no attempt is made here to suggest the dominance of one over the other. We can, however, at least get a rough idea of NEE response to different radiation intensities using light response curves to test whether changes in light response may exist

during frontal events. Using such curves, appropriate tests for this study include: 1) whether light response curves have different signatures in the model compared to observations, 2) if unique signatures at different times relative to frontal passage exist compared to the typical signature for the summer, and 3) if there are light response differences between sites that might relate to vegetation differences.

These tests are addressed in Figure 3.19. The most important result is the general agreement between observed and modeled summer responses and observed and modeled frontal responses (except SGP); i.e., there are no large apparent deviations in the model. There are also few differences in the response depending on day relative to frontal passage (except perhaps observed responses at LEF and SGP). Furthermore, there doesn't appear to be much difference between observed frontal and summer responses or modeled frontal and summer responses. Perhaps arguments can be made that more observed uptake occurs during fronts at WPL or more modeled uptake occurs during fronts at WPL and LEF (both consistent with Figure 3.18), but this is only suggestive; more data may be needed.

A couple additional points worth noting include: 1) the strong observed uptake at HRV compared to the model, which is expected, 2) with regard to the model, the stronger slopes during less intense radiation and the tendency to level off after 200 W/m^2 (except SGP), and 3) model stress beyond 250 W/m^2 at SGP in the model not present in the observations. This last feature is probably an artifact of prescribed C3 vegetation rather than C4, the former of which is more vulnerable to temperature stress under intense radiation. This may also explain the stronger model uptake suggested in the 100-300 W/m^2 regime compared to GSP observations. Overall, SiB results are favorable and suggest that SiB, although experiencing weaker frontal variations compared to those observed, is basically behaving as might be expected.

The results in this section apply only to a few stations. Although modeled NEE response to frontal weather may be in better agreement with observations at some sites (HRV) compared to others (WPL), without generalizing too much it appears that model
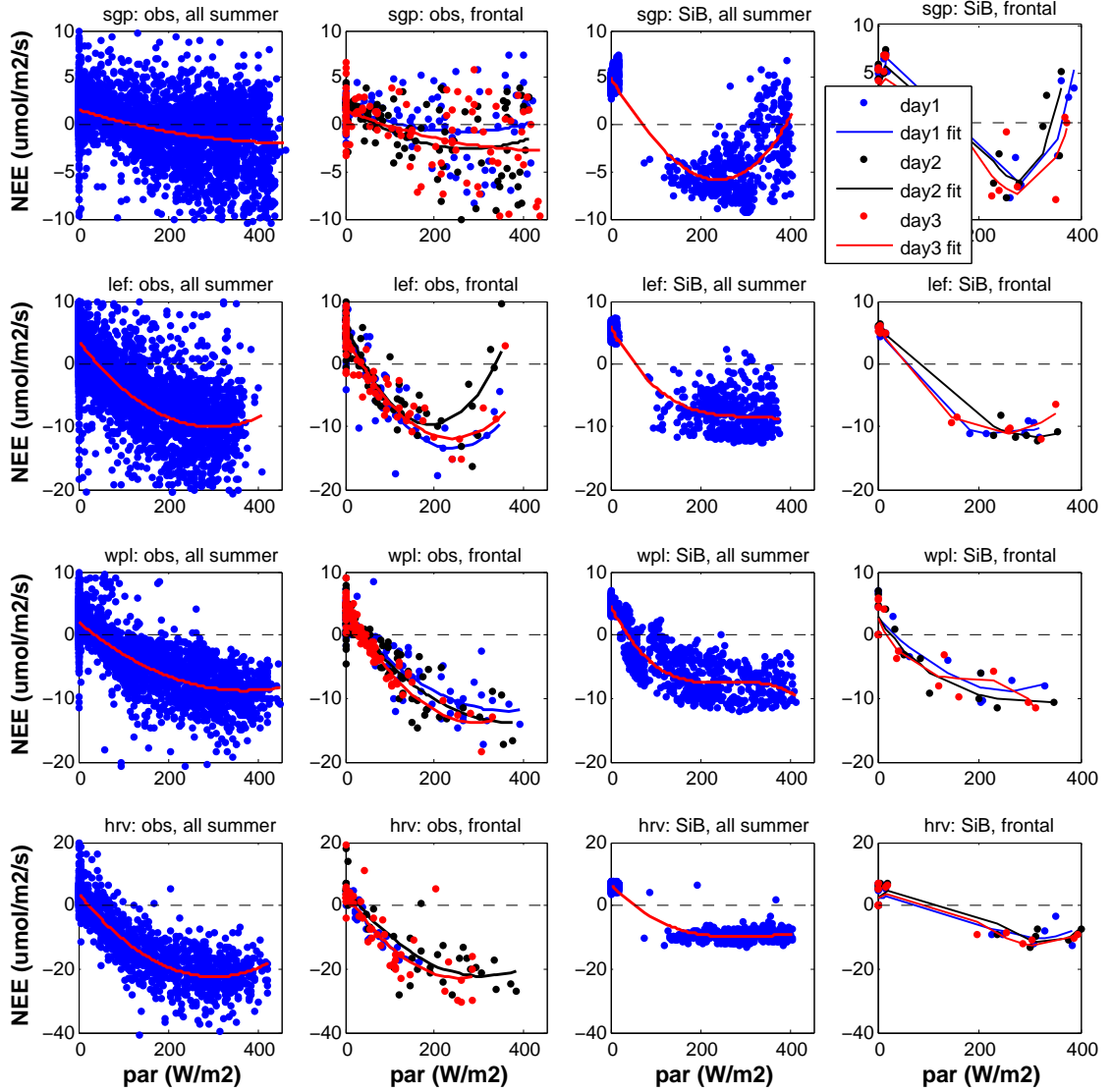
Figure 3.19: Light response curves (NEE vs photosynthetically active radiation (PAR)). Light response curves are represented by polynomial fits to the scatterplots; 2nd degree fits are used for observations and, because of a lack of data between 0 and 150 W/m^2, 3rd degree fits for the model. Each row represents one site. Column 1 is observed (hourly) summer curves, 2 is observed frontal, 3 is modeled (6 hourly) summer, and 4 is modeled frontal. Multiple fronts are included. Columns 2 and 4 have multiple curves: blue is the day before frontal passage (day1), black is the day of (day 2), and red is the day after (day3).

responses are going to be weaker than observed. It is difficult to make any conclusions about SiB regarding NEE response to frontal weather with this simple analysis, but, except for HRV, there isn't necessarily any reason to suggest SiB isn't responding correctly to frontal weather, although weak correlations at these sites may be related to model stress suggested

in the diurnal composites shown in Figure 3.7.

3.7   Vertical Mixing

We have seen evidence through coherent events that horizontal transport must contribute to a large portion of synoptic variations, at least in some cases. Also associated with fronts are vertical motions due to converging winds, adiabatic ascent (at synoptic scales), and latent heating, which separately or combined can cause mixing of vertical gradients. Regardless of the process at work (these will be discussed in more detail in Chapter 4) we need some way to assess the extent to which vertical mixing is accomplished in PCTM.

Figure 3.20 shows 9 profiles across NA in the spring of 2003. The results suggest that PCTM does a reasonable job matching the basic vertical gradient. There are no obvious systematic biases such as too little or too much mixing. There are a lot of high frequency vertical variations in the observations that PCTM is not expected to capture. There are several instances where the vertical gradient is stronger than modeled, such as at 18zMay29 in the Pacific Northwest, and opposite that observed, such as on 21zMay31 and 17zJun11. The model gradient is stronger than observed on 13zJun03, although this occurs in the morning and likely results from some model delay in mixing of nocturnal buildup.

Most days shown are fair weather except 21zMay31 and 17zJun11, which occur just prior to frontal passage. These happen to be two days for which the model gradient is opposite that observed, as if daytime profiles in the boundary layer are too low prior to frontal passage at these sites. Further investigation should be carried out in the future to determine if a link exists or not.
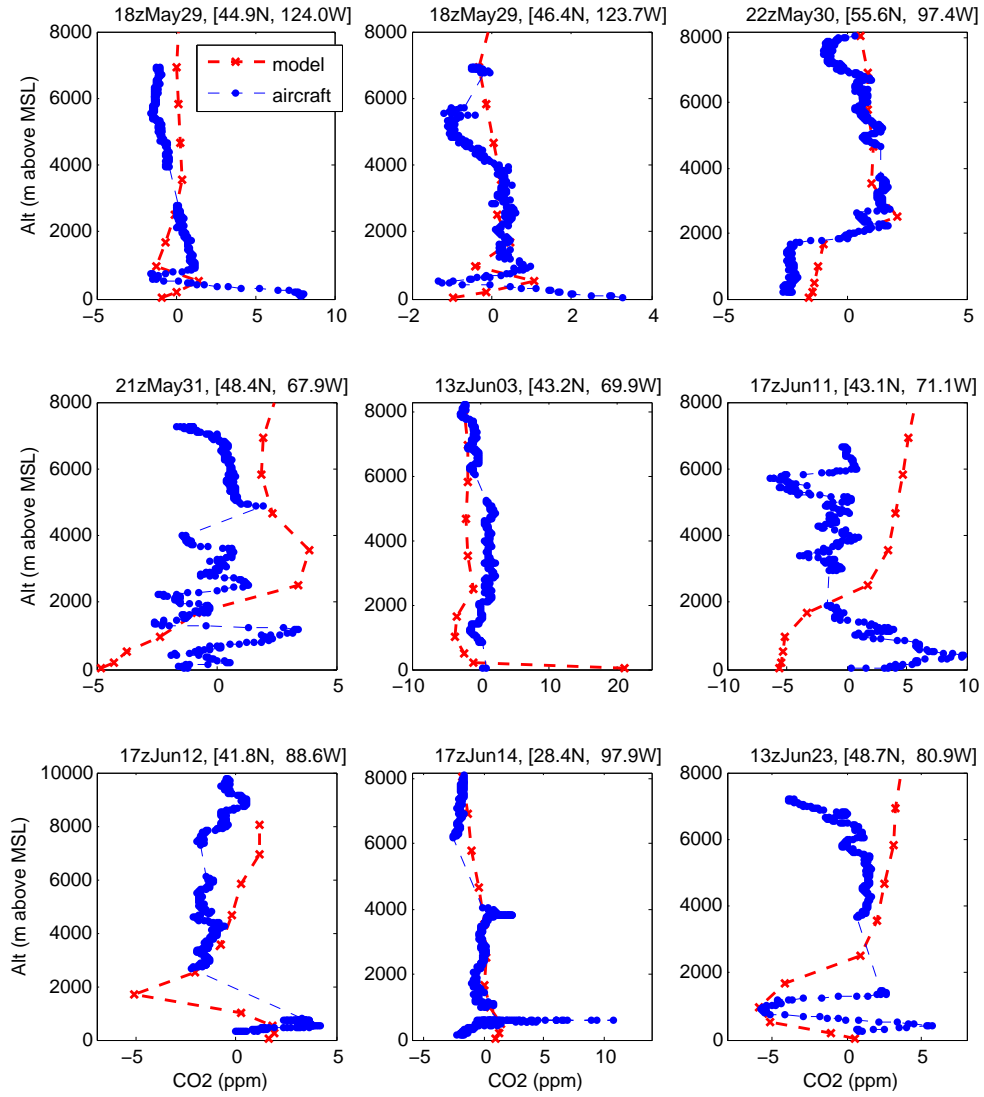
Figure 3.20: Vertical profiles of aircraft and modeled CO_2. Aircraft profiles are chosen during descents or ascents between the free troposphere and PBL during the COBRA North America 2003 campaign. Times are in UTC. PCTM is sampled vertically near the time of ascent/descent. Column means have been removed from all profiles so that only vertical gradients are conveyed.

Chapter 4

ANALYSIS OF PHYSICAL AND BIOLOGICAL MECHANISMS

What makes the synoptic signal so interesting and important is that there are certain times of the year when the sign of surface CO_2 flux does not match changes in boundary layer CO_2 (Hurwitz et al., 2004). Hurwitz et al. (2004) examined several cold front passage events in the spring and winter at a station in northern Wisconsin and found that the timing of CO_2 spikes and dips corresponded well with wind shifts at the surface, implying the existence of advection of horizontal CO_2 gradients. Since it is very unlikely that spikes and dips can be attributed to local variations in NEE only, we need to pay special attention to horizontal and vertical transport processes.

The Hurwitz et al., 2004 study also hints that different air masses associated with the cold fronts may contribute uniquely to CO_2 signals at the station, air mass influence depending on wind direction. Similarly, a study by Worthy et al. (2003) found distinct differences in CO_2 measurements at a Canadian tower when influenced by air masses from NA compared to those from the Arctic/North Atlantic.

In Chapter 3 we investigated the performance of PCTM compared to continuous observations of atmospheric CO_2 over NA at seasonal an synoptic time scales. We found that PCTM was able to reproduce observed trends in mid-afternoon CO_2 for several summer cold front passage events at eight sites across NA; furthermore, several coherent events were identified that suggested the importance of horizontal advection over scales greater than 500 km. This analysis suggested that PCTM, coupled with a realistic land surface model and assimilated winds, would be a good diagnostic tool for the study of mechanisms leading to

synoptic CO_2 variations.

Having established that the coupled model can predict synoptic variations in CO_2, we now use the 4D fields in the model to quantitatively analyze various mechanisms that could control these variations. This Chapter investigates the influence of upstream fluxes and passing weather disturbances on synoptic CO2 variations using PCTM. We build a set of tools to explain variations associated with midlatitude cyclones in terms of a set of mechanisms most important in synoptic flow, including local ecosystem response to synoptic weather and vertical and horizontal transport (Geels et al., 2004). This method is also used to evaluate mechanisms at work on monthly scales.

Continental observation sites in NA, which were discussed in detail in Chapter 3, are used in the analysis but we try to extend the investigation as much as possible to the entire region under the influence of synoptic flow. We investigate different sources for upstream influences, including large-scale flow moving over a continent and regional variations in NEE. An analysis of large-scale inflow is done to also consider its importance as lateral boundary forcing for regional simulations. A planetary boundary layer budget equation for CO_2 is used to quantify the various terms most important in controlling synoptic CO_2 variations. We also investigate how CO_2 gradients may be established and later acted on by deformational flow associated with midlatitude cyclones.

4.1   Budget Calculations

4.1.1   Budget Equation

We are interested in using a governing equation for CO_2 in the atmosphere to help explain synoptic variations near the surface in general, i.e., not just those that occur along a cold front as discussed in Chapter 3. Variations in the PBL are of particular interest because: 1) that is where most continental observations are and 2) it is the part of the atmosphere most strongly influenced by the surface. Bakwin et al. (2004) analyzed processes that influence CO_2 in the continental PBL on monthly and seasonal time scales. They assume

horizontal advection is negligible on monthly time scales and that CO_2 in the PBL is influenced only by monthly averaged local surface fluxes and vertical exchanges between the free troposphere and the PBL through advection.

A similar analysis can be performed on synoptic time scales using model output rather than observations. In this way we can try to predict changes in PBL CO_2 (dC/dt) over time scales that resolve large jumps seen in the observations ($\sim$ 3-6 hours for example) in a similar way as the transport model, based on simplified transport and surface flux terms. Each term can then be evaluated separately during synoptic events. The intent is not to predict the evolution of CO_2 over some time period, only to see if changes over small time intervals can be reproduced in order to assess mechanisms causing those changes.

A similar PBL budget equation to Equation 1 of Bakwin et al., 2004 is used for this study. The differential version is given as

$$\frac{\partial C}{\partial t} + \frac{RT}{p}\frac{\partial F_c}{\partial z} + W\frac{\partial C}{\partial z} + V_h \bullet \nabla_H C + g\frac{\partial(CM)}{\partial p} = 0 \qquad (4.1)$$

where C is the molar CO_2 mixing ratio (μmol CO_2 per mol dry air, ppm), F_c is the net turbulent flux of CO_2 (μmol/m^2/s), R is the universal gas constant, T is temperature (in K), p is pressure (in Pa), W and V_h are vertical and horizontal wind speeds (m/s), g is gravity, and M is the net convective mass flux. The first term represents the time rate of change of CO_2, the second is turbulent exchange, the third is vertical advection, the fourth is horizontal advection, and the fifth is vertical cloud transport. Together, these terms represent all processes leading to variations in CO_2 modeled by PCTM. Effort is taken below to simplify each term so that we can make approximate contributions by each term to the total change in CO_2 in the PBL over a three hour period.

Equation 4.1 is rewritten by using a similar procedure as in Bakwin et al., 2004: 1) apply finite differencing to first, fourth, and fifth terms, 2) integrate each term over the depth of the PBL, 3) apply the continuity equation and the condition that W=0 at the

surface to vertical advection, and 4) let F_c absorb RT/p for convenience,

$$\langle\frac{\Delta C}{\Delta t}\rangle + \frac{F_c^o}{z_i} + \frac{F_c^{z_i} + WC|_{z_i}}{z_i} + \langle U\frac{\Delta C}{\Delta x} + V\frac{\Delta C}{\Delta y}\rangle - g\frac{\Delta(CM)}{\Delta p} = 0 \qquad (4.2)$$

where angled brackets represent layer averages over the depth of the PBL, denoted by z_i. F_c^o is CO_2 emitted from the surface, where F_c (embedded within F_c^o) is the biogenic and fossil fuel surface flux (from SiB and constant, respectively) which we assume to mix instantly throughout the PBL. This is an approximation in that PCTM mixes more slowly through vertical diffusion, but is a valid assumption over multi-hout time steps. Horizontal winds, temperature, pressure, and cloud mass flux are provided by GEOS4.

z_i is a diagnostic variable included in the GEOS4 gridded product and is solved for using the Vogelezang and Holtslag (1996) formulation. Details regarding this formulation can be found in Kiehl et al. (1998). Here we assume that z_i represents the interface between the PBL and free troposphere.

We use a similar formulation as in Bakwin et al. (2004) for vertical advection,

$$\frac{F_C^{z_i} + WC|_{z_i}}{z_i} = \frac{C_{FT} - \langle C\rangle}{\tau} \qquad (4.3)$$

where τ is the residence time (expressed as $z_i/\bar{w}$), $\bar{w}$ is the average vertical wind of model layers above and below z_i, C_{FT} is the average CO_2 in the free troposphere, and a sign change has been made. Vertical exchange in the PBL is such that PBL CO_2 is assumed to respond instantly to mixing with the free troposphere. This is an approximation but valid for multi-hour time steps. Vertical velocity ($w = Dz/Dt$) is diagnosed using the hydrostatic approximation such that $w = -\omega/(\rho g)$, which is assumed valid for synoptic scale motions. ω is diagnosed within PCTM using mass flux divergence.

Vertical cloud transport out of the boundary layer is solved for according to the formulation in Kawa et al., 2004,

$$g\frac{\Delta(CM)}{\Delta p} = \frac{g}{\Delta p_k}[M_{k+1}(C_{k+1} - C_k) - M_k(C_k - C_{k-1})] \qquad (4.4)$$

where M_k and M_{k+1} are the net convective mass flux at the upper and lower edges of layer

k and $\Delta p_k/g$ is the mass of air in layer k. We integrate over all layers within the boundary layer to attain total transport by convection.

Vertical advection of CO_2 by the mean vertical wind assumes that CO_2 on either side of the inversion can penetrate the inversion (z_i) through vertical advection. There are four different scenarios for advection by the vertical wind, as illustrated in Figure 4.1. For cases 1 and 2 we assume that any upward motion, including convection, will cause PBL CO_2 to decrease, regardless of the vertical CO_2 gradient. The scenario denoted by 'Case 1' is labeled as 'False' because, even though the equation for advection suggests PBL CO_2 should increase, it is more intuitive that advection of high CO_2 out of the PBL will decrease PBL CO_2. These scenarios are assumed to be independent of horizontal advection and cloud transport, which will typically combine in some way to compensate for vertical motion.

4.1.2   Reynolds Decomposition of Vertical and Horizontal advection Terms

Vertical exchange can be broken down if we consider that CO_2 has time mean and perturbation components, $C = \bar{C} + C'$, such that Equation 4.3 can be expressed as

$$\frac{C_{FT} - \langle C \rangle}{\tau} = \frac{\bar{C}_{FT} - \langle \bar{C} \rangle}{\tau} + \frac{C'_{FT} - \langle C' \rangle}{\tau} \tag{4.5}$$

where $\bar{C}_{FT} - \langle \bar{C} \rangle$ denotes the 30-day average difference between CO_2 in the free troposphere and the PBL, while $C'_{FT} - \langle C' \rangle$ the anomaly from the 30-day day average, given as $C'_{FT} - \langle C' \rangle = [C_{FT} - \langle C \rangle] - [\bar{C}_{FT} - \langle \bar{C} \rangle]$. The same average 3-hr vertical wind is used for each term on the RHS of Equation 4.5.

Similarly, we can represent horizontal advection such that the fourth term in Equation 4.2 can be expressed as

$$\langle U \frac{\Delta C}{\Delta x} + V \frac{\Delta C}{\Delta y} \rangle = \langle U \frac{\Delta C'}{\Delta x} + V \frac{\Delta C'}{\Delta y} + U \frac{\Delta \bar{C}}{\Delta x} + V \frac{\Delta \bar{C}}{\Delta y} \rangle \tag{4.6}$$

where $\bar{C}$ denotes 30-day average PBL averaged CO_2 and C' denotes anomalous CO_2, which we solve for as $C' = C - \bar{C}$. The same 3-hour horizontal winds are used for advection of time mean and anomalous CO_2 gradients.
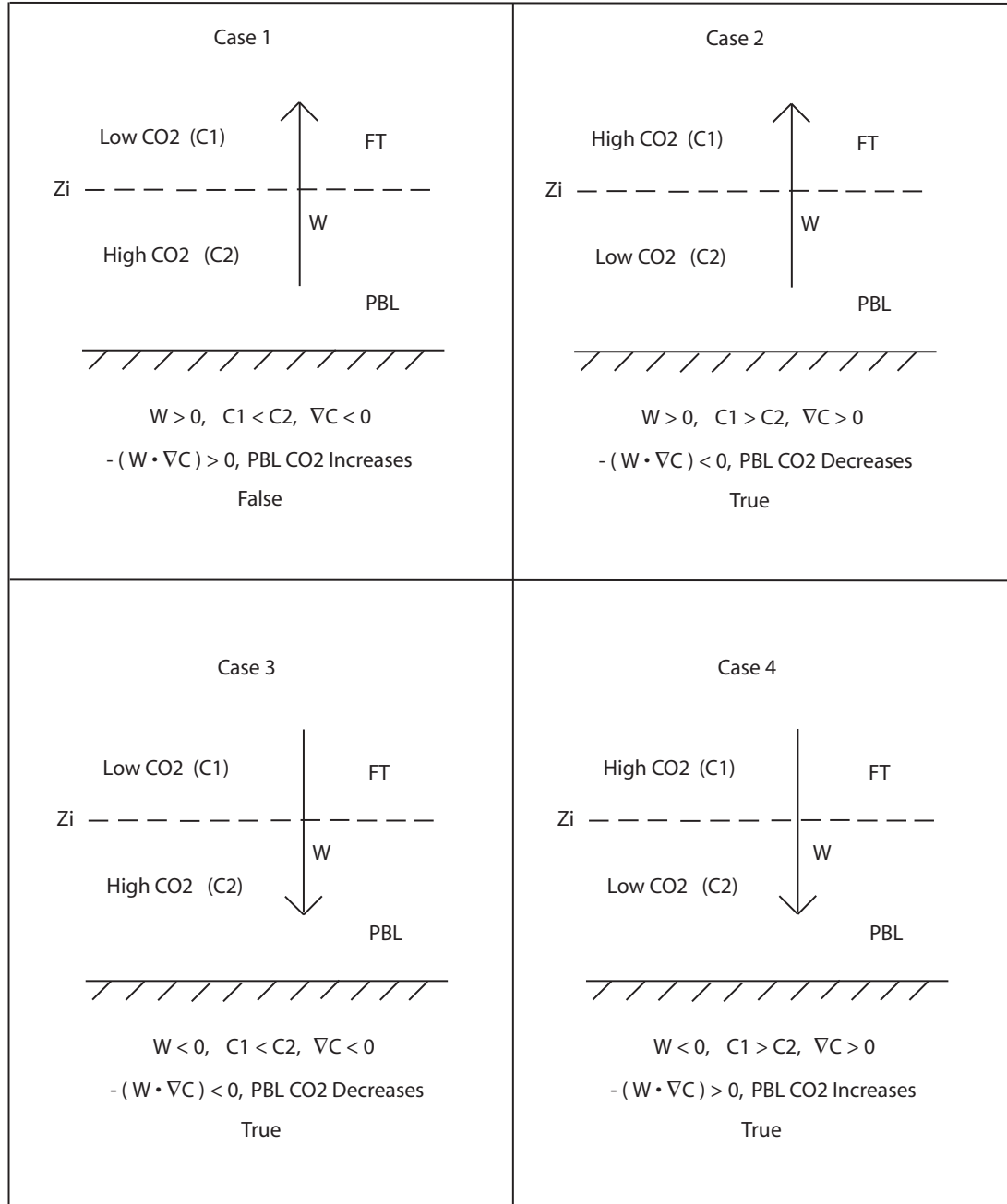
Figure 4.1: 4 scenarios (indicated by case number) for vertical advection of CO_2 depending on the vertical CO_2 gradient (∇C) and the vertical wind speed ($\bar{w}$, represented here as W, the direction of which is indicated by the vertical arrow). Zi is PBL height (dashed line), C1 is the average CO_2 in the FT (free troposphere), and C2 is the average PBL CO_2. Text labeled 'True' or 'False' refers to whether the statement above it is valid for our representation of vertical advection.

We apply this perturbation principle to vertical and horizontal advection because we are interested in relative contributions to the synoptic signal by synoptic weather acting separately on time mean spatial CO_2 gradients compared to anomalous spatial gradients. Details on anomalous vs time means gradients are discussed in Section 4.5.3. We assume time mean CO_2 is affected by average weather, which includes the average of synoptic and fair weather events acting within a grid cell over a month. Anomalous CO_2 are perturbations from the time mean controlled by synoptic weather.

4.2 Large Scale Influences

Total atmospheric CO_2 in the continental PBL can be thought of as a combination of contributions from local NEE and fossil fuel, horizontal and vertical advection of gradients established over the continent, and mixing of background concentrations in the free troposphere carried along with the large-scale flow moving in over continental boundaries (typically the west coast). Signals carried along with the large-scale inflow are associated with seasonal and spatial differences in global uptake and fossil fuel emissions (fossil fuels only varies spatially). Background CO_2 is therefore a result of months of mixing of global surface fluxes by atmospheric transport. Its value in synoptic variations, and day-to-day variations in general, can be evaluated using PCTM.

A simple test to examine the influence of large-scale flow on synoptic variations was done as follows. For convenience, the main PCTM experiment described in the previous chapters is referred to from here on out as EX1. In the second experiment, EX2, all SiB fluxes between 180°W and 10°W are set to zero such that only Eastern Hemisphere (EH) terrestrial fluxes are allowed to interact with the atmosphere. The experiment is run for 2004 with the modified SiB fluxes and without fossil fuel and ocean fluxes, using the same assimilated winds, grid configuration, and initial conditions as in EX1. The idea is to test the effect of baroclinic mixing on latitudinal gradients advected off Asia under conditions where the atmosphere is unperturbed by surface sources/sinks as it crosses over NA, and

how this might contribute to variations at the surface.

Some of the results found are outlined in Figure 4.2, which shows seasonal cycles as a function of latitude, experiment, month, and longitude transect. The most important result
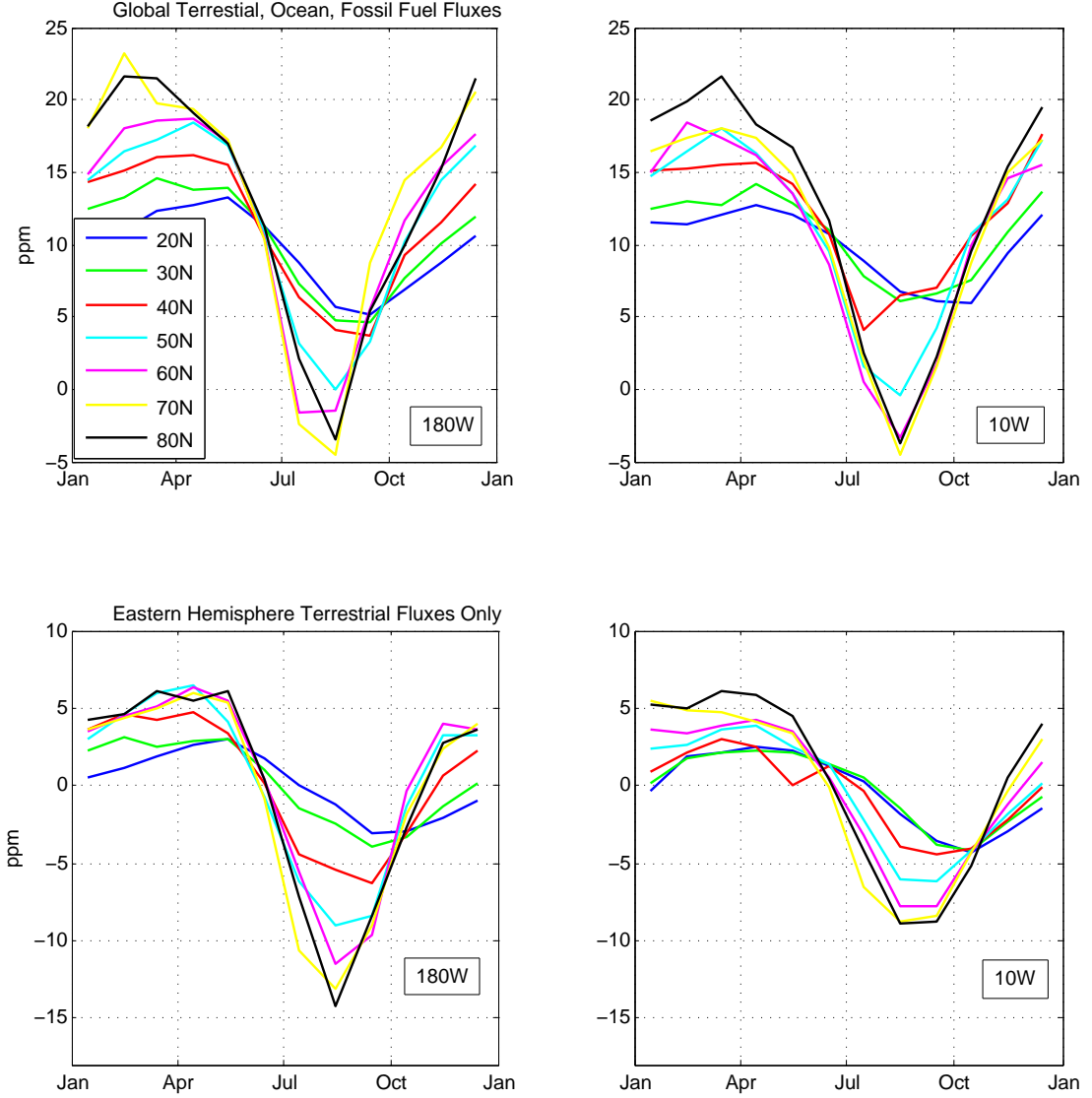
Figure 4.2: Seasonal cycles of monthly mean surface CO_2 at $180°W$ (left) and $10°W$ (right) from 20-80°N for EX1 (top) and EX2 (bottom). The 180°W transect is just off the Asia coast to represent gradients flowing off of Asia. 10°W represents gradients modified by baroclinic eddies just before reaching Europe.

demonstrates the importance of baroclinic eddies in mixing CO_2, such that when summer surface sources/sinks over NA are not interacting with the atmosphere, the latitudinal

gradient coming off of Asia (bottom left) decreases moving east over NA to just west of Eurasia (bottom right). This is in contrast to EX1, in which surface sources/sinks over NA (biogenic and anthropogenic) seem to help maintain latitudinal gradients as they flow across NA.

Sampling CO_2 from EX2 for composite cold front events (as was done for EX1, see caption in Figure 4.13 for description) indicates that synoptic variations at the surface can occur purely as a result of mixing of large-scale inflow (not shown), more so in the summer when inflow gradients are typically stronger (Figure 4.2). The patterns take the same general shape at each station, with CO_2 rising prior to frontal passage and decreasing afterwards (except for SOBS which, unlike the other sites, experiences counterclockwise wind shifts prior to frontal passage, where wind direction is more steady out of the south at the other sites). This result is not surprising since wind direction is typically southwesterly prior to frontal passage, bringing in higher CO_2, and northwesterly after the frontal wind shift frontal, bringing in lower CO_2 from the north; this is consistent with the sign of the inflow latitudinal gradient interacting with each station. In many cases the shapes are similar to patterns from EX1, but the magnitude of the variation is much weaker.

Theoretically, the magnitude of variability should be less if, for example, the weaker inflow gradient from EX1 (which is slightly more realistic since global fluxes are allowed to interact with the atmosphere) were used as inflow for EX2 (see Figure 4.2 for comparison of inflow gradients). Taking this one step further, flask observations over the Pacific Ocean suggest the inflow gradient is weaker than modeled in EX1 in the summer and winter (see Figure 4.3). Assuming weaker inflow gradients lead to weaker variations over the continent, these comparisons of inflow gradients, which become weaker as the atmosphere approaches reality and a world which contains sinks for fossil fuel, suggest large scale influences might not be quite as significant in the real world atmosphere.

So the question that remains to be answered pertaining to this study is how important background CO_2 is in creating observed synoptic variations compared to mixing of CO_2
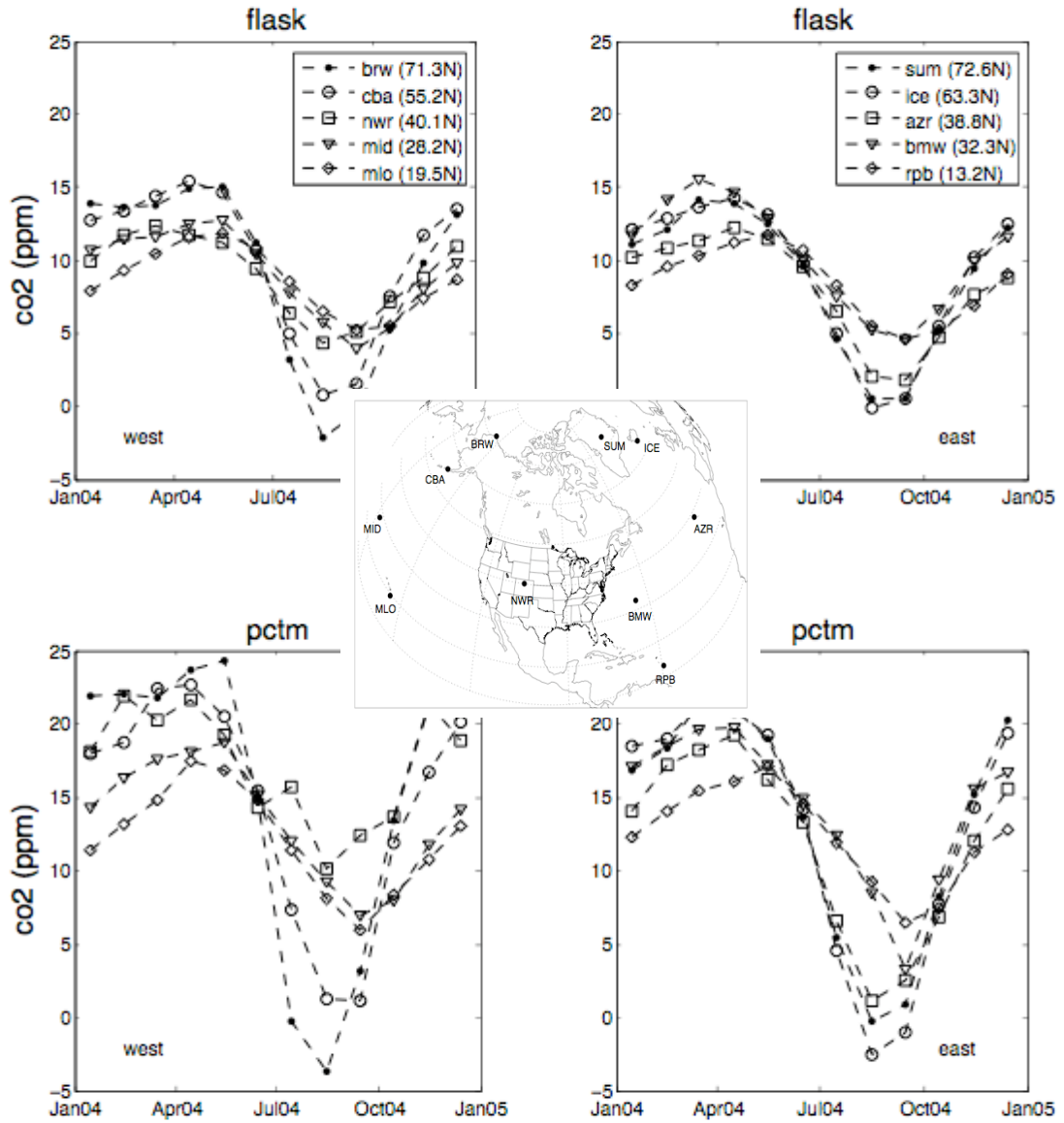
Figure 4.3: Seasonal cycles of monthly mean CO_2 at remote flask sites (NOAA GMD) surrounding the east and west coast of NA. The top plots are observed flask data for 2004; the bottom plots are model results sampled at the grid cell containing the flask locations. The middle image shows flask locations west and east of NA.

gradients created by continental surface fluxes. Making correlations between day-to-day variations at grid points in EX1 and EX2 can give a partially satisfying answer to this. Correlation maps between the two experiments are constructed over North America in January and July and are shown in Figure 4.4. They show that the correlation is strongest
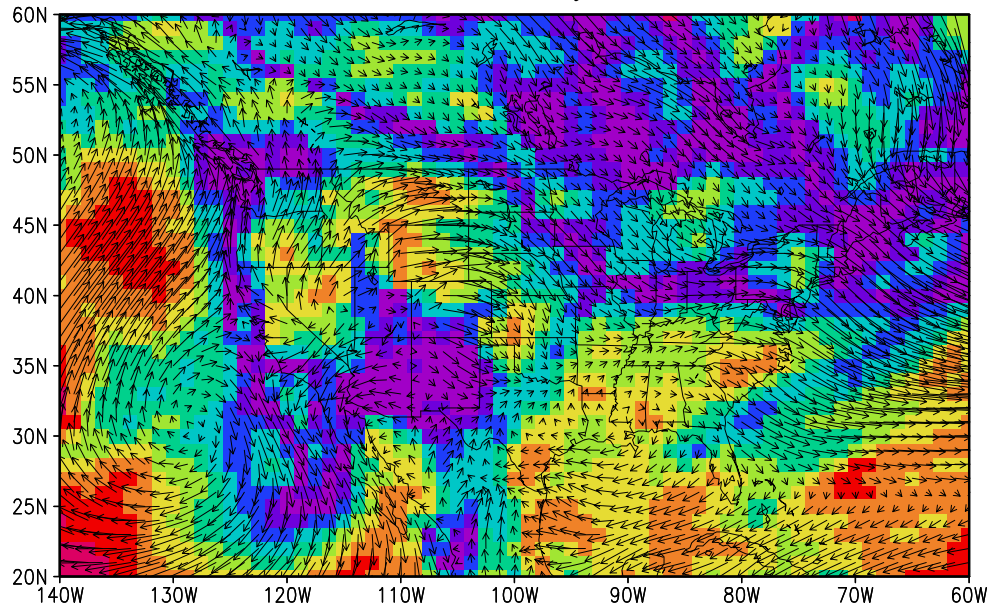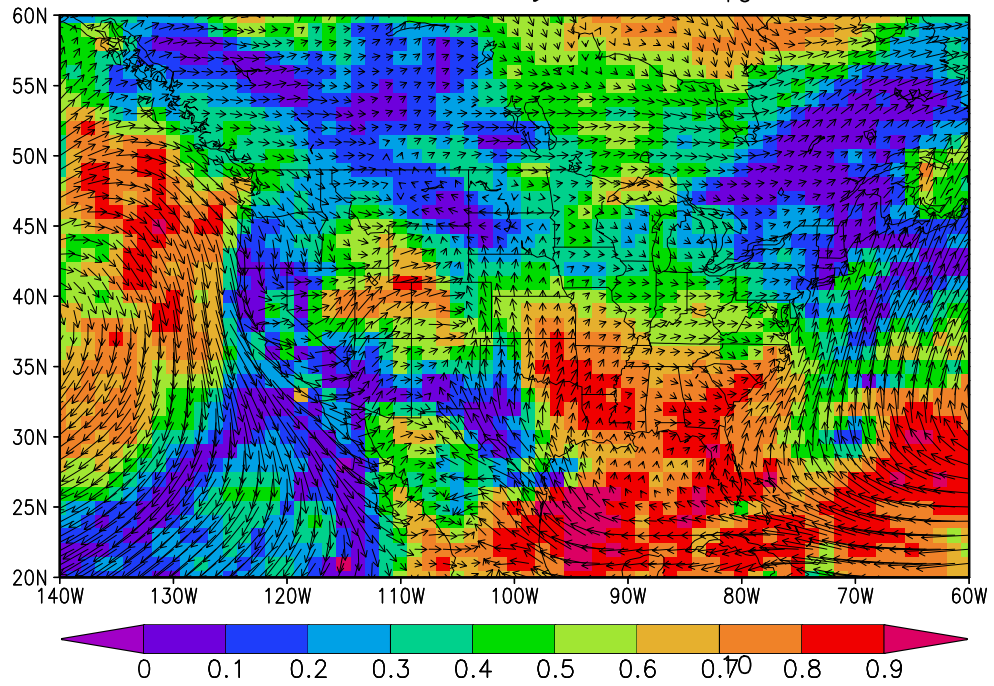
Figure 4.4: Correlation map of mid-afternoon CO_2 from EX1 and EX2 in January and July at the lowest model level.

(¿ 0.6) in January and July off the Pacific Northwest coast, over the Rockies, in the Gulf of Mexico, and in the Southwest. These regions have the common factor of ambient background air experiencing weak to nonexistent NA terrestrial influence. The correlation is much weaker inland (¡ 0.5), suggesting that the amount of large-scale inflow influence depends on the amount of regional terrestrial influence and that: 1) large-scale inflow should be considered as a lateral boundary condition for regional simulations since mixing of large scale flow causes some variability at the surface (more depending on the amount of large scale flow reaching the surface) and 2) mixing of PBL CO_2 established by regional surface fluxes appears to dominate continental synoptic variations with large scale inflow responsible for about 0-25% of the variance (more in the Southwest).

4.3   Terrestrial Controls

CO_2 within the PBL is largely controlled by local anthropogenic and biogenic surface fluxes. The magnitude and sign of daytime NEE depends strongly on relationships between photosynthesis, vegetation type and solar radiation. Spatial differences in vegetation plays a large role in establishing time-averaged horizontal NEE and CO_2 gradients. This is particularly important at regional and continental scales where differences in biome type are more important (e.g., agricultural transition to mixed forest in upper Midwest, Hurwitz et al., 2004). Anomalous NEE and CO_2, which we define to occur at synoptic scales, can arise locally from plant response to alternating weather patterns within a region (Higuchi et al., 2003) associated with midlatitude cyclones and/or remotely transport of upstream fluxes. Spatial differences in fossil fuel fluxes also contribute to CO_2 gradients. This section analyzes how NEE gradients may be established at monthly and synoptic time scales. Fossil fuel influences are also considered.

A good way to characterize time mean spatial NEE gradients is to make comparisons to NDVI. Figure 4.5 shows the modeled relationship between GiMMSg NDVI (30-day maximum value composite) and NEE in January and July in NA in 2004. Exceptions ex-

ist in the Southeast and Pacific Northwest in the summer where NDVI detects plants but soil/atmospheric stress suppresses photosynthetic uptake.
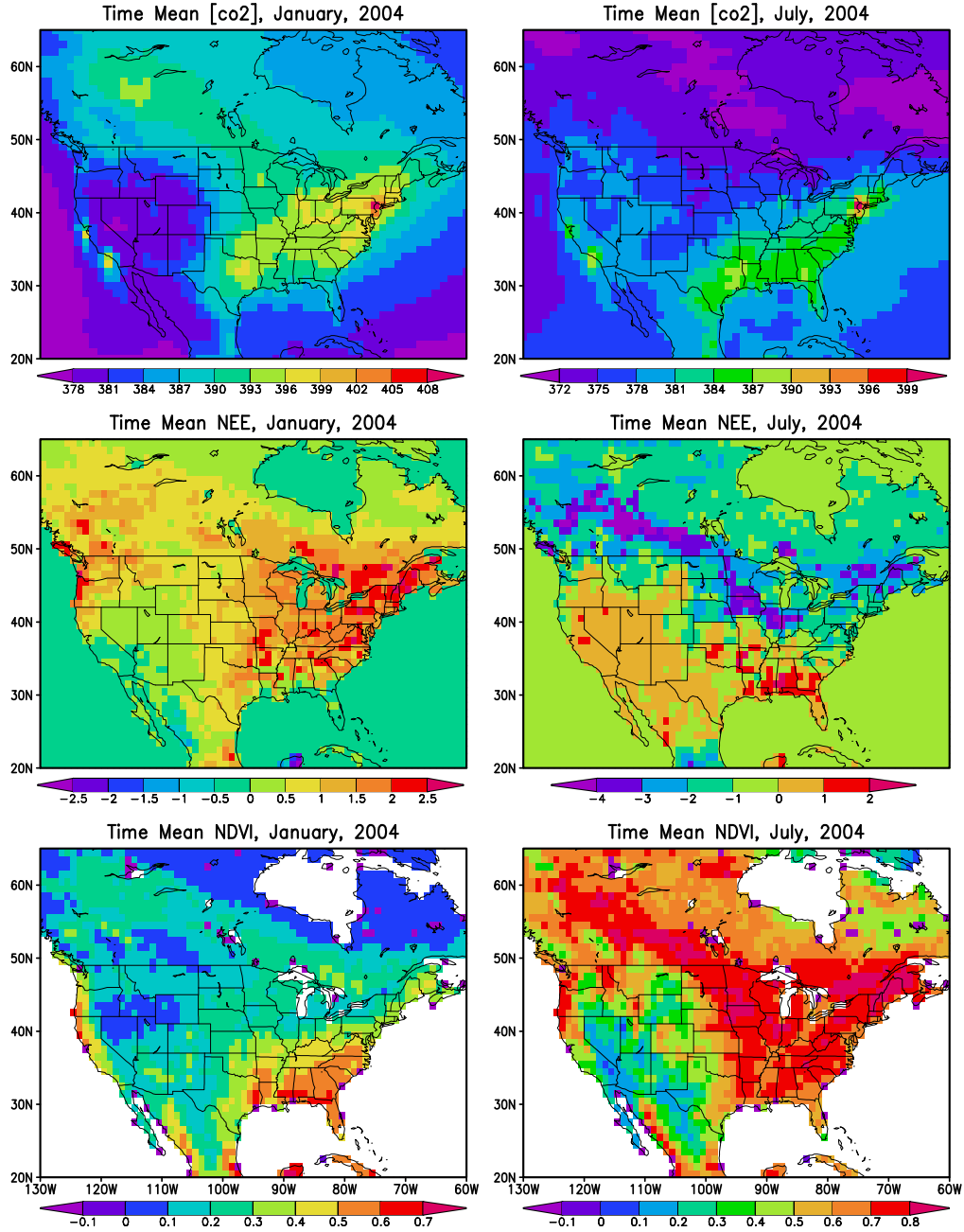
Figure 4.5: Model dependence of time mean CO_2 (30-day, top) at lowest model level on NEE (middle) and NDVI (bottom) in winter (left) and summer (right)

Atmospheric CO_2 at the lowest model level tends to follow the sign and strength

of NEE, as well as its seasonality, especially in boreal Canada and upper Midwest. The correlation is masked somewhat in regions where fossil fuel emissions are the largest, such as in the Northeast where buildup in the PBL by fossil fuel seems to exceed photosynthetic drawdown over a monthly average. Also note how the transition from net release to net drawdown above $40°N$ from January to July, with relatively weak transitions below $40°N$, tends to alter spatial gradients in CO_2 between seasons, especially North-South (N-S) gradients. Here we hypothesize that the seasonality of sign and strength of time mean spatial gradients, coupled with systematic clockwise wind shifts associated with cold fronts, plays an important role in determining the shape of synoptic CO_2 patterns.

Two types of synoptic weather are considered for creating anomalous CO_2 gradients. The first is associated with air mass development that occurs during the period in between frontal episodes when high-pressure ridges settle in and fair weather dominates. This will have varying effects on NEE depending on ecosystem and time since frontal passage last occurred. Postfrontal airmass modification, for example, often leads to enhanced drawdown (Freedman et al., 2001), setting up an environment conducive to negative CO_2 anomalies in the PBL due to negative surface fluxes. If a region, on the other hand, has been exposed to fair weather for extensive periods such that plants become biologically stressed, positive anomalies may result. This may happen under prolonged influence of a high-pressure ridge that causes large-scale subsidence, hot and sunny weather, and reduced precipitation (unless thunderstorms are common in the area in which case environmental stress is less likely). If CO_2 anomalies occur downstream of a cold front they have the potential to be carried along with the front under deformational flow (see next section for discussion).

The second type of synoptic weather occurs along cold front boundaries and is typically characterized by forced convection, deep convective clouds, precipitation (sometimes), and reduced radiation, all of which tend to reduce photosynthesis at the time of frontal passage. This study is not limited to fronts that produce precipitation, so variable NEE responses due to synoptic weather alone are expected. We consider this as local ecosystem

response to synoptic weather and assume the signal is left behind the cold front (second term of equation 4.2).

An important distinction between NEE and fossil fuel emissions is that fossil emissions only contribute to positive CO_2 anomalies. Like NEE, the magnitude of fossil fuel influence depends on season and location, but for different reasons. Table 4.1 summarizes the correlation of observed hourly CO_2 variations to the fossil fuel tracer of PCTM for winter (DJF) and summer (JJA) at several NA sites. Over 50% of observed winter variations at LEF and AMT can be explained by advection of fossil fuels from nearby industrial centers

	SUMMER			WINTER		
	r	RR	b	r	RR	b
SGP	0.240	0.058	2.350	0.597	0.357	1.818
LEF	0.242	0.058	3.670	0.725	0.528	1.729
SOBS	-0.224	0.050	-8.567	0.648	0.420	3.568
FRS	0.118	0.014	1.900	0.513	0.264	0.946
AMT	0.131	0.017	0.611	0.762	0.580	1.008

Table 4.1: Statistics comparing fossil fuel tracer to observed CO2 in the summer and winter for 5 stations with eddy covariance data. Shown is the correlation (r), percent of variance explained (RR), and regression coefficient (b).

(see Chapter 2 for discussion of industrial influence by site), with fairly high values at the other sites in the winter as well. The correlation of the fossil fuel tracer to total model CO_2 (fossil fuel + SiB + ocean) is also very strong, indicating that a significant portion of both model and observed synoptic variations are explained by fossil fuel emissions. The influence is much stronger in the winter than summer because of fossil fuel buildup within the stably stratified winter PBL (signal diluted by convection in the summer) and reduced magnitude of NEE from summer to winter relative to fossil fuels. The SiB tracer is also important in the winter, also leading to positive anomalies, but is clearly more dominant in the summer.

4.4 Organization of Gradients Along Frontal Boundaries

The timing of many of the large spikes/dips in the simulations and observations seems to correlate fairly strongly with the passage of bands of high/low CO_2, or zones of strong horizontal gradients in general, along the surface. There are many examples in the simulations where gradients appear to organize along frontal boundaries and take the shape of cold fronts (compared to surface maps and model diagnostics of frontal location), as if frontogenesis were acting on CO_2 as it does on density fields. There are instances where CO_2 bands evolve out of smaller CO_2 anomaly pools that then organize along converging wind fields associated with cold fronts (see Figure 4.6 for example).

One theory for this phenomenon is that CO_2 gradients at the surface are acted on by horizontal shear caused by a combination of shearing and stretching deformation flow along cold front boundaries. If CO_2 is treated as a passive tracer in a horizontal flow field using kinematic theory (Holton, 2004), deformational forces can act to weaken or strengthen gradients at the surface according to

$$\frac{D_g}{Dt}(\frac{\partial C}{\partial x} + \frac{\partial C}{\partial y}) = -(\frac{\partial u_g}{\partial x}\frac{\partial C}{\partial x} + \frac{\partial v_g}{\partial x}\frac{\partial C}{\partial y}) - (\frac{\partial u_g}{\partial y}\frac{\partial C}{\partial x} + \frac{\partial v_g}{\partial y}\frac{\partial C}{\partial y}) \quad (4.7)$$

where shear deformation (2nd and 3rd terms on RHS) can rotate a parcel through shear vorticity, concentrating CO_2 gradients along lines of maximum shear, and stretching deformation (1st and 4th terms) deforms tracer fields through stretching parallel to the shear vector (shrinking perpendicular to shear vector) such that CO_2 concentrates along the axis of dilation. Figure 4.4 demonstrates this nicely. In a nonhydrostatic atmosphere CO_2 diverges vertically under horizontal convergence at the surface, which it seems to do in the simulations (example shown later), but this is still a good model for explaining how gradients may be concentrated, strengthened and/or maintained along frontal boundaries.
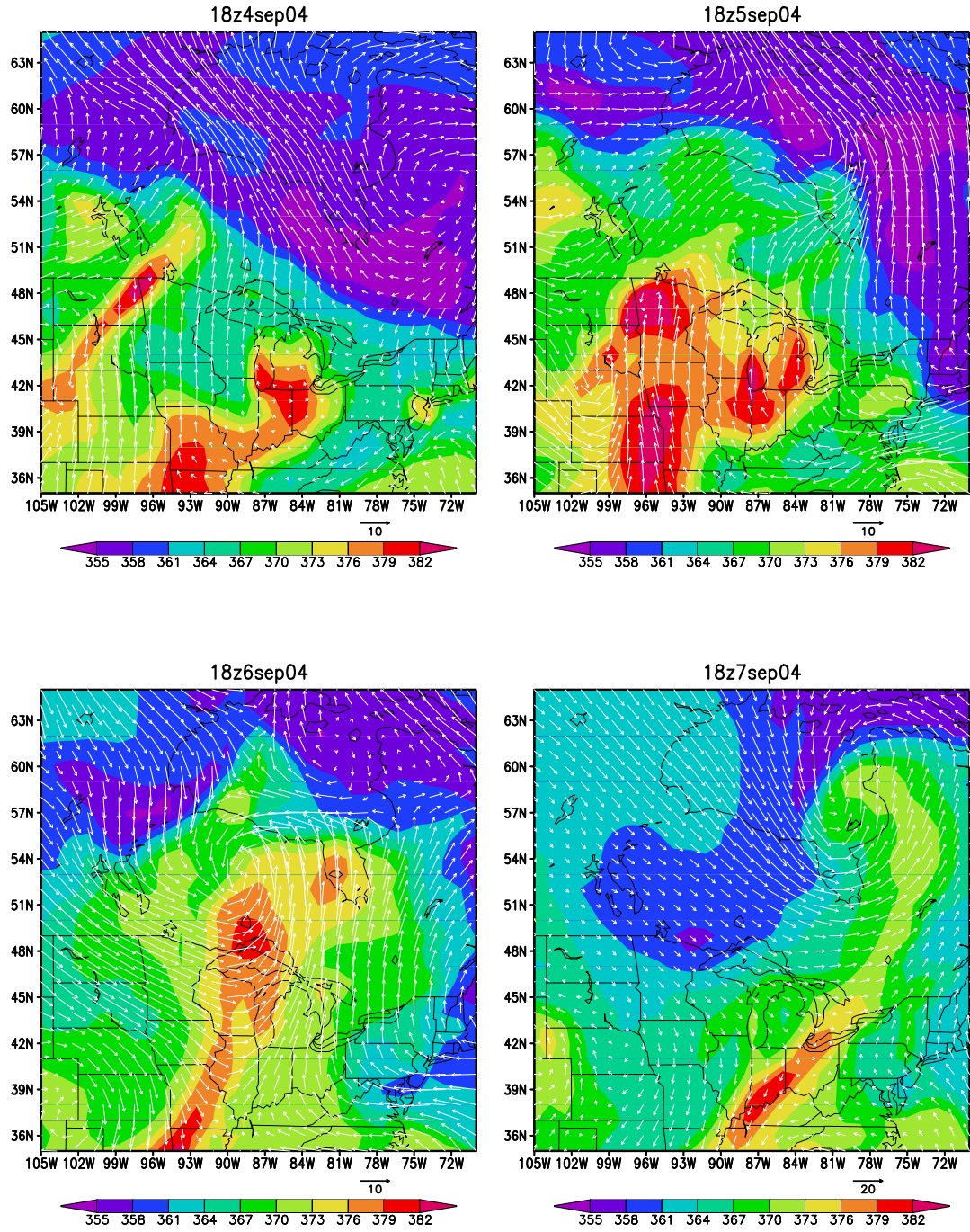
Figure 4.6: Evolution of positive CO_2 surface anomalies over 4-day period (from left to right, top to bottom, each image is a snapshot) into string taking shape of cold front through deformational flow. CO_2 is shaded with wind vectors overlaid to show deformation field.

4.5   Maps of CO$_2$ Budget Terms

We attempt to explain synoptic variations in the PBL in terms of mixing and local ecosystem response to synoptic weather by making maps of each term in the budget equation. This provides a means to reconstruct CO$_2$ signals associated with mid-latitude cyclones in terms of atmospheric dynamics and local variations in NEE to determine when and where each term in the budget equation is most important.

In order to assess the relative importance of each term of Equation 4.2 to PBL averaged CO$_2$, we solve for ΔC using $\Delta t = 3$ hours (since this is the output interval of PCTM) to get the change in concentration in the PBL over 3 hours as a function of 3 hour aggregated NEE and transport. For convenience, we then divide by 3 to get 1-hour tendencies. We quantify each term both as a tendency (ppm/hr) and as a percent contribution to the modeled (PCTM output) change in CO$_2$ by dividing by the sum of terms, such that if flux (referred to as NEE in text, flux in plots, and represents flux emissions into the PBL) is denoted by F, vertical advection by V, horizontal advection by H, vertical cloud transport by C, and all mechanisms by T, the percent contributions would be F/T, V/T, H/T, and C/T. Negative values represent negative contributions and vice versa. A value of 1 means that term explains 100% of positive tendencies in PBL averaged CO$_2$ (-1 represents 100% of negative tendencies). This is useful because our simplified budget equation (simplified, for example, in that a simpler formulation than in PCTM is used for vertical transport) will most likely be unable to perfectly reconstruct 1 hour changes modeled by PCTM; it should be close, however, and this method is designed to quantify and explain the relative importance of four mechanisms at various scales.

In the following sections, monthly and daily mean mechanisms are analyzed. Only daylight hours are considered in order to avoid potentially large variations due to nocturnal buildup which would tend to dominate other variations in the summer. By ignoring night-time processes the chances of seeing the effect of weather and climate on NEE is greatly improved.

4.5.1   *Monthly Budget*

Monthly averaged components are analyzed by taking the 30-day daytime-only average of each term in Equation 4.2 to get time mean 1-hour changes in PBL CO_2; results for the summer are shown in Figure 4.7. It is useful to first assess the ability of the budget equation to reconstruct monthly mean dC/dt modeled by PCTM. For this we compare the top two plots of Figure 4.7. The results show that the budget equation successfully predicts the spatial pattern of dC/dt and, for the most part, the correct magnitudes. Now we try to explain monthly mean dC/dt in terms of individual mechanisms.

Horizontal advection is essentially negligible on monthly time scales compared to NEE and vertical transport. This is especially true in the continental interior where fair weather events, combined with advection of both positive and negative CO_2 anomalies during synoptic events, cause advection to zero out over long enough time scales. This result is consistent with Bakwin et al. 2004 where only surface fluxes and vertical mixing were assumed most important at monthly time scales. This is not true on the coast or at industrial centers, however, where horizontal gradients tend to be more constant over seasonal time scales (e.g., Los Angeles, New York, Chicago).

The results also show that CO_2 tends to be depleted on average over 1 hour in the daytime over all of NA. This is especially true east of the Rockies and along the agricultural belt and up into Canada. The zone of depleted CO_2 is centered in the South in Arkansas, the magnitude of which weakens moving out from that point. This low CO_2 zone is not solely a result of negative NEE; rather, it is a combination of vertical mixing and surface fluxes.

Assuming horizontal advection is indeed negligible, there are three reasons PBL CO_2 may be depleted at monthly time scales: 1) NEE removes CO_2 faster than vertical advection supplies it, 2) vertical advection removes CO_2 faster than NEE supplies it, or 3) uptake and depletion by vertical advection combine to remove CO_2. Since daytime NEE causes CO_2 to be depleted on average, reason 2 does not appear to apply in the summer. Reason 3
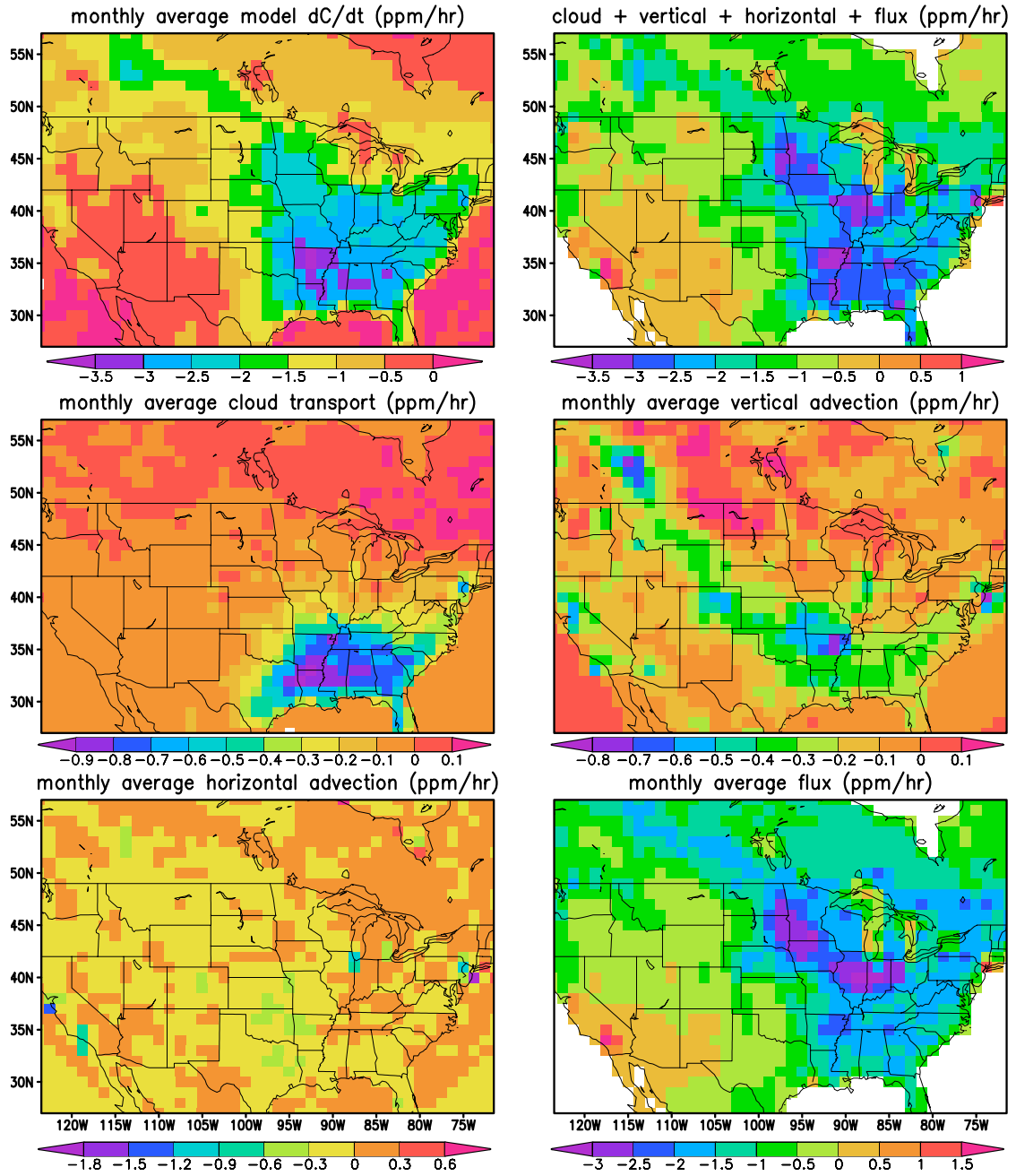
Figure 4.7: Time mean 30-day average terms in budget equation. Absolute concentration (in ppm) are shown. Time is centered on July 22, 2003. The middle and bottom rows represent mechanistic components that cause changes to PBL averaged CO_2. Reconstructed changes over 1 hour are shown in the top right (dC/dt, sum of all terms); changes modeled by PCTM are shown in the top left (also dC/dt). The top right represents best guess values for the top left plot.

is somewhat valid in the Rockies, Great Plains, and Southeast. To a good approximation, however, monthly average daytime drawdown simply reflects NEE.

CO_2 is most depleted around Arkansas because of the third reason listed. Reason 3 is also partially true in the Southeast but the budget is still heavily dominated by NEE. Reason 1 is true in the upper Midwest and along the lee side of the Rockies north of about 40°N, where cloud transport is zero and vertical mixing by subsidence transports relatively higher CO_2 air from the free troposphere into the PBL, but vegetative uptake removes CO_2 at a faster rate. Vertical advection and NEE contribute weakly along the Rockies.

We can get an idea of relative contributions of each term by making maps of each term as fractions of the total (see Figure 4.8). This map clearly shows that horizontal
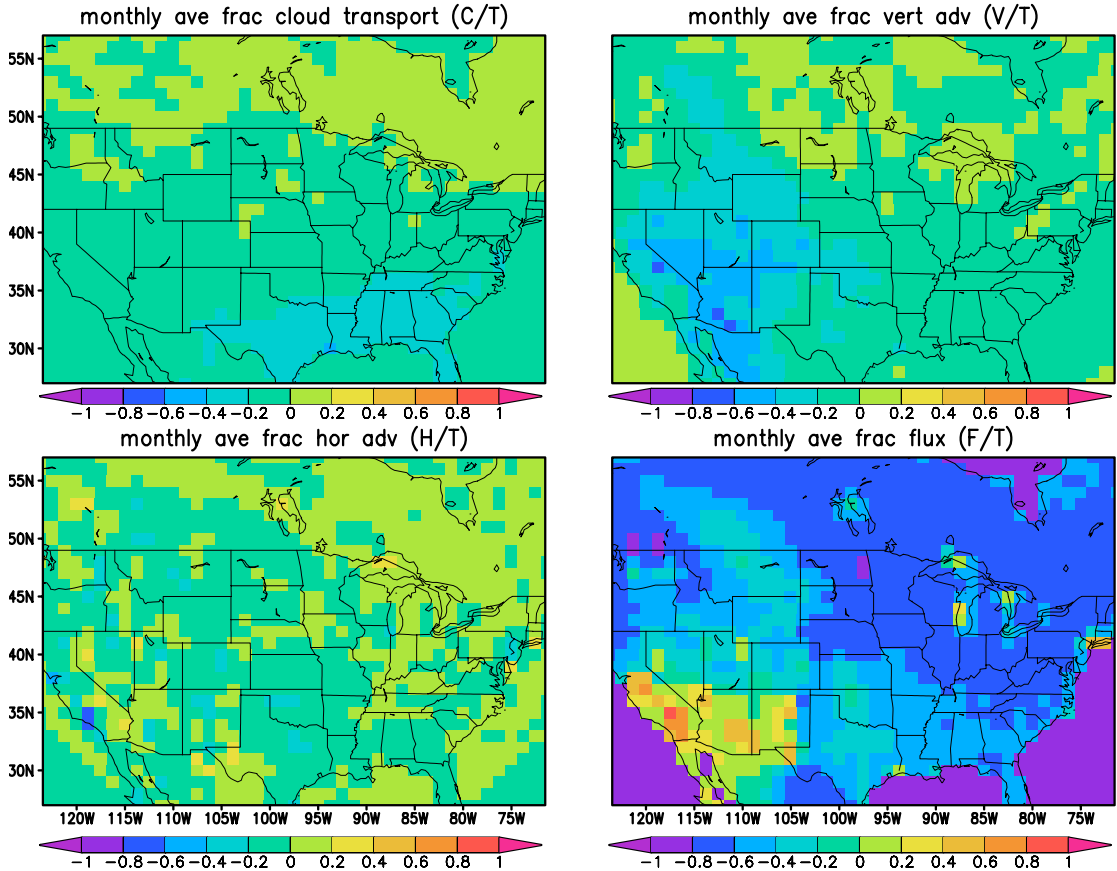
Figure 4.8: Same as middle and bottom rows of Figure 4.7 except time mean fractional contributions are plotted. Reconstructed and modeled dC/dt are excluded.

advection is negligible, negative vertical advection is strongest in the West and along the Rockies, positive vertical advection by subsidence is strongest in the lee of the Rockies in Canada, vertical cloud transport is strongest in the Southeast, and that NEE is negative everywhere except in the Southwest and almost completely dominant everywhere east of the Rockies ($\sim$ 80%, less so in the South). These mechanisms combined lead to depleted CO_2 in the summer PBL over NA.

Patterns are quite different in the winter (not shown). dC/dt is slightly negative everywhere ($<$ .2 ppm/hr) except over industrial areas, the Southeast and along the east coast up into the Northeast ($\sim$ 0-1 ppm/hr). There is just enough uptake to deplete the PBL in the Southeast but only by $\sim$ 1 ppm/hr. Vertical cloud transport is almost completely negligible everywhere except in the Pacific Northwest ($\sim$ -.3 ppm/hr) and in the Northeast ($\sim$ -.2 ppm/hr), both regions of which typically experience a lot of storm activity in the winter. In the Northeast, negative vertical advection and cloud transport compensate just enough for positive NEE to cause slightly depleted PBL's in the winter. Everywhere else, in the Midwest and Canada for example, negative vertical advection and positive NEE essentially balance. Vertical advection is likely too strong in the budget equation in the winter as it was in the summer nocturnal PBL such that mismatches are partly attributed to excessive vertical advection. In all, PBL CO_2 is slightly (everywhere except Southeast) to moderately (Southeast) depleted. Each terms is much weaker than its summer counterpart.

4.5.2   Synoptic Budget

The budget equation behaves much differently at synoptic scales. A summer cold front in the Midwest demonstrates this nicely. Daily mean 1-hr tendencies are shown in Figure 4.9, The cold front is fairly zonal at about 35°W moving east to Alabama, at which point it becomes oriented to the northeast (see Figure 4.10). The Low core center lies around the Great Lakes. The results again show that the budget equation successfully reconstructs spatial patterns and magnitudes of dC/dt when under the influence of mid-latitude cyclonic
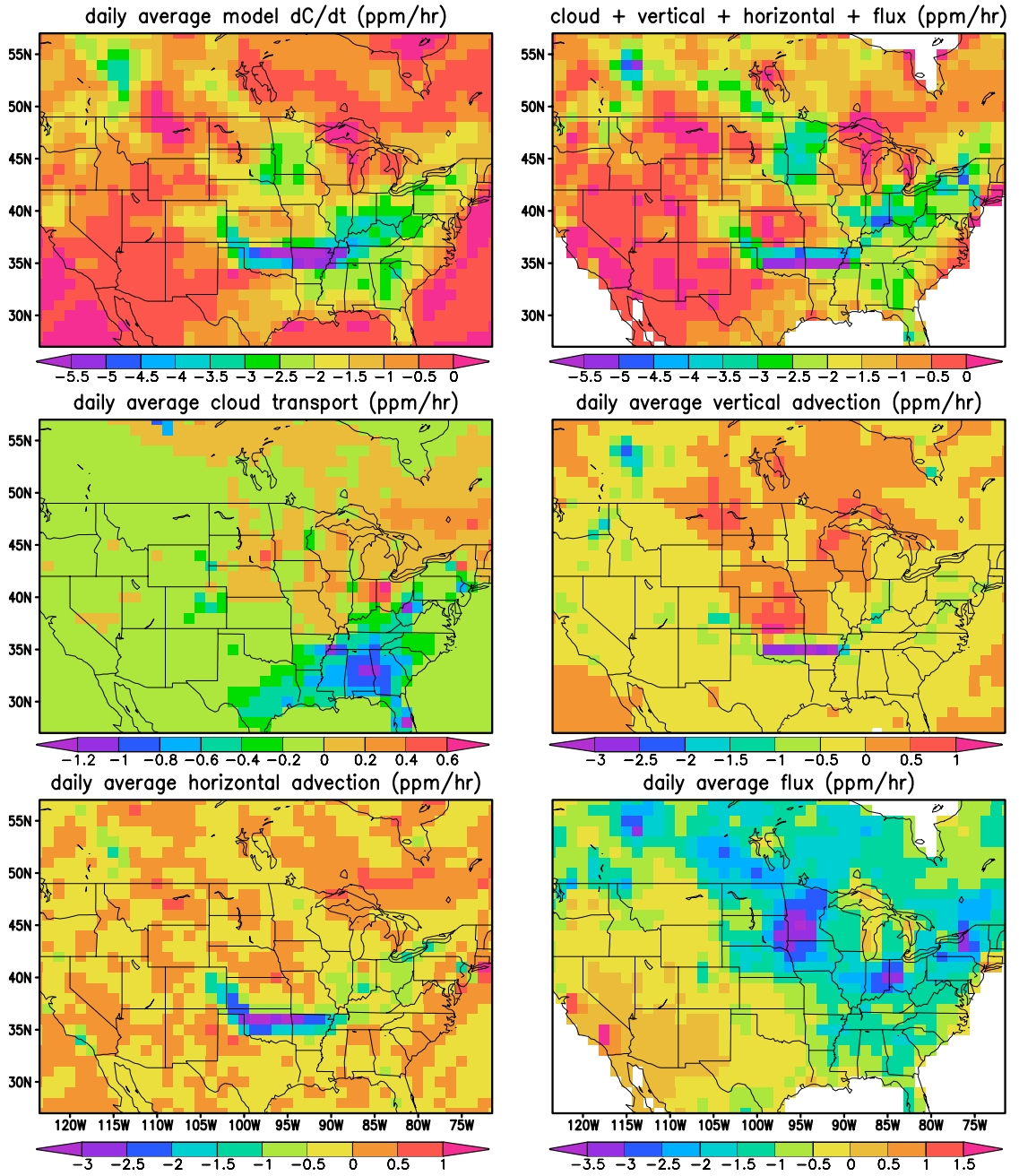
Figure 4.9: Same as Figure 4.7 except for daily means.

activity, most importantly the negative CO_2 anomaly along the cold front. There are few differences compared to the pattern predicted by PCTM.

All four terms have much spatial variability. Let's first consider mechanisms that occur along the cold front boundary where dC/dt is the largest ($\sim$ 10-20 ppm per day, top
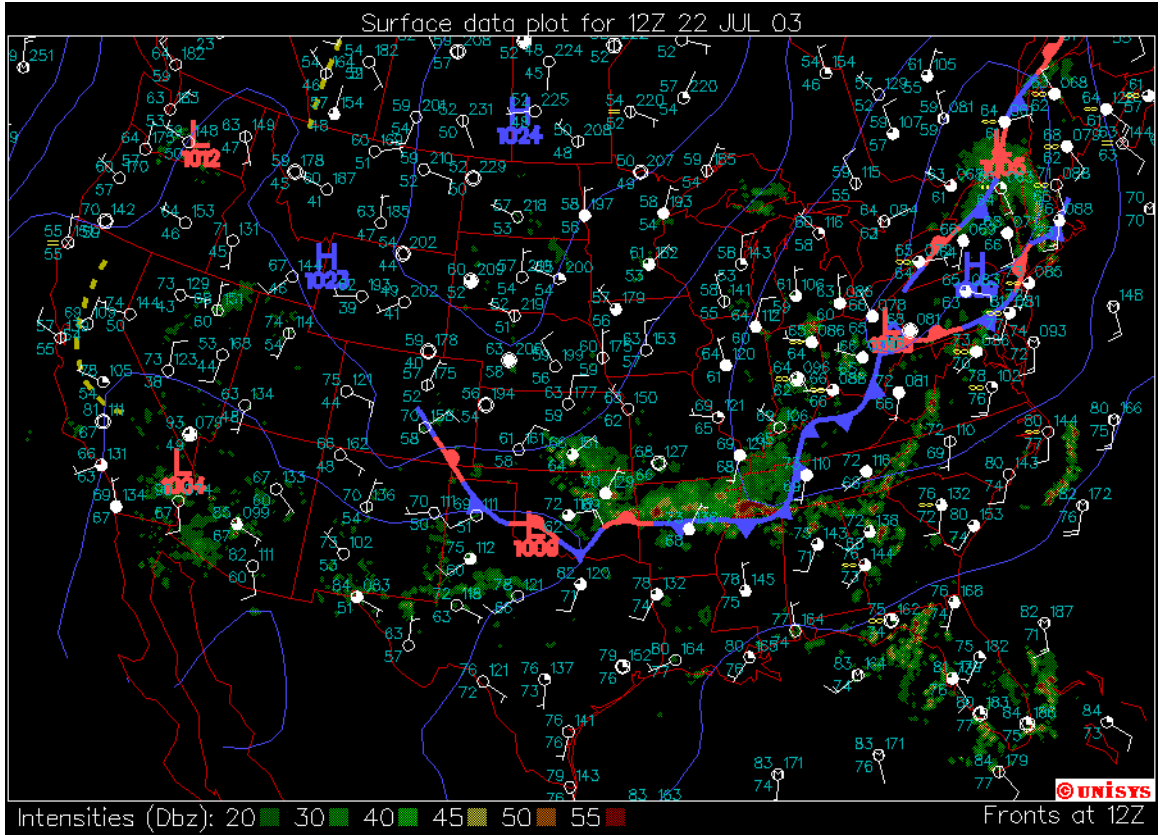
Figure 4.10: Surface composite map containing radar summary (color filled areas), surface data plot (composite station model), frontal locations (in various bold lines) and pressure contours (in thin blue lines). Unisys.

plots of Figure 4.10). This example shows that horizontal and vertical advection contribute strongly negatively throughout the entire length of the cold front boundary. Vertical cloud transport also plays a fairly strong role along the diagonal portion of the front.

Vertical and horizontal advection have the same sign at the edge of the cold front, most likely because of mass flux divergence. We can look at this in more detail by analyzing a vertical cross section running N-S across the front (see Figure 4.11). The front is approximately between 36 and 37°N. The first thing to note is that surface winds are northerly behind (north of) the front and southwesterly out ahead (to the south). This converging wind field helps give rise to vertical motion at 36°N, helping CO_2 penetrate deep into the free troposphere such that the vertical advection term is negative and removes CO_2 from the PBL. At the frontal boundary winds advect low CO_2 air south, the CO_2 gradient of

which is due to N-S gradients in NEE. The atmospheric dynamics, couple with NEE, cause these terms to be strongly negative along the front.
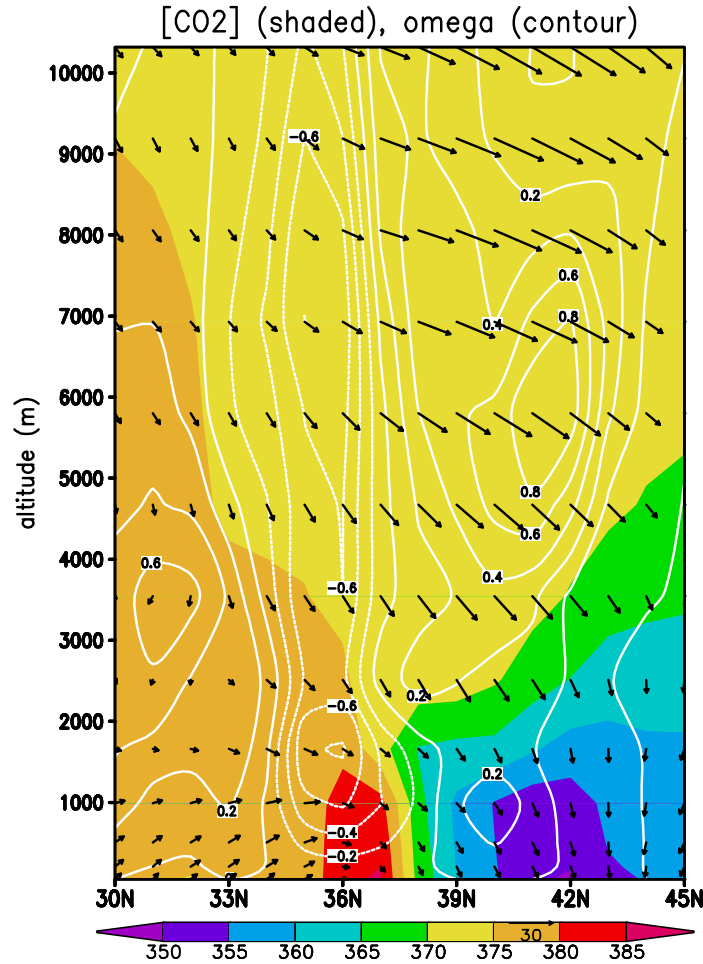
Figure 4.11: Vertical cross section along latitudinal transect at 93°W at 0z, July 22, 2003. CO_2 is shaded, omega (Pa/s) in white contours, wind vectors (m/s, northerly if arrow points down, easterly if left, etc).

The sign, magnitude, and pattern of synoptic NEE look fairly similar to its time mean component, consistent with the model light response curves of the top 2 right plots of Figure 3.19, which suggest little or no difference relative to the rest of the summer (although more data is needed). There are several places, however, where the average tendency over 1 day is slightly weaker, especially along the front near Arkansas, which

in this case produced significant cloud cover such that a large part of the South and East under the influence of the surface front and Low core center were exposed to cloud cover and reduced shortwave radiation (bottom plot of Figure 4.12). The reduced NEE appears to be a result of suppression of GPP and R_g due to reduced shortwave radiation (GPP more so than R_g relative to each other), at least when compared to the time mean (top and middle plots of Figure 4.12), although a combination of other factors may also be responsible. This result is consistent with Chan et al. (2004) and Wang et al. (2005).

Separate from convection that already occurs in the Southeast, vertical cloud transport tends to take the shape of the diagonal portion of the front. Cloud transport depletes CO_2 by up to 1-2 ppm/hr on average for this event. Although the pattern of daily vertical cloud transport does not differ much from its time mean component in this case, analysis of other frontal events that occur further north reveal similar patterns of bands of negative cloud transport on the order of 0.5-2 ppm/hr. Another common characteristic is the abrupt transition behind the front to nearly 0 ppm/hr, which is not surprising since both free and forced convection are more likely to be suppressed. The strength of transport tends to be strongest when the front is oriented from SW to NE in the Southeast where PBL buildup by positive NEE is strongest. It is also possible that this frontal orientation may be more favorable for convective mass fluxes.

Behind the cold front, along the border between Minnesota and the Dakotas, south into Iowa and Missouri, and north into Canada, NEE is clearly the more dominant process, as can be seen in the map of daily fractional contributions (see Figure 4.13). Although NEE was positive (net release) at the time of frontal passage (a day earlier in the Plains) due to reduced GPP under suppressed radiation, negative NEE on July 22, which is slightly stronger and more widespread (up into Canada) than in the time mean, may relate to post-frontal airmass modification, where the atmosphere is more favorable for uptake, especially by agriculture.

Also behind the cold front, in particular directly behind the front in Kansas and
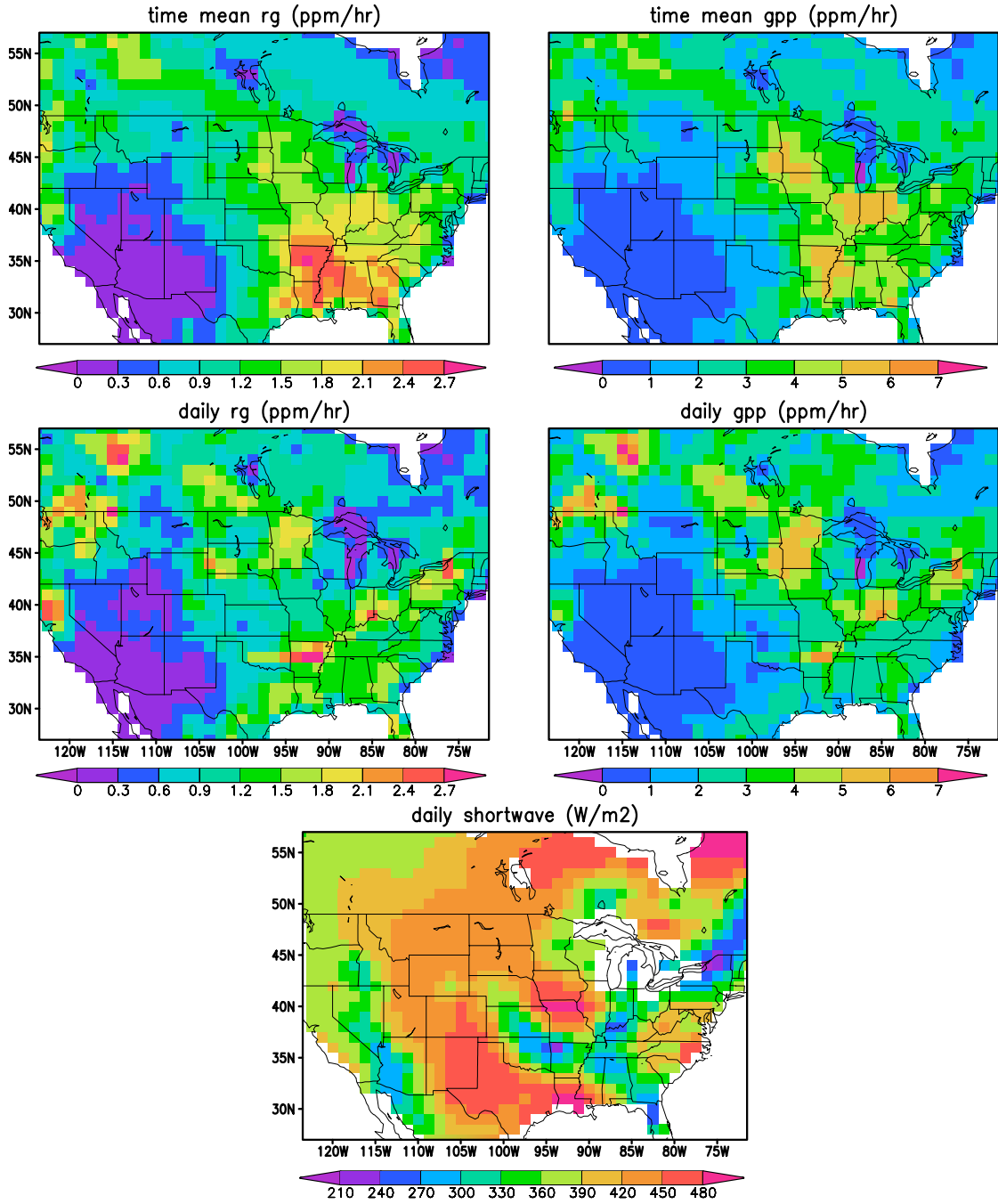
Figure 4.12: Comparison of monthly and daily average R_g and GPP and their relation to NCEP2 shortwave radiation during the July 22, 2003 cold front.

farther north in Wisconsin and western North Dakota, vertical advection contributes positively. This is probably associated with the cold conveyor belt, where cold air advection behind the surface front tends to cause sinking motion. This subsidence also suppresses any
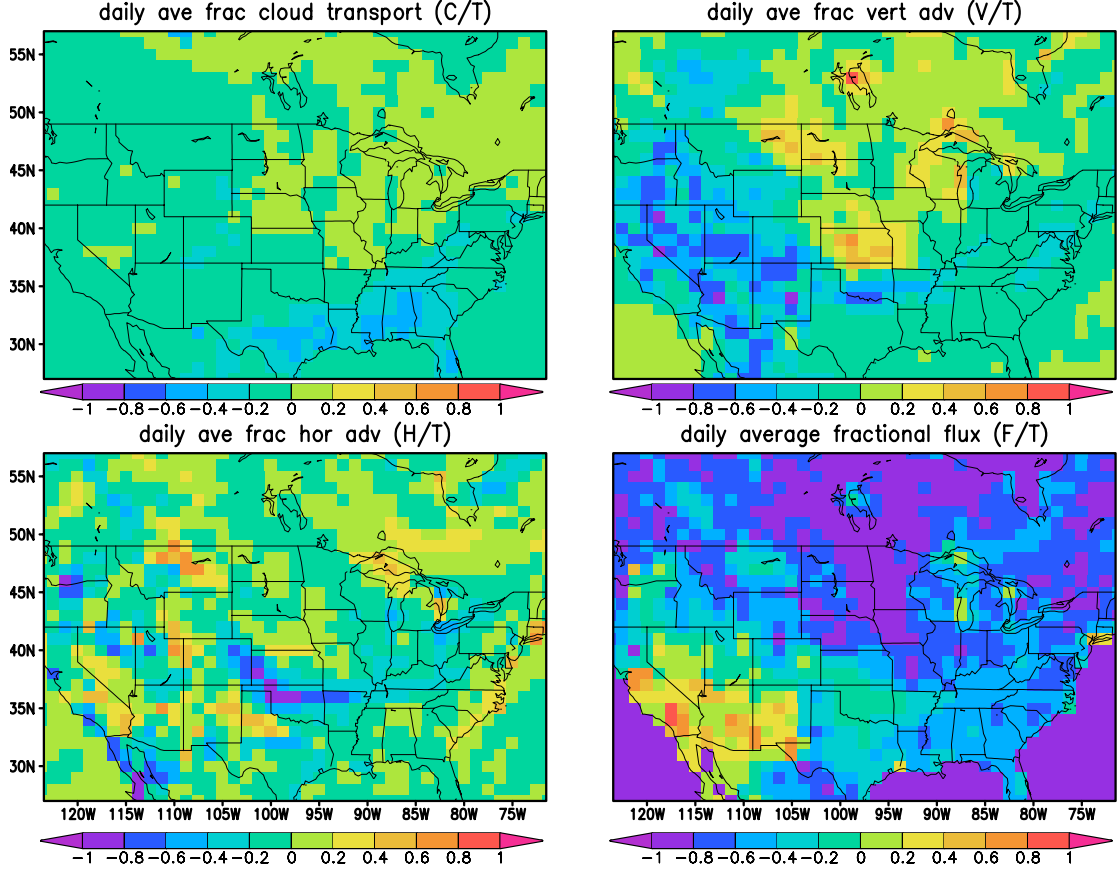
Figure 4.13: Same as Figure 4.8 except for daily means. Time is valid for July 22, 2003 (terms correspond to concentrations in Figure 4.9.

cumulus convection. In this case subsidence occurred in a region where the vertical CO_2 gradient was strongly positive because of strong surface uptake (see Figure 4.11).

To complete our model cyclone we should also expect to see rising motion in the warm sector between the cold front and warm front with southwesterly winds. This is clear in maps of vertical and horizontal wind and is also indicated in the middle right plot of Figure 4.9 along the Appalachians and Ohio River Valley by advection of CO_2 out of the PBL through adiabatic ascent. This is more clearly seen in the vertical cross section in Figure 4.14. The model of rising south and sinking north seems to be simulated in PCTM and conveyed in the budget equation.

Our analysis of all mechanisms combined leads us to an important conclusion. Since
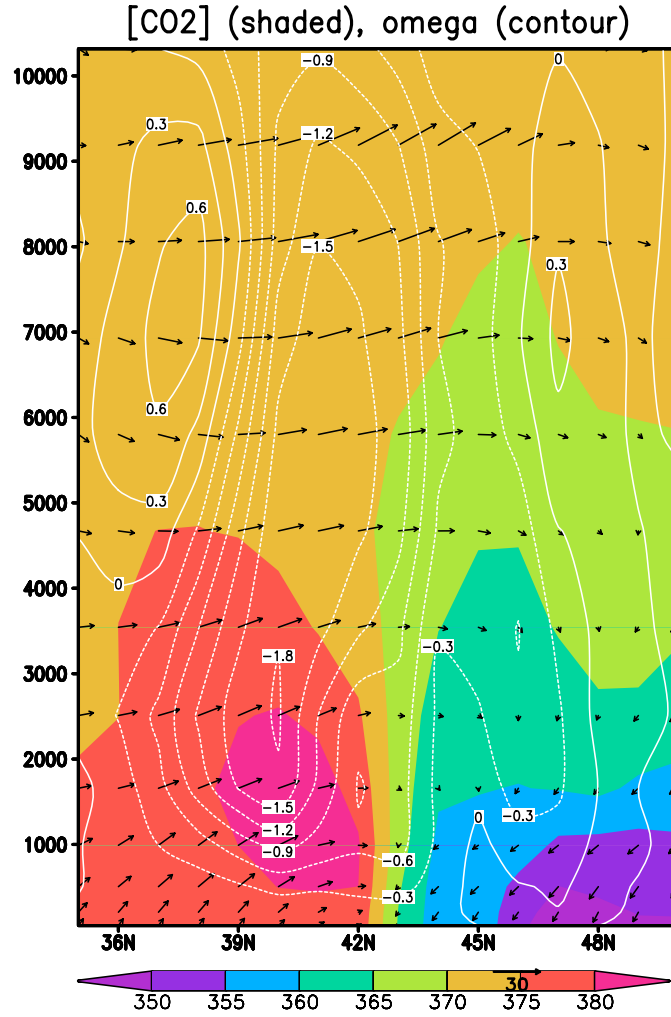
Figure 4.14: Same as Figure 4.11 except for a warm front along the 84W N-S transect between 35 and 50°N.

the negative CO_2 anomaly is stronger along the front than behind or ahead of it, there is indication that advection is more favorable for sudden CO_2 spikes/dips along the front, especially in this case where horizontal and vertical mixing have equal sign. Vertical cloud transport also contributes significantly to negative frontal anomalies. This, however, does not rule out the importance of flux response to frontal weather; only one case has been analyzed thus far.

Analysis of other summer midlatitude cyclones in NA reveals very similar patterns as in the above case study, with horizontal and vertical transport (advection and via clouds)

strong at the frontal boundary and negative NEE anomalies and positive vertical advection common behind the front, especially in the upper Midwest. The strength of all transport processes varies with each front, as does the magnitude of surface flux and its response to frontal weather. Horizontal advection depends on wind direction, wind speed, and the sign/magnitude of CO_2 anomalies advected along with or in the path of the front. Horizontal advection leads to the largest spikes/dips right at the front because horizontal CO_2 gradients are strongest there.

A look at frontal passage events at the 8 NA continuous CO2 sites quickly rules out any generalizations about transport across the country compared to surface fluxes (see Figure 4.15) beyond that it is present during most frontal events. The figure shows that frontal average surface fluxes are small relative to transport at only 3 of the 8 sites (SGP, WKT, FRS). All transport terms are important surrounding frontal passage at these sites and cause strong depletion during and after frontal passage at SGP and WKT and significant increases at FRS before frontal passage. Surface fluxes are much stronger at HRV compared to transport in which case they typically cause depletion and look remarkably similar to the 'total' curve. Surface fluxes and the individual transport terms have about the same magnitude at the other sites. For the most part, horizontal and vertical transport are responsible for the large sudden day-to-day variations (e.g., SGP, WKT, SOBS, AMT, and WPL), but flux variations also contribute in a few cases due a sudden positive flux (LEF) or negative flux after being neutral for several days (WPL). It is important to note that only daytime average tendencies are shown; if nighttime values were included, the flux and vertical advection terms would change significantly. Daytime values only show the effect of frontal weather on NEE.

These results suggest that, although the case study showed that horizontal and vertical transport can be quite significant and dramatic, generalizations about frontal mechanisms should not be made and that each case should be analyzed separately since so many factors can come into play (i.e., most cases are unique). Examples of such factors include the
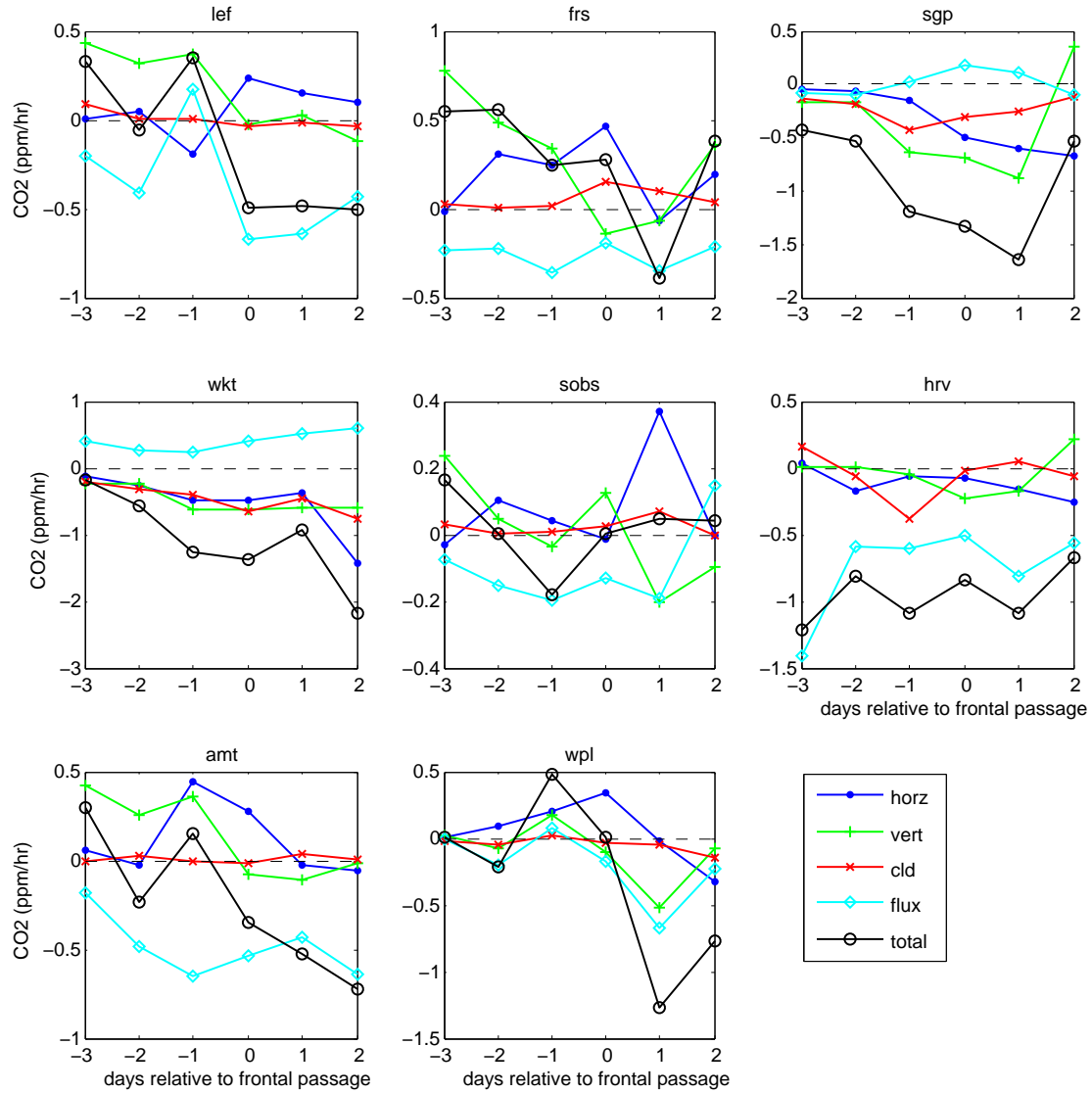
Figure 4.15: Frontal composites of mechanisms. The averaging procedure and frontal cases used are identical to the CO_2 composites in Figure 3.14 except that individual terms from the budget equation are plotted. The blue curve is horizontal advection, green is vertical advection, red is cloud transport, turquoise is surface flux, and black is the sum of the other curves. Each value represents a 1-hr mixing ratio tendency averaged each day during daylight hours only.

presence of upstream CO_2 anomalies (and their sign and strength), vertical motion, type of vegetation, condition of vegetation prior to frontal passage (e.g., temperature and/or moisture stressed), weather associated with cold front (precipitation, cloud cover, type of radiation allowed through, temperature, etc.).

The budget equation behaves differently in the winter in terms of relative importance of each term. Vertical advection is almost always negative in the PBL since vertical gradients are predominately negative (positive NEE in winter combined with fossil fuel emissions), and any vertical motion either removes high CO_2 in the PBL during convection (typically along cold front or around Low core center) or mixes in low CO_2 from the free troposphere during subsidence (behind front). Horizontal advection acts in the same way as in the summer. The magnitude of vertical advection is much stronger in the winter because of the buildup of negative vertical CO_2 gradients under stable winter PBLs. NEE is predominantly weakly positive in NA and is essentially unresponsive to synoptic weather. Positive anomalies seem to develop when vertical advection is weak, NEE is positive, and deformational flow concentrates gradients, which are then translated as spikes in the observations when acted on by horizontal advection. What is therefore typically seen during wintertime frontal passage is prefrontal spikes followed by depletion as vertical advection along the front dilutes the PBL. Figure 3.12 shows examples at several NA stations.

4.5.3   Reynolds Averaged CO_2

Here we analyze Reynolds averaged CO_2 using Equations 4.5 and 4.6 and consider vertical and horizontal advection of time mean and anomalous CO_2 gradients. The July 22 Midwest cold front is used for a summer analysis and the results are plotted in Figure 4.16. The results for this case show that horizontal advection along the cold front is dominated by anomaly CO_2 gradients, suggesting strong horizontal gradients have been established through a combination of anomalously strong N-S NEE gradients and deformational flow.

Horizontal advection of time mean gradients has a slightly different pattern and weaker signal (1-2 ppm compared to 5-7 ppm). The pattern is, however, consistent with time mean gradients in the upper right plot of Figure 4.5. This signal tends to counter the total advective signal but only slightly. Analysis of other synoptic events gives similar results and suggests advection of time mean gradients is negligible at the frontal boundary
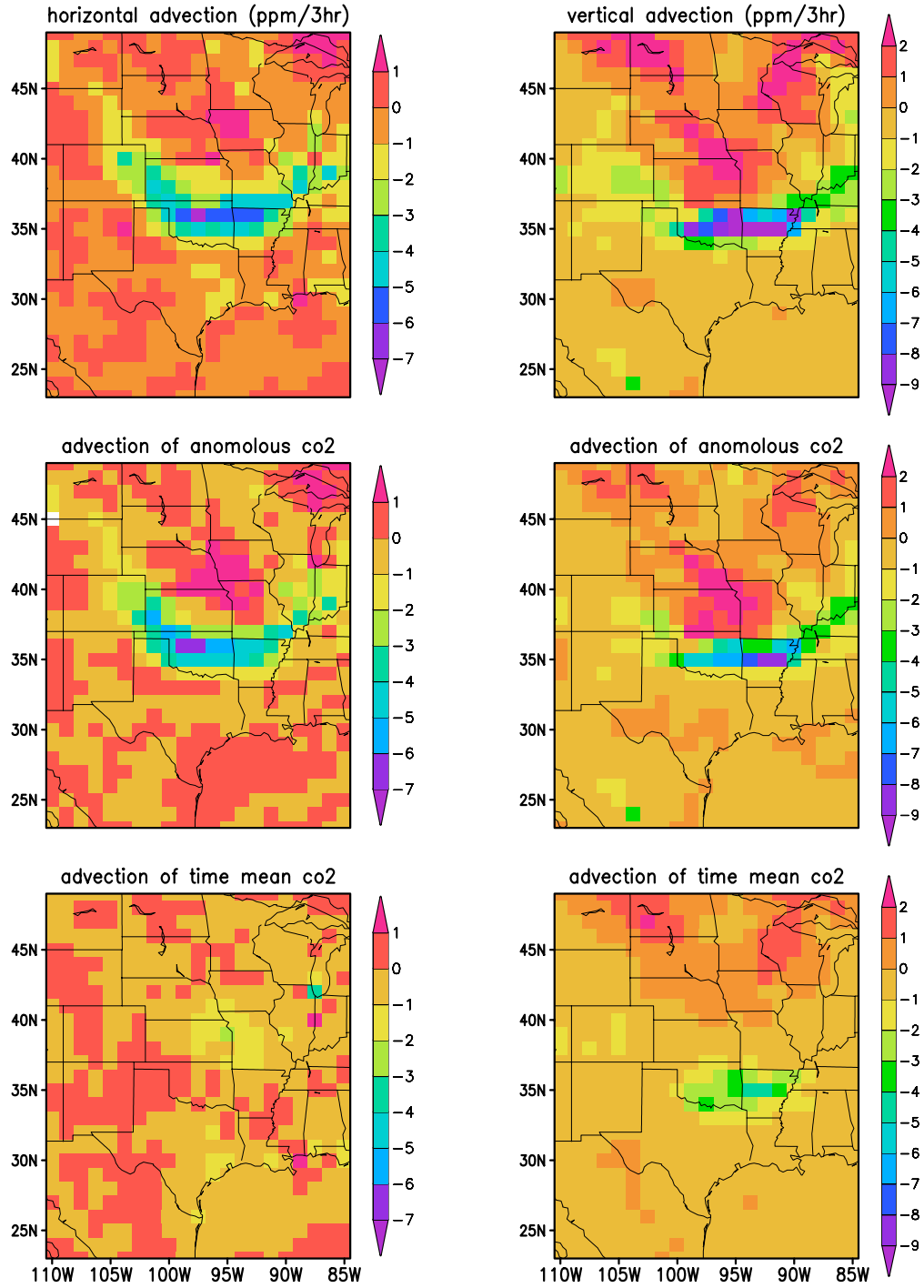
Figure 4.16: Horizontal (left) and vertical (right) advection of total (top), anomalous (middle), and time mean (bottom) components of PBL averaged CO2 concentration during a cold front on July 22.

compared to advection of anomalous gradients. Our hypothesis that systematic mixing of time mean gradients by frontal winds explains a large portion of frontal CO_2 variations does not appear to hold. Although advection along the front is enhanced somewhat, advection of anomaly CO_2 is likely most responsible for large frontal variations.

Vertical advection of anomalous CO_2 is also stronger than advection of time mean CO_2 at the frontal boundary where vertical gradients are stronger than normal because of NEE response to weather. Advection of time mean and anomaly CO_2 behind the front near the Dakotas is very similar. This analysis suggests that similar patterns of vertical advection of time mean and anomalous gradients exist everywhere; the strength of anomaly signals, however, is much larger surrounding fronts. The same is true for other events. This result does not hold for horizontal advection.

Chapter 5

CONCLUSIONS AND FUTURE WORK

5.1   Review of Objectives and Summary of Research

The major objective of this research was to gain a better understanding of mechanisms that cause variations in CO_2 within a PBL under the influence of cyclonic activity. In particular, huge day-to-day variations in observations are seen throughout the year at many continuous sites across NA and this study sought out to reproduce and explain those variations. Insight gained in such a study improves the ability to learn about CO_2 source and sink distributions through information contained in frontal weather systems.

To achieve this objective the study was broken into 2 major components: 1) model evaluation and 2) analysis of mechanisms. Model evaluation was essential for this study to determine whether SiB coupled to PCTM produced spurious CO_2 variations or not. To our knowledge such a detailed analysis of hourly SiB and PCTM had not been performed in the past. It was therefore critical to analyze SiB and GEOS4 in addition to PCTM coupled offline to SiB through GEOS4 to make sure correct results were not produced for the wrong reasons. Interpretation of CO_2 variations produced by PCTM was made possible once model limitations were more clearly understood.

Once satisfied the models were producing the correct frontal CO_2 patterns for the right reasons, analysis of mechanisms causing those patterns followed. A PBL budget equation was presented as the tool of choice for analysis of both biological (NEE) and physical (transport) mechanisms. Since transport mechanisms are mostly important for large CO_2 variations when CO_2 gradients exist across the atmosphere, discussion of processes that

cause the gradients was necessary. Maps of each term in the budget equation could then be made and interpreted with relative ease.

5.2   Conclusions

CO_2 observations across NA show huge day-to-day variations that are associated with passing weather disturbances manifested as surface cold fronts, often on the order of 10-20 ppm. Although ecosystem response to frontal weather plays a role, most of the variation (70-90% in most cases) along the front in the case study is due to a combination of vertical and horizontal mixing. NEE is a more dominant process, along with vertical mixing by subsidence, behind the front, but also appears to be important in some other cases in the daytime less intensely analyzed (LEF AND WPL, for example). Coherent CO_2 patterns at stations 500-1000 km suggested horizontal advection was an important mechanism for transporting strong CO_2 gradients across the continent associated with CO_2 anomalies, which without would make frontal CO_2 variations considerably weaker. These anomalies can be remotely generated and concentrated through deformational flow and strong uptake or release when vegetation is exposed to a high pressure system for long enough.

A method for frontal identification in time at a point in space was tested. With the aid of wind shifts and surface weather maps the method was found to be a good objective tool for identifying cold fronts in weather reanalysis consistent with those in the observations, regardless of season and location, and many of which experienced the large day-to-day CO_2 variations seen the observations.

Although PCTM, forced by GEOS4 reanalysis, accurately predicted the shape and timing of frontal CO_2 patterns, a tribute to the ability of SiB to correctly establish CO_2 gradients and GEOS4 to transport those gradients around, it tends to overestimate amplitude in the winter, most typically at the northern sites, and miss amplitude in general in the summer. NEE is clearly overestimated in the winter compared to observations, especially at the northern sites. This is fairly strong evidence suggesting overestimation of CO_2

amplitude in the winter was at least partially a result of excessive model buildup in the winter PBL due to strong respiration. There is also evidence that weak vertical mixing in the winter, a feature that appears to be common in transport models, exacerbates buildup of CO_2 near the surface in the winter.

The summer amplitude errors likely have several sources. The exclusion of fire emissions does is one, and although frontal fire tracer variations are modeled to be small, they are more likely larger in reality as fire burning is concentrated over smaller time scales.

Another source of error is NEE response to frontal weather. There are several instances where NEE is observed to decrease in the daytime as cloud cover reduces GPP but modeled not to change much at all, and vice versa. This occurs at most of the sites with eddy covariance data. This may be related in part to inconsistencies between SiB driver weather (NCEP2 induced) and PCTM driver weather (GEOS4).

Since SiB has no net annual sources or sinks, which is clear in the summer at sites such as HRV and SGP (and other agricultural sites not discussed), CO_2 gradients across the continent (and vertically) may have the correct sign but incorrect strength. Another source of incorrect NEE strength appears to be weather induced stress, which is evident in several model diurnal NEE composites. It is likely these translate directly to a third source of amplitude error as those gradients are mixed around. This is fortunate, however, in that information about source and sink distributions are contained in the weather (although it is is unfortunate that this error is superimposed on plant stress). The forward modeling approach should be combined with top down approaches to help determine sources and sinks.

The influence of large scale inflow to frontal variations depends on the strength of the latitudinal gradient moving off Asia and the strength of the terrestrial gradient upstream of a station. The amount of large scale influence drops off moving inland. Also, in reality, where winter frontal variations are observed to be much weaker than in the summer (see composite plots), inflow is probably more influential (i.e., explains larger part of variance)

in the winter as the large scale latitudinal gradient approaches the strength of the terrestrial gradient.

Finally, the budget equation, which was adapted from Bakwin et al. to represent PBL averaged processes, was presented as a very useful tool for the study of mechanisms associated with variations in CO_2 within the PBL. It was shown to be useful for understanding large variations along a cold front, weaker variations behind cold fronts and along warm fronts, and time mean variations in the Southeast, Mountains, and Plains. The approach is general enough to analyze variations in other parts of the world where the Coriolis Force is less relevant, such as in the Tropics. It will be interesting to apply the budget equation to different parts of the world to see how mechanisms behave and interact with each other.

5.3   Future Work

This study was limited to NA primarily because at the start of the study it was more convenient to compile a fairly large network of well calibrated continuous observations over NA than on other continents. There are, however, plenty of observations available in Europe and results from this work have made it easier to acquire them. Future work will involve similar analysis of CarboEurope data, first to see if variations can be reproduced and if synoptic patterns exist as was seen in NA, and if so to then quantify those variations using the budget equation.

European data is very diverse in that it isn't limited to isolation within the continental interior. Sites are spread out over the mountains, along coasts, within the Mediterranean Sea, and well above the Arctic circle, setting up the perfect environment for study of many different types of air mass influence. It will be interesting to see how PCTM performs overseas and whether the budget equation holds up or not.

The credibility of this work is compromised somewhat by the use of two separate reanalysis datasets to drive SiB (NCEP2) and PCTM (GEOS4). Comparison of horizontal winds between the datasets suggests that horizontal transport is probably about the same

regardless of the reanalysis used. It does, however, affect such things as vertical cloud transport and NEE along a front. If, for example (not necessarily true but plausible) GEOS4 simulates clouds along a front but NCEP2 does not, this would likely cause vertical cloud transport in PCTM without reduction in photosynthesis because shortwave radiation is not reduced in NCEP2 and SiB. This leads to inconsistencies in model processes and should of course be avoided if possible. Effort was made in this study to drive SiB with GEOS4 but there were too many complications.

Although PCTM simulations would be more realistic with the inclusion of fire emissions it is not as simple as including them as an additional tracer. This would be inconsistent with SiB, which might simulate strong uptake at a grid cell when fire inventories suggest the opposite. SiB also needs to include the effect of combustion on vegetation within that grid cell. SiB needs to know, for example, that NEE might go to zero during a fire so that it doesn't mistakenly photosynthesis after vegetation burns or becomes dormant.

REFERENCES

Ameriflux. ARM Southern Great Plains site- Lamont- Oklahoma. http://public.ornl.gov/ameriflux/Site_Info/siteInfo.cfm?KEYID=us.lamont.01. March 2007.

Amiro, B.D., J.B. Todd, B.M. Wotton, K.A. Logan, M.D. Flannigan, B.J. Stocks, J.A. Mason, D.L. Martell, K.G. Hirsch, 2001: Direct carbon emission from Canadian forest fires, 1959-1999, *Can. J. For. Res.*, 31, 512-525.

Andres, R. J., G. Marland, I. Fung, and E. Matthews, 1996: A 1 degrees x 1 degrees distribution of carbon dioxide emissions from fossil fuel consumption and cement manufacture, 1950-1990. *Global Biogeochem. Cy.*, 10, 419-429.

Andrews, A., 2007: Readme file of Atmospheric Carbon Dioxide Mixing Rations from the NOAA GMD Tower Network. [Available over the internet at ftp://ftp.cmdl.noaa.gov/ccg/towers/README_tower_co2.html].

Baker, D. F., et al. (2006): TransCom 3 inversion intercomparison: Impact of transport model errors on the interannual variability of regional CO_2 fluxes, 1988-2003, *Global Biogeochem. Cycles*, 20, GB 1002, doi: 10.1029/2004GB002439

Baker, I, A. S. Denning, N. Hanan, L. Prihodko, M. Uliasz, P. Vidale, K. Davis, and P. Bakwin, 2003: Simulated and observed fluxes of sensible and latent heat and CO2 at the WLEF-TV tower using SiB2.5. *Global Change Biol.*, 9, 1262-1277

Bakwin, P. S., P. P. Tans, D. F. Hurst, and C. Zhao, 1998: Measurements of carbon dioxide on very tall towers: Results of the NOAA/CMDL program. *Tellus*, 50B, 401-415.

Baldocchi, D., Falge, E., Gu, L., Olson, R., Hollinger, D. et al. 2001. FLUXNET: a new tool to study the temporal and spatial variability of ecosystem-scale carbon dioxide, water vapor and energy flux densities. *Bull. Am. Meteorol. Soc.*, 82, 2415-2434.

Barford, C.. C., Wofsy, S. C., Goulden, M. L., Munger, J. W., Pyle, E. H. et al. 2001: Factors controlling long- and short-term sequestration of atmospheric CO_2 in a mid-latitude forest. *Science*, 294, 2415-2434

Bloom, S., A. da Silva, D. Dee, 2005: Documentation and Validation of the Goddard Earth Observing System (GEOS) Data Assimilation System Version 4. Technical Report Series on Global Modeling and Data Assimilation.

Chan, D., C. W. Yuen, K. Higuchi, A. Shashkov, J. Liu, J. Chen, D. Worthy., 2004: On the CO2 exchange between the atmosphere and the biosphere: the role of synoptic and mesoscale processes. *Tellus*, 56B, 194-212.

Chen, B., J. M. Chen, J. Liu, D. Chan, K. Higuchi, A. Shashkov, 2004: A vertical diffusion scheme to estimate the atmospheric rectifier effect. *J. Geo. Res.*, 109, D04306, doi:10.1029/2003JD003925.

Collatz G. J., Ball J. T., Grivet C., et al. 1991: Physiological and environmental regulation of stomatal conductance, photosynthesis, and transpiration: a model that includes a laminar boundary layer. *Agriculture and Forest Meteorology*, 54, 107-136.

Collatz G. J., M. Ribas-Barbo, J. A. Berry, 1992: Coupled photosynthesis-stomatal conductance model for leaves of C4 plants. *Australian Journal of Plant Physiology*, 19, 519-538.

Clarke, L. C. and Renard, R. J., 1965: Experiments in numerical objective frontal analysis. *Mon. Weather Rev.*, 93, 547-556.

Davis, K. J., P.S. Bakwin, C. Yi, B. W. Berger, C. Zhao, R. M. Teclaw, and J. G. Isebrands, 2003: The annual cycle of CO2 and H2O exchange over a northern mixed forest as observed from a very tall tower. *Global Change Biol.*, 9, 1278-1293.

Denning, A. S., J. G. Collatz, C. Zhang, D. A. Randall, J. A. Berry, et al, 1996a: Simulations of terrestrial carbon metabolism and atmospheric CO2 in a general circulation model. Part 1: Surface carbon fluxes. *Tellus*, 48B, 521-542

Denning, A. S., D. A. Randall, G. J. Collatz, P. J. Sellers, 1996b: Simulations of terrestrial carbon metabolism and atmospheric CO2 in a general circulation model. Part 2: Spatial and temporal variations of atmospheric CO2. *Tellus*, 48B, 453-567.

Denning, A. S., M. Nicholls, L. Prihodko, I. Baker, P. Vidale, K. Davis, and P. Bakwin., 2003: Simulated variations in atmospheric CO2 over a Wisconsin forest using a coupled ecosystem-atmosphere model. *Global Change Biol.*, 9, 1241-1250.

Denning, A.S. et al., 2005: *Science Implementation Strategy for the North American Carbon Program.* Report of the NACP Implementation Strategy Group of the U..S. Carbon Cycle Interagency Working Group. Washington, DC: U.S. Carbon Cycle Science Program, 68 pp.

Douglass, A. R., and S. R. Kawa, 1999: Contrast between 1992 and 1997 high-latitude spring Halogen Occultation Experiment observations of lower stratospheric HCl. *J. Geophys. Res.*, 104, 18, 739-54.

Eugster, W. and S. Siegrist, 2000: The influence of nocturnal CO_2 advection on CO_2 flux measurements, *Basic and Applied Ecology*, 1, 177-188.

Fan, S., M. Gloor, J. Mahlman, S. Pacala, J. Sarmiento, T. Takahashi, and P. Tans, 1998: A large terrestrial carbon sink in North America implied by atmospheric and oceanic carbon dioxide data and models. *Science*, 282, 442-446.

Farquhar G. D., S. von Caemmerer, J. A. Berry, 1980: A biochemical model of photosynthetic CO2 assimilation in C3 plants. *Planta*, 14, 78-90.

Geels, C., S. C. Doney, R. Dargaville, J. Brandt, and J.H. Christensen, 2004: Investigating the sources of synoptic variability in atmospheric CO2 measurements over the Northern Hemisphere continents: a regional model study. *Tellus*, 56B, 35-50.

Gerbin, C., J. C. Lin, S. C. Wofsy, B. C. Daube, A. E. Andrews, B. B. Stephens, P. S. Bakwin, and C. A. Grainger, 2003: Toward constraining regional-scale fluxes of CO2 with atmospheric observations over a continent: 1. Observed spatial variability from airborne platforms, *J. Geophys. Res.*, 108(D24), 4756, doi:10.1029/2002JD003018.

GLOBALVIEW-CO$_2$: Cooperative Atmospheric Data Integration Project - Carbon Dioxide. CD-ROM, NOAA GMD, Boulder, Colorado [Also available on Internet anonymous FTP to ftp.cmdl.noaa.gov, Path: ccg/co2/GLOBALVIEW], 2006.

Gloor, M., P. Bakwin, D. Hurst, L. Lock, and R. Draxler, 2001: What is the concentration footprint of a tall tower? *J. Geophys. Res.*, 106, 17, 831-840.

Gurney, K. R., and Coauthors, 2002: Towards robust regional estimates of CO2 sources and sinks using atmospheric transport models. *Nature*, 415, 626-630.

Gurney, K. R., Y.-H. Chen, T. Maki, S. R. Kawa, A. Andrews, and Z. Zhu (2005), Sensitivity of atmospheric CO2 inversions to seasonal and interannual variations in fossil fuel emissions, *J. Geophys. Res.*, 110, D10308, doi:10.1029/2004JD005373.

Hack, J. J., 1994: Parameterization of moist convection in the National Center for Atmospheric Research community climate model (CCM2). *J. Geophys. Res.*, 99, 5551-5568.

Hansen, M. C., R. S. DeFries, J. R. G. Townshend, et al, 2000: Global land cover classification at 1km spatial resolution using a classification tree approach. *International Journal of Remote Sensing*, 21, 1331-1364.

Heimann, M., 2001: The carbon cycle and atmospheric CO2, in *Atmospheric Inversion Calculations Performed for IPCC Third Assessment Report*, chap. 3, Max-Planck-Inst. Fr Biogeochem., Jena, Germany.

Higuchi, K., D. Worthy, D. Chan, A. Shashkov, 2003: Regional source/sink impact on the diurnal, seasonal and inter-annual variations in atmospheric CO2 at a boreal forest site in Canada. *Tellus*, 55B, 115-125.

Holtslag, A. A. M., and B. A. Boville, 1993: Local versus non-local boundary layer diffusion in a global climate model. *J. Climate*, 6, 1825-1842.

Houghton, R. A. 1999. The annual net flux of carbon to the atmosphere from changes in land use 1850-1990. *Tellus* 51B, 298-313

Hurwitz, M. D., D. M. Ricciuto, P. S. Bakwin, K. J. Davis, W. Wang, C. Yi, and M. P. Butler, 2004: Transport of carbon dioxide in the presence of storm systems over a Northern Wisconsin Forest. *J. Atmos. Sci.*, 61, 607-618.

Intergovernmental Panel on Climate Change (IPCC), 2001: Climate Change 2001: The Scientific Basis. Contribution of the Working Group I to the Third Assessment Report of the Intergovernmental Panel on Climate Change (Houghton, J. T. et al., eds), Cambridge and New York.

Jones, PW. 1999. First- and Second-Order Conservative Remapping Schemes for Grids in Spherical coordinates. *Mon. Weather Rev.* Vol. 127, Issue 9, p 2204, 7 p.

Kanamitsu M., W. Ebisuzaki, J. Woollen, S., K.-S. Yang, J. J. Hnilo, M. Fiorino, and G. L. Potter, 2002: NCEP-DOE AMIP-II reanalysis (R-2). *Bull. Amer. Meteor. Soc.* 83, 1631-1643.

Kawa, S. R., D. J. Erickson III, S. Pawson, and Z. Zhu, 2004: Global CO2 transport simulations using meteorological data from the NASA data assimilation system. *J. Geophys. Res.*, 109, D18312, doi:10.1029/2004JD004554.

Kiehl, J. T., J. J. Hack, G. B. Bonan, B. A. Boville, D. L. Williamson, and P. J. Rasch, 1998: The National Center for Atmospheric Research Community Climate Model: CCM3. *J. Climate.*, 11, 1131-1149

Law, R. M., P.J. Rayner, L.P. Steele, I. G. Enting, 2002: Using high temporal frequency data for CO_2 inversions. *Global Biogeochem. Cy.* 16(4), 1053, doi:10.1029/2001GB001593

Law, R., W. Peters, C. Rodenbeck, 2005: Protocol for TransCom continuous data experiment, Retrieved from http://www.purdue.edu/transcom/protocolv5.pdf.

Lin, S. J., and R. B. Rood, 1996: Multidimensional flux-form semi-Lagrangian transport schemes. *Mon. Weather Rev.*, 124, 2046-2070.

Los S. O., Collatz G. J., Sellers P. J. et al., 2000: A global 9-yr biophysical land surface dataset from NOAA AVHRR data. *Journal of Hydrometeorology*, 1, 183-199.

Nielson, J. 2000. Documentation for the Three-Dimensional Parameterized Chemistry and Transport Model. Emergent Information Technologies, Inc. NASA Goddard Space Flight Center.

Pacala, S. W., Hurtt, G. C., Baker, D., Perlin, P., Houghton, R. A. et al. 2001. Consistent land- and atmosphere-based U.S. carbon sink estimates. *Science* 292, 2316-2320.

Pickett-Heaps, C. and Rayner, P., 2006: Protocol for TransCom Upper Air Inter-Comparison Project, Personal Communication

Pinzon, J. E., M. E. Brown, C. J. Tucker, 2004. Satellite Time Series Correction of Orbital Drift Artifacts Using Empirical Mode Decomposition. NASA Goddard Space Flight Center.

Randall, D. A., D. A. Dazlich, C. Zhang, A. S. Denning, P. J. Sellers, C. J. Tucker, L. Bounoua, J. A. Berry, G. J. Collatz, C. B. Field, S. O. Los, C. O. Justice, I. Fung, 1996c: A revised land surface parameterization (SiB2) for GCMs. Part III: The Greening of the Colorado State University General Circulation Model. *J. Climate*, 9, 738-763.

Randerson, J. T., G. R. van der Werf, L. Giglio, G. J. Collatz, and P. S. Kasibhatla, 2006: Global Fire Emissions Database, Version 2 (GFEDv2). Data set. Available on-line [http://daac.ornl.gov/] from Oak Ridge National Laboratory Distributed Archive Center, Oak Ridge, Tennessee, U.S.A.

Rotman, D. A., et al. (2001), Global Modeling Initiative assessment model: Model Description, integration, and testing of the transport shell, *J. Geophys. Res.*, 106, 1669-1691.

Schimel, D. S., et al., 2001: Recent patterns and mechanisms of carbon exchange by terrestrial ecosystems. *Nature*, 414, 169-172

Schultz, D. M., 2005: A review of cold fronts with prefrontal troughs and wind shifts. *Mon. Weather Rev.*, 133, 8, 2449-2472

Sellers P. J., Y. Mintz, Y. C. Sud, et al., 1986: A simple biosphere model (SiB) for use within general circulation models. *J. Atmos. Sci.*, 43, 505-531.

Sellers, P. J., D. A. Randall, G. J. Collatz, J. A. Berry, C. B. Field, D. A.. Dazlich, C. Zhang, and L. Bounoua, 1996a: A revised land surface parameterization (SiB2) for atmospheric GCMs. Part I: Model formulation. *J. Climate*, 9, 676-705

Sellers, P. J., S. O. Los, C. J. Tucker, C. O. Justice, D. A. Dazlich, G. J. Collatz, D. A. Randall, 1996b: A revised land surface parameterization (SiB2) for atmospheric GCMs. Part II: Generation of global fields of terrestrial biophysical parameters from satellite data. *J. Climate*, 9, 706-737

Soil Survey Staff, 1994: *State Soil Geographic Database (statsgo)*. US Department of Agrictulture, Natural Resources, Conservation Service, Fort Worth, TX

Syed, K. H., L. B. Flanagan, P. J. Carlson, A. J. Glenn, K. E. V. Gaalen, 2004: Environmental control of net ecosystem CO2 exchange and carbon balance in a treed, moderately rich fen in northern Alberta.

Takahashi, T. S., S. C. Sutherland, C. Sweeney, A. Poisson, N. Metzl, B. Tilbrook, N. Bates, R. A. Feely, C. Sabine, J. Olafsson, and Y. Nojiri, 2002: Global Sea-Air CO2 flux based on climatological surface ocean pCO2 and seasonal biological and temperature effects. *Deep-Sea Research Part II*, 49, 1601-1622.

Teillet P. M., E. Saleous N, M. C. Hansen et al., 2000: An evaluation of the global 1-km AVHRR land dataset. *International Journal of Remote Sensing*, 21, 1987-2021.

Unisys, (2005). Surface Maps. Retrieved January 2, 2006 from http://weather.unisys.com/archive/sfcmap

Wang, J. W., A. S. Denning, L.. Lu, I. T. Baker, and K. D. Corbin, 2005: Observations and simulations of synoptic, regional, and local variations in atmospheric CO2. *J. Geophys. Res.*, Submitted

Worthy, D. E., I. Levin, N. B. Trivett, A. J. Kuhlmann, J. F. Hopper, and M. K. Ernst, (1998): Seven years of continuous methane observations at a remote boreal site in Ontario, Canada. *J.. Geophys. Res*, 103, 15995-16007.

Zhang, G. J., and N. A. McFarlane, 1995: Sensitivity of climate simulations to the parameterization of cumulus convection in the Canadian flimate center general-circulation model. *Atmos. Ocean*, 33, 407-446.